UTS UNIVERSITY OF TECHNOLOGY SYDNEY

Cytotoxicity and Metabolic Study of New Psychoactive Substances

by Huey Sze Leong

Thesis submitted in fulfilment of the requirements for the degree of

Doctor of Philosophy (Science)

under the supervision of Professor Shanlin Fu and Professor Paul Kenneth Witting

University of Technology Sydney
Faculty of Science

March 2021

CERTIFICATE OF ORIGINAL AUTHORSHIP

I, *Huey Sze Leong* declare that this thesis, is submitted in fulfilment of the requirements for the award of *Doctor of Philosophy*, in the *School of Mathematical and Physical Sciences/ Faculty of Science* at the University of Technology Sydney.

This thesis is wholly my own work unless otherwise referenced or acknowledged. In addition, I certify that all information sources and literature used are indicated in the thesis.

This document has not been submitted for qualifications at any other academic institution.

This research is supported by the Australian Government Research Training Program.

Signature:

Production Note:
Signature removed prior to publication.

Date: 24 March 2021

Acknowledgements

Firstly, I would like to express my upmost gratitude to Professor Shanlin Fu for all his kindness, support and invaluable guidance. I would particularly like to thank him for his patience and belief in me, which enabled me to finally arrive at the final stage of this challenging but rewarding journey. This academic pursuit would not have been accomplished without him.

To my co-supervisor, Professor Paul Kenneth Witting, I would like to thank him for his varied support in the laboratory and advice given to me throughout my candidature. Without his external collaboration, the success of this project would not be possible. I would also like to thank colleagues at the Discipline of Pathology, The University of Sydney, Mr Martin Simone for helping me to get orientated in the laboratory and instructing me with regard to cell biology, which added a new dimension to my science journey. Furthermore, I would also like to thank the staff at The Charles Perkin Centre, The University of Sydney, especially Mr Craig Jackson for providing administrative and technical support as well as instrumentation training whenever needed in the laboratory.

I thank all the academic and professional staff at UTS who supported me throughout my candidature. I wish to especially thank Ms Jane Cameron and Ms Zofia Winiarski for the technical support with the fungus study and allowing me the access to the incubation facility. I must also thank Dr Ronald Shimmon and Dr Dayanne Bordin Mozaner Bordin for all the support in the laboratory especially with the LC-MS instruments.

I would also like to thank Professor Claude Roux and the Centre for Forensic Science for their strong support, particularly with the attendance of conferences.

To the UTS friends especially colleagues from Drugs and Toxicology Group that I have made over the last couple of years, thank you for making my PhD enjoyable. Your thoughtful comments during our discussions added insight and shaped my perspectives throughout my candidature. I would also like to thank Mr Ahmad Yusri Mohd Yusop for being a great colleague with me at conferences and always extending help whenever I needed some.

Lastly, I want to express my deepest gratitude to God and my family for supporting me throughout my PhD journey both emotionally, mentally and spiritually. Your prayers and encouragement for me have spurred me on to do my best and empowered me to achieve something that I never thought possible. I love you all dearly.

Table of Contents

List of papers/publications

The following papers for Chapter 3 and Chapter 4 are reproduced in this thesis with the permission from the publishers (Creative Commons Attribution 4.0 International License, CC BY 4.0). Paper for chapter 5 has been submitted for peer-reviewed publications.

For Chapter 3

Leong, H.S.; Philp, M.; Simone, M.; Witting, P.K.; Fu, S. Synthetic Cathinones Induce Cell Death in Dopaminergic SH-SY5Y Cells via Stimulating Mitochondrial Dysfunction. *Int. J. Mol. Sci.* **2020**, *21*, 1370
https://doi.org/10.3390/ijms21041370

For Chapter 4

Huey Sze Leong, Shimpei Watanabe, Unnikrishnan Kuzhiumparambil, Ching Yee Fong, Hooi Yan Moy, Yi Ju Yao, Paul K Witting, Shanlin Fu. Monitoring metabolism of synthetic cannabinoid 4F-MDMB-BINACA via high-resolution mass spectrometry assessed in cultured hepatoma cell line, fungus, liver microsomes and confirmed using urine samples.
Forensic Toxicol. **2021**, *39,* 198–212
https://doi.org/10.1007/s11419-020-00562-7

For Chapter 5

Huey Sze Leong, Morgan Philp, Paul Kenneth Witting, Shanlin Fu. The Detox Factory: Toxicology Profile of New Psychoactive Substances.

List of Figures

diamond, respectively) with control (empty circle). Individual mitochondrial function parameters of EC_{15} and EC_{40} for (D) butylone (clear and grey diagonal bars, respectively), (E) pentylone (clear and grey horizontal bars, respectively), and (F) MDPV (clear and grey vertical bars, respectively): (i) basal respiration ($^{\#\#}p < 0.01$ vs. EC_{15} pentylone, and $^{\#\#\#\#}p < 0.0001$ vs. EC_{15} MDPV), (ii) proton leak ($^{\#\#}p < 0.01$ vs. EC_{15} MDPV), (iii) maximal respiration ($^{\#\#\#\#}p < 0.0001$ vs. EC_{15} pentylone and EC_{15} MDPV), (iv) non-mitochondrial respiration, and (v) spare respiratory capacity ($^{\#\#\#\#}p < 0.0001$ vs. EC_{15} pentylone, and $^{\#\#}p < 0.01$ vs. EC_{15} MDPV). The spare respiratory capacity was calculated from the difference between maximal and basal respiration. Data are Mean ± SD obtained from at least four independent experiments normalized to the % confluence of cells. Different to the control; * $p < 0.1$, *** $p < 0.001$ and **** $p < 0.0001$

Figure 3.5 Intracellular levels of adenosine triphosphate (ATP) after 24 h of treatment of EC_{15} and EC_{40} for butylone, pentylone, and MDPV. Data are Mean ± SD obtained from three independent experiments normalized to total protein. Different to the control; *** $p < 0.001$ and **** $p < 0.0001$

Figure 3.6 Representative merged images of Cal-520AM staining in (A) the control, (B) EC_{15} butylone, (C) EC_{15} pentylone, and (D) EC_{15} MDPV using the IncuCyte® live-cell imaging system (scale bar: 100 μm) at different time points (8, 12, and 22 h) after drug treatments. Triangular arrowhead shows cell axons, the filled arrow shows the focal distribution, and the broken arrow shows the dispersed distribution of Cal-520 AM staining. (E) Quantification of Cal-520 AM fluorescence after 24 h of treatment of EC_{15} and EC_{40} for butylone, pentylone, and MDPV. Data shown in panel E are Mean ± SD obtained from four independent experiments. $^{\#\#\#\#}p < 0.0001$ vs. EC_{15} butylone, EC_{15} pentylone and EC_{15} MDPV. Different to the control; ****$p < 0.0001$

Figure 3.7 Effect elicited by EC_{15} and EC_{40} for butylone, pentylone, and MDPV in the activation of caspase 3 and 7 after 24 h of treatment. Data are Mean ± SD obtained from four independent experiments normalized to the % confluence of cells. $^{\#\#\#\#}p < 0.0001$ vs. EC_{15}. Different to the control; **** $p < 0.0001$

Figure 4.1 Product ion spectra and structures with the suggested fragmentation patterns from the three *in vitro* models: *C. elegans* (F), human liver microsomes (M) and HepG2 (H). Bracket indicates spectra obtained from one of the *in vitro* models with CE 10 or 20 eV. The exact position of the hydroxylation was not determined

Figure 4.2 Proposed metabolic pathway of 4F-MDMB-BINACA. *In vivo* metabolites were in italics and bold. The exact position of the metabolites with hydroxylation structure were not determined

Figure 4.3 (A) Common *in-vitro* metabolites among the seven most abundant metabolites in (B) *C. elegans* (C) HLM and (D) HepG2 model. *C. elegans*, HLM and HepG2 are represented by horizontal, diagonal and vertical bar lines, respectively. Error bars reflect the relative abundance variation of a specific metabolite within the analyzed group (n = 3)

Figure 5.1 Normalized dose-response curves after 72 h drug treatment with (A) butylone, (B) pentylone, (C) MDPV and (D) 4F-MDMB-BINACA in HepG2 cells. Data are mean ± SD obtained from at least three independent experiments for the CyQuant assay. Table: Mean EC_{50} values obtained from dose-response curves of CyQuant assay. ($^{\#}p < 0.1$ vs 4F-MDMB-BINACA)

Figure 5.2 Linear regression plot of lipophilicity and EC_{50} values of butylone, pentylone, MDPV and 4F-MDMB-BINACA

Figure 5.3 Chemical structures and lipophilicity values (expressed in terms of Consensus LogP) of butylone, pentylone, MDPV and 4F-MDMB-BINACA

Figures 5.4 Representative merged images of orange-red TMRE and blue Hoechst 33342 staining in 300 μM of (A) butylone, (B) pentylone, (C) MDPV; 120 μM of (D) 4F-MDMB-BINACA; and (E) the control using fluorescence phase-contrast microscope with a 20x objective (scale bar: 50 μm) after 72 h of drug treatments in HepG2 cells. Quantification of TMRE fluorescence after 72 h of treatment in (F) 100 and 300 μM of SCs: butylone, pentylone and MDPV, and (G) 60 and 120 μM of 4F-MDMB-BINACA.

Data shown in panel F and G are mean ± SD obtained from four independent experiments. #### $p <$ 0.0001 vs 300 μM pentylone and 300 μM MDPV. Different to the control; * $p < 0.1$, ** $p < 0.01$ and **** $p < 0.0001$. RFU: Relative Fluorescence Unit

List of Tables

Abstract

The unprecedented growth of new psychoactive substances (NPS) render identification a challenging issue to both the forensic and clinical laboratories. NPS readily available in myriad of unknown formulation, posing serious threat and acute harm for the users. At present, there is paucity of information on the potential potency, toxicity mechanisms, and toxicokinetic parameters associated with the use of these drugs. The present study aimed to investigate the neurotoxicity potency and cellular mechanism of NPS. Hepatoxicity potency potential, metabolic stability and subsequent metabolism pathway of specific NPS is also explored for better understanding of the toxicokinetics of these NPS.

The neurotoxicity potential and mechanism of synthetic cathinones (SCs) butylone, pentylone and 3,4-methylenedioxypyrovalerone (MDPV) was investigated using differentiated SH-SY5Y cell line. Viability assays and end-point measurements that include markers of oxidative stress, mitochondrial bioenergetics, intracellular calcium (Ca^{2+}) and cell death pathways were employed. All the three SCs displayed dose-dependent neurotoxicity with the following order of potency: butylone (least cytotoxic) < pentylone < MDPV (most cytotoxic). The activation of apoptotic cell death pathway implicated the orchestration of mitochondrial-mediated neurotoxicity mechanisms via oxidative stress, compromised bioenergetics balance and changes in Ca^{2+} homeostasis ($p < 0.0001$ vs. control).

The metabolism of synthetic cannabinoid (SCB), 4F-MDMB-BINACA was investigated using *in vitro* models: HepG2 liver cells, fungus *Cunninghamella elegans* (*C. elegans*) and pooled human liver microsomes (HLM). Tentative structure elucidation of the *in vitro* metabolites was performed using high-resolution mass spectrometry whilst twenty authentic human urine samples were retrospectively analysed using liquid chromatography-orbitrap mass spectrometry. A total of twenty-five *in vitro* metabolites and eight *in vivo* metabolites were tentatively identified. Ester hydrolysis and ester hydrolysis dehydrogenation 4F-MDMB-BINACA metabolites were recommended as urinary markers for 4F-MDMB-BINACA intake. *C. elegans* has the potential to be used

as a complementary model to predict and characterise human metabolites, as well as identifying possible drug toxicities for emerging SCBs.

The metabolic stability and hepatotoxicity potential of butylone, pentylone, MDPV and 4F-MDMB-BINACA were studied using HLM and HepG2 liver cells, respectively. Drug-treated HepG2 exhibited the following cytotoxicity potency: butylone (least cytotoxic) < pentylone < MDPV < 4F-MDMB-BINACA (most cytotoxic). For the metabolic stability study, NPS incubated in HLM were collected at various time points and subsequently analysed by liquid-chromatography tandem mass spectrometry. Calculated *in vitro* half-lives together with estimated intrinsic clearance values categorised butylone, pentylone and MPDV as low clearance drugs and 4F-MDMB-BINACA as high clearance drug.

Keywords: New psychoactive substances, cytotoxicity, metabolic profile, *in vitro*

Chapter 1
Introduction

1.1 Background

Many new psychoactive substances (NPS) synthesized and patented a few decades ago, had their chemical structures modified my entrepreneurial chemists to produce new compounds with psychoactive effects similar to the traditional illicit drugs of abuse. Importantly, small structural differences from previously controlled compounds can result in a big difference in terms of biological activity, toxicokinetic parameters, and identification [1]. These NPS have proliferated in ways intended to evade law enforcement. Varying potency, concentration and formulation in product content with lack of information of the active ingredients have increased unknown risks for the users, resulting in fatal intoxications [2, 3]. The rapid emergence of novel NPS with a constantly increasing abuse and addiction are persistent public health concerns that exert global health problems [4, 5]. There is a need to investigate the cellular toxicity and its associated mechanism of NPS as intervention measure since scientific data on these remains scarce. Predicting which NPS is likely to result in severe toxic effects, prior to the actual occurrence aids in risk assessment, which could eventually improve public health [6].

Unlike traditional drugs of abuse, little is known about NPS metabolism and toxicokinetic data on NPS are still largely unknown. Moreover, most of the synthetic cannabinoids (SCBs) were demonstrated to undergo extensive metabolism in the human body, leading to negligible levels of parent drug in examined biological fluids, making detection of parent drug difficult [7-9]. As detection and quantification of parent drug in biological fluids are key steps in the diagnosis and treatment of emergency cases, there is an urgent need for the development of highly sensitive analytical methods for the detection and quantification of metabolites. Toxicology laboratories previously focused on narrow range of drugs, are now challenged to detect plethora of NPS analogs. As most of the NPS were not detected by routine drugs of abuse immunoassay screening methods, liquid chromatography-coupled to various mass analyzers have been proposed to detect newly emerging NPS [10]. Combined *in vivo* and *in vitro* metabolism approaches have been proven useful in the identification of emerging NPS metabolites due to non-availability of reference standards.

1.2 Research Objectives

The research objectives were outlined as follows:

- To evaluate the neurotoxicity potency potential and toxicity mechanism of butylone, pentylone in relation to 3,4-methylenedioxypyrovalerone (MDPV).
- To assess the suitability of three *in vitro* models in monitoring metabolism of methyl (2S)-2-([1-(4-fluorobutyl)-1H-indazole-3-carbonyl]amino)-3,3-dimethylbutanoate (4F-MDMB-BINACA) and to propose suitable urinary marker(s).
- To use key screening strategies to gauge biological effects of butylone, pentylone, MDPV and 4F-MDMB-BINACA in predicting its potentially hazardous hepatotoxicity and to investigate the *in vitro* metabolic stability of these NPS.

1.3 Research Scope

- Neurotoxicity potency potential and toxicity mechanistic pathway of butylone, pentylone and MDPV were investigated using various end-point and real-time measurements via well-established human dopaminergic SH-SY5Y cell line (Chapter 3).
- Metabolism pathway of NPS was studied using three different *in vitro* models: HepG2 liver hepatoma cell line, fungus *Cunninghamella elegans (C. elegans)* and human liver microsomes (HLM). Since metabolism studies of butylone, pentylone and MDPV have been well explored [11-13], metabolism pathway of emerging 4F-MDMB-BINACA was investigated and validated using *in vivo* authentic human urine samples. The identification of the relevant urinary marker(s) was based primarily upon the prevalence of the *in vivo* metabolites and its presence in all the *in vitro* models especially in the *C. elegans* model where scaling up metabolites production allow isolation, characterization of metabolites as well as the identification of active metabolites for future toxicity studies (Chapter 4).
- The order of cytotoxicity potency potential of butylone, pentylone, MDPV and 4F-MDMB-BINACA in HepG2 liver hepatoma cell line was determined and compared using two approaches: EC_{50} values obtained from dose-response viability curve and screening baseline value from mitochondrial membrane potential assay. *In vitro* half-lives and estimated intrinsic clearance were investigated using HLM and compared with existing literature where possible. These *in vitro* metabolic stability data were then used to predict the unknown *in vivo* toxicokinetic of emerging 4F-MDMB-BINACA (Chapter 5).

1.4 References

1. Zawilska, J. B. & Andrzejczak, D. (2015) Next generation of novel psychoactive substances on the horizon – A complex problem to face, *Drug and Alcohol Dependence.* **157**, 1-17.

2. UNODC (2020) World Drug Report: Cross-cutting Issues: Evolving Trends and New Challenges, *United Nations publication, Sales No E20XI6.* **Booklet 4**, 1-119.

3. Zamengo, L., Frison, G., Bettin, C. & Sciarrone, R. (2014) Understanding the risks associated with the use of new psychoactive substances (NPS): High variability of active ingredients concentration, mislabelled preparations, multiple psychoactive substances in single products, *Toxicology Letters.* **229**, 220-228.

4. Baumann, M., Solis, E., Watterson, L., Marusich, J., Fantegrossi, W. & Wiley, J. (2014) Bath Salts, Spice, and Related Designer Drugs: The Science Behind the Headlines, *Journal of Neuroscience.* **34**, 15150-15158.

5. Madras, B. K. (2017) The Growing Problem of New Psychoactive Substances (NPS), *Current Topics in Behavioral Neurosciences.* **32**, 1-18.

6. Hondebrink, L., Zwartsen, A. & Westerink, R. H. S. (2018) Effect fingerprinting of new psychoactive substances (NPS): What can we learn from in vitro data?, *Pharmacology and Therapeutics.* **182**, 193-224.

7. Diao, X. & Huestis, M. A. (2019) New Synthetic Cannabinoids Metabolism and Strategies to Best Identify Optimal Marker Metabolites, *Frontiers in Chemistry.* **7**, 109.

8. Kevin, R. C., Lefever, T. W., Snyder, R. W., Patel, P. R., Fennell, T. R., Wiley, J. L., McGregor, I. S. & Thomas, B. F. (2017) In vitro and in vivo pharmacokinetics and metabolism of synthetic cannabinoids CUMYL-PICA and 5F-CUMYL-PICA, *Forensic Toxicology.* **35**, 333.

9. Kong, T., Kim, J.-H., Kim, D. & Lee, H. (2018) Synthetic cannabinoids are substrates and inhibitors of multiple drug-metabolizing enzymes, *Archives of Pharmacal Research.* **41**, 691-710.

10. Huestis, M. A., Brandt, S. D., Rana, S., Auwärter, V. & Baumann, M. H. (2017) Impact of Novel Psychoactive Substances on Clinical and Forensic Toxicology and Global Public Health, *Clinical Chemistry.* **63**, 1564-1569.

11. Meyer, M. R., Wilhelm, J., Peters, F. T., Maurer, H. H. (2010) Beta-keto amphetamines: studies on the metabolism of the designer drug mephedrone and toxicological detection of mephedrone, butylone, and methylone in urine using gas chromatography-mass spectrometry, *Analytical and Bioanalytical Chemistry.* **397**(3), 1225-1233.

12. Richter, L.H.J., Flockerzi, V., Maurer, H.H., Meyer, M.R. (2017) Pooled human liver preparations, HepaRG, or HepG2 cell lines for metabolism studies of new psychoactive substances? A study using MDMA, MDBD, butylone, MDPPP, MDPV, MDPB, 5-MAPB, and 5-API as examples, *Journal of Pharmaceutical and Biomedical Analysis.* **5** (143), 32-42.

13. Mueller, D.M., Rentsch, K.M. (2012) Generation of metabolites by an automated online metabolism method using human liver microsomes with subsequent identification by LC-MS(n), and metabolism of 11 cathinones. *Analytical and Bioanalytical Chemistry.* **402**(6), 2141-2151.

Chapter 2
Literature Review

2.1 New Psychoactive Substances

New psychoactive substances (NPS) are classes of drugs that mimics the psychoactive effects of "traditional" illicit recreational drugs such as heroin, cocaine, amphetamines and cannabis [1]. NPS also known as "legal high" or "designer drugs" have dominated the drug scene globally during the last decade due to the ease of purchase over internet, relatively low cost resulting from large-scale production, aggressive marketing strategies to attract consumers and low detection rate from routine drug screening methods, hence evading laws regulation on the sale and use of controlled substances [2-5]. NPS-related epidemiological trends indicated that NPS are popular among younger individuals who abuse multiple substances, associated with criminal history, lived in metro area and experienced homelessness [6-8]. Manufactured typically in clandestine laboratories in China and India, NPS are then distributed into the global markets [9]. Attractive NPS brand names were used to allure consumers, especially teenagers, the names often refer to popular movies (e.g., "Black Mamba", 'Vanilla Sky"), cartoons (e.g., "Scooby snax", "Kryptonite"), animals (e.g., "Magic Dragon", "Meow Meow") or landscapes ("Ocean snow", "Rainbows") [10]. The names on the commercial products are often inconsistent, with similarly named products having different chemical compositions [10, 11]. Moreover, the list of active ingredients on the product package often do not contain indication of the presence of single or multiple psychoactive substances, exposing NPS users to severe risk factors. Alterations in cognition and mood, depression, psychosis, agitation, and suicidality were amongst the effects that were significantly associated with NPS use [8].

By Dec 2019, the number of NPS identified and reported to the United Nations Office on Drugs and Crime World Drug Report (UNODC) reached 950, which is more than three times of the internationally controlled drugs. Most of these synthetic NPS identified in the period 2009-2019 had stimulant effects (mostly cathinones and phenethylamines), followed by synthetic cannabinoids and hallucinogens [12]. This study will focus mainly on the synthetic cathinones (SCs) and synthetic cannabinoids (SCBs), as these are the two most prevalent groups of NPS that have received substantial media attention [4, 8]. Although both SCs and SCBs were synthesized in the early twentieth century, new derivatives are constantly being detected globally [4]. These two classes of NPS are composed of pharmacologically diversified compounds with multiple

mechanisms of action. The main mechanisms of action for the SCs is the inhibition and/or reversal of monoamine reuptake transporters, whilst the activation of cannabinoids receptors is the main mechanisms of action for the SCBs [13]. SCs and SCBs have been linked to mortalities as well as to adverse physical and psychiatric conditions [14-20]. The prevalence of NPS appearing on the global market has become a major public health concern because of the paucity of scientific research and general lack of information on newly manufactured NPS and the possibility of serious health risks.

2.1.1 Synthetic Cathinones

Cathinone, specifically S(-) cathinone was identified in 1975 as the stimulant component of the cultivated perennial shrub khat, *Catha edulis* (native to East Africa/ Arabian Peninsula). More recently, the term "cathinone" refers to racemic or (±) cathinone unless stereochemistry is specifically defined. Cathinone is beta-ketone amphetamine analogue (Figure 2.1), that can be structurally modified to give rise to large number of psychoactive synthetic compounds [21]. These SCs have surfaced as popular alternative to other illicit drugs of abuse, such as methamphetamine, 3,4-methylenedioxymethamphetamine (MDMA) or ecstasy and cocaine due to their potent psychostimulant and empathogenic effects [22]. The most common substitutions of the SCs at the N-terminus are methyl or ethyl groups, or a pyrrolidine ring [23]. Additionally, the length of the alkyl chain at the α-position is commonly modified [24]. SCs are primarily sold online as "plant food," "bath salts," or "research chemicals" and labelled as "not for human consumption," in order to evade potential regulation [25]. Common routes of administration include snorting and ingesting orally with some users having mix routes administration. Rectal and intramuscular administration are the less common routes for SCs administration [26, 27]. Clinical effects of SCs are individual-, dose- and route of administration-dependent. The "sought-after" effects of SCs include euphoria, empathy, increased sexual performance, and increased sociability [28]. SCs exert their stimulant effects via interaction with monoamine membrane transporters, namely dopamine (DAT), serotonin (SERT), and noradrenaline (NET) [29]. Although a number of different cathinones have been detected in "bath salts" product, IUPAC name 1-(1,3-benzodioxol-5-yl)-2-pyrrolidin-1-ylpentan-1-one or 3,4-methylenedioxypyrovalerone (MDPV) have been one of the most prevalent SCs found globally [30]. MDPV has a pyrrolidine ring and a tertiary

amino group with propyl substitution at the α-position (Figure 2.1). MDPV's lipophilic properties allow it to cross the blood brain barrier easily [31]. MDPV is highly selective and potent uptake blocker at DAT and NET when compared to cocaine, predicting serious potential for abuse. Butylone and pentylone was found to be mixed with MDMA or as a replacement in common party pill such as "Molly" [32, 33]. Butylone and pentylone contain ethyl and propyl at the α-position with IUPAC name 1-(1,3-benzodioxol-5-yl)-2-(methylamino)butan-1-one and 1-(1,3-benzodioxol-5-yl)-2-(methylamino)pentan-1-one, respectively. Both butylone and pentylone involve non-selective inhibition of monoamine reuptake (resembling cocaine, which shows greater selectivity toward the DAT than the SERT) and promotion of release of serotonin (similar to MDMA) [34]. A number of negative cardiac, psychiatric, and neurological adverse effects associated with SCs use have been reported, emphasizing growing use of SCs might constitute an important public health issue. Acute toxicity of SCs is the leading cause of SCs-induced fatalities [35].

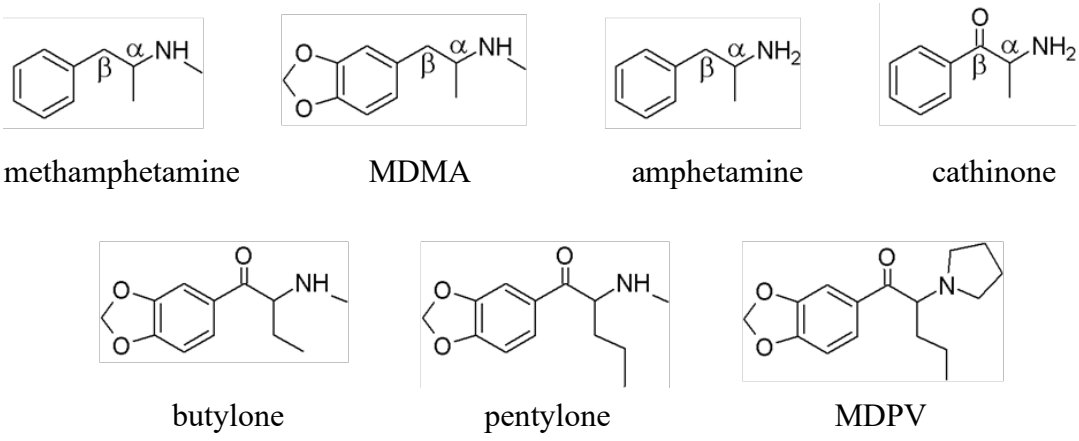

Figure 2.1 Chemical structures of butylone, pentylone and MDPV, and their relationship to methamphetamine, MDMA, amphetamine and cathinone

2.1.2 Synthetic Cannabinoids

SCBs were initially developed in the legitimate search for potential novel therapeutic agents that target the neuroregulatory cannabinoid system via central (predominantly CB_1) and peripheral (predominantly CB_2) receptors [36]. As clandestine laboratory

chemists recognize that SCBs mimic the effects of delta-9-tetrahydrocannabinoid (Δ^9-THC), the main psychoactive component of cannabis [37], products for recreational use were created and marketed as 'natural herbal blends' such as 'spice' and 'K2' [38]. Similar to Δ^9-THC, SCBs exert its pharmacological effects through human cannabinoid type 1 (CB_1) and type 2 (CB_2) G-protein coupled receptors [39]. Stimulation of the central CB_1 receptors produces the desired euphoria and relaxation effects sought by the SCBs' users, while CB_2 receptors, represent a potential therapeutic opportunity and are critical for immune functions. SCBs binds at higher potency and efficacy at CB_1, posing greater risk of abuse and dependence compared to the traditional cannabis [40, 41]. Inhalation is found to be the main route of administration of SCBs where it is delivered mainly via conventional smoking and gaining popularity more lately, is the electronic cigarette (e-cigarette) [42, 43]. SCBs are generally classified based on the chemical structure consisting of a core, linker, linked group and tail sections (Figure 2.2) [44]. The complex chemical structure of SCBs offers numerous opportunities for modification to evade legal controls based on novel chemical structures created. Compounds with indole or indazole core groups constitute the largest group of the abused SCBs [45], with indazole carboxamide groups being the most abundant and prevalent classes identified, with many compounds still emerging [46-48]. Common metabolic pathways include hydroxylation at various sections of the molecule and hydrolysis of compounds with amide or ester functional groups to carboxylic acid metabolites via various CYP, CES, and amidase enzymes [48]. Importantly, many of the hydroxylated metabolites have been demonstrated to be pharmacologically active [49, 50]. Adverse effects of SCBs administration including toxicity to multiple organ systems, neurological, psychiatric, cardiorespiratory, and gastrointestinal effects have been reported [51-53]. Although most of the common clinical toxicities were not life threatening, more severe outcomes that includes fatality have been described [17, 51, 54, 55].

Lately since 2018, 4F-MDMB-BINACA with IUPAC name methyl (2S)-2-([1-(4-fluorobutyl)-1H-indazole-3-carbonyl]amino)-3,3-dimethylbutanoate, has been reported with increasing frequency as a contributory factor in deaths, creating morbidity and mortality risks for drug users [56-60]. However, there is limited toxicology information on synthetic cannabinoid, 4F-MDMB-BINACA currently.

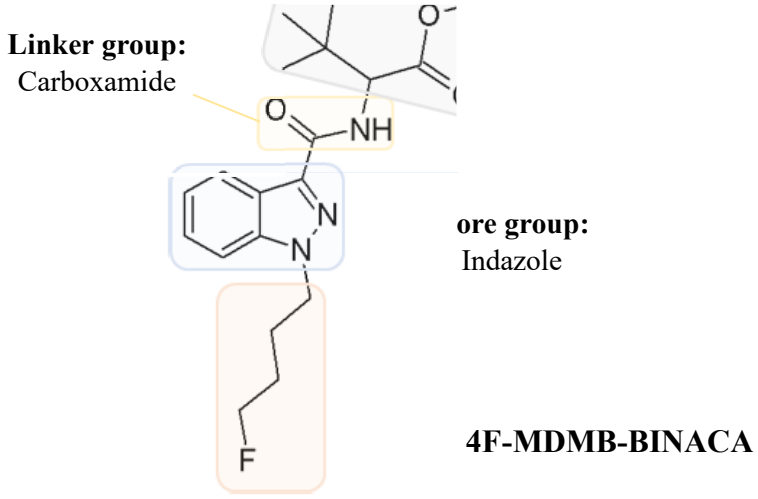

Figure 2.2 General structure depiction of synthetic cannabinoids (SCBs) based on their different sections

2.2 Cytotoxicity and Mechanism of Toxicity

Drug-induced oxidative stress is implicated as a mechanism of toxicity in numerous organ systems, such as liver, cardiovascular, nervous systems and so on [61]. Toxic damage in cells can cause organ dysfunction resulting in severe health problem. [62]. Oxidative stress has been reported to damage the mitochondrial respiratory chain, alter membrane permeability, induce mitochondrial DNA mutations, and influence intracellular calcium (Ca^{2+}) homeostasis, leading to cell toxicity [63]. Knowledge and insight gained from mechanistic toxicity study is useful in cell toxicity protection, treatment and prevention of the drug adverse effects, which eventually aid in risk assessment of the constantly evolving NPS. Traditional toxicological evaluation has largely relied on animal models that have been used to predict potentially harmful effects in humans. While the animal models have provided valuable information on the safety of the drugs, they are costly, low throughput and time-consuming [64].

There was a paradigm shift of toxicological testing towards replacing animal models with alternative test methods and strategies at the advent of technological innovations in molecular and cellular biology [65]. These new approaches include *in vitro*, *in chemico* and *in silico* methods. In this study, human cell-based *in vitro* methods

for the assessment of potential cytotoxicity and mechanism of toxicity will be discussed.

2.2.1 *In vitro* cell-based models

Replacement of animal models is motivated by ethical and scientific concerns. Therefore, non-animal high-throughput methods are now of great interest in the field of toxicology [66]. Cell-based *in vitro* models are relatively low costs and higher throughput when compared to animal models. Since 1959, the development and use of *in vitro* cell cultures have increased dramatically, driven primarily by advances in molecular biology techniques. Despite the reductionist *in vitro* cell-based approach in determining toxicological profiles of NPS, *in vitro* assessments can provide a good approximation of the expected effects *in vivo* by comparing the obtained toxicology profiles to data of well-characterized psychoactive substances [67] and hence, may provide an alternative to animal models.

Current cell-based *in vitro* methods are typically based on two-dimensional (2D) cultures of cell lines, primary cells or induced pluripotent stem cell (iPSC)-derived cells growing in multi-well plates. Drugs-induced cellular changes are then either assessed via colorimetric-, fluorescence- or luminescence-based assays, or by high-throughput automated imaging. These data provide information on cellular injury and mechanism of toxicity pathway perturbation.

The determination of toxicological profiles can be studied using various well-established optimized assays. Toxicology profile such as cytotoxicity potencies can be assessed using EC_{50} values for *in vitro* toxicity assessment. However, EC_{50} values depend on assay conditions and are often not comparable between laboratories. The inclusion of reference compounds (well-known psychostimulants such as MDMA and methamphetamine) in the screening of NPS can help to compare EC_{50}-based findings between laboratories.

For the assessment of toxicity mechanisms, the most commonly used type of cell culture is the 2D cell model, although three-dimensional (3D) cell model has been gaining in popularity lately [68]. The primary cell line mimics the *in vivo* human features most accurately as it contains populations of different cell types present in the source tissue. However, the correct cell types are often difficult to isolate and isolated cells have

relatively short life span for continuous experiments. An alternative option is the use of established popular cancer cell line such as SH-SY5Y and HepG2 cell lines.

The neuroblastoma SH-SY5Y cell line is a subline of the SK-N-SH cell line which was established in culture in 1970 from a bone marrow biopsy of a metastatic neuroblastoma of a 4-year-old female that has undergone three rounds of clonal selection [69]. SH-SY5Y cell line display a catecholaminergic phenotype since it has the machinery to synthesize both dopamine and noradrenaline. It should be noted that SH-SY5Y cells are not purely dopaminergic because the cell line was obtained as a neuroblastoma derivative and its cancerous properties possess physiological characteristics which may differ from the normal dopaminergic neuronal features [70]. Despite these limitations, SH-SY5Y cell line was extensively used for Parkinson's disease research, as well as other areas of neuroscience, including research on psychostimulant NPS-induced neurotoxicity [71-78]. The phenotype of SH-SY5Y cells can be induced to terminal neural phenotype specifically, dopaminergic-like neurons more efficiently by sequential treatment with retinoic acid (RA) and 12-*O*-Tetradecanoylphorbol-13-acetate (TPA) [79]. As most of the amphetamine-type psychostimulant drugs are neurotoxic and involve deficits in and alterations to dopaminergic pathways in the brain [80], differentiated dopaminergic SH-SY5Y cells are employed for the neurotoxicity investigation of psychostimulant SCs in this study.

Human hepatoblastoma cell line HepG2 derived from liver tissue of a 15-year-old Caucasian male, were developed with the intention that it would be an alternative to primary human hepatocytes in early toxicology screening as they display many genotypic and phenotypic characteristics of human hepatocytes [81]. Low levels of expression of phase I (CYPs) enzymes and drug transporters have been reported for HepG2 cells, but the unlimited cell supply and stable clonality [82] have made these cell line popular as liver-based *in vitro* cytotoxicity screening tool for NPS [83-86]. Moreover, metabolic competence of HepG2 was reported to develop and toxicity expresses itself after 3 days of exposure to drugs [87].

2.2.2 End-point and real-time measurements

Cytotoxicity analysis allows the cells to be assessed for viability after being exposed to a particular drug for a period of time. Cytotoxicity and cell viability assays are based on

various cell functions. A broad spectrum of assays is beneficial in the determination of mechanisms of actions of a drug that is useful in the field of toxicology and pharmacology. The assays in general could be grouped into four categories according to their type of end-point measurement: dye exclusion, colorimetric, fluorometric and luminometric assays [88].

In dye exclusion method, viable cells exclude dyes. Trypan blue (TB) is a dye exclusion assay whereby large negatively charged TB are excluded from entering live cells that possess intact cell membranes. Viable cells will have a clear cytoplasm, whereas dead cells will have a blue cytoplasm [89]. Number of viable and/or dead cells per unit volume is determined by light microscopy as a percentage of untreated control cells. TB has been used extensively as the method is simple, inexpensive and a good indicator of membrane integrity. However, it could be laborious to count cells manually with a hemocytometer, hence semi-automated or fully automated instrumentation has been introduced to supplement this traditional cell counting method [90]. As TB dye exclusion assay cannot be used to distinguish between the healthy cells and viable cells that are losing cell functions, it is often performed complimentary with another *in vitro* cytotoxicity assay.

A widely used approach to determine drug-induced cytotoxicity involves measuring cellular metabolic activity at the conclusion of an experiment using colorimetric assays. Reagents used in colorimetric assays develop a colored biochemical marker in response to the viability of cells, allowing the colorimetric measurement of cell viability. Colorimetric assays are economical and easy to perform. Colorimetric method based on the tetrazolium salt XTT (2,3-bis(2-methoxy-4-nitro5-sulphophenyl)-5-carboxanilide-2H-tetrazolium, monosodium salt is excellent in quantitating cells and determining their viability [91]. This assay is based on the ability reduction of the tetrazolium salt XTT to water soluble orange-colored formazan compounds by metabolic active cells, in which the intensity can be measured with a spectrophotometer. XTT assay is highly sensitive, accurate and easy to implement.

Lactate dehydrogenase (LDH) assay is a colorimetric method of assaying cellular cytotoxicity. The assay measures the stable, cytosolic LDH enzyme quantitatively that is released into the cell culture media when cell membrane is compromised [92]. The released LDH is measured by a coupled enzymatic reaction that results in the conversion of tetrazolium salt 2-(4-iodophenyl)-3-(4-nitrophenyl)-5-phenyltetrazolium chloride

(INT) into a red color formazan by diaphorase. In the first step, LDH catalyze conversion of lactate to pyruvate and in the second step, INT is reduced to red formazan by catalyst diaphorase. The loss of intracellular LDH and its release into the cell culture media is an indicator of irreversible cell death due to damaged cell membrane.

Fluorometric assays are easy to perform with the use of a fluorescence microscope, fluorometer, fluorescence microplate reader or flow cytometer. Fluorometric assays are generally more sensitive than colorimetric assays [93].

Fluorescent probes for monitoring mitochondrial membrane potential are frequently used for assessing mitochondrial function. In particularly, the mitochondrial membrane potential ($\Delta\psi_m$) is an important physiologic mitochondrial parameter as it relates to cells' capacity to generate ATP by oxidative phosphorylation, which is the key indicator of cell health or injury. Lipophilic cationic tetramethylrhodamine ethyl ester (TMRE) have become an important tool for directly measuring the $\Delta\psi_m$ component [94]. The lipophilic cations are highly efficient in crossing the hydrophobic membranes and attracted to the negative potential across the inner mitochondrial membrane, where they preferentially accumulate into the mitochondria of the living cells. Polarized mitochondria (hyperpolarized, where the interior is more negative) will accumulate more cationic dye, and depolarized mitochondria (interior is less negative) will accumulate less dye. Fluorescent dye accumulation in mitochondria is then optically detected and measured.

Overproduced reactive species such as reactive oxygen species (ROS) and reactive nitrogen species (RNS) can cause oxidative stress leading to cellular damage. Fluorescent probes are excellent indicators of the highly reactive species due to their high sensitivity as they can be oxidized by the reactive species to form highly fluorescent moieties. Reduced dyes are often non-fluorescent, whereas their oxidized products are highly fluorescent [95]. Fluorescein probes such as 2',7'-dichlorofluorescin diacetate (DCFHDA) and its analogues are the most frequently used for detecting intracellular ROS [96]. Cell-permeable DCFHDA readily diffuses into cells, where it is deacetylated by cellular esterases, and the resultant non-fluorescent carboxylate anion, 2',7'-dichlorofluorescin (DCFH) which is retained in cell, is further oxidized to the highly fluorescent 2', 7'-dichlorofluorescein (DCF) which can be monitored by fluorescence-based technique.

The regulation of protons and other ion concentrations is crucial for mitochondrial

functionality. Some ions, particularly calcium is a second messenger that regulates many fundamental physiological processes. Excess of calcium in the mitochondria causes the opening of the mitochondrial permeability transition pore, eventually leading to cell death. Fluorescent approaches to evaluate the rate of calcium influx or efflux in mitochondria such as Cal-520 AM is a choice indicator among the green-emitting small-molecule indicators [97, 98]. Cell permeable Cal-520 AM are cleaved by esterases, resulting in a negatively charged fluorescent dye that stays inside cells. Its fluorescence is greatly enhanced upon binding to intracellular Ca^{2+} and can be measured by fluorescence instrumentation. Real-time system such as IncuCyte® allow for the tracking of intracellular Ca^{2+} over the entire time course of the experiment.

Another real-time system is that of the sensitive high-throughput Seahorse XF Extracellular Flux Analyzer in assessing mitochondrial oxidative phosphorylation function through determination of oxygen consumption rate of cells. The system utilizes novel fluorescent sensor-containing cartridges for reagent mixing and measuring oxygen consumption. Mitochondrial respiratory electron transport system inhibitors distributed in ports surrounding the sensor are then sequentially injected to each well including background correction wells to normalize the data to background plate noise. Real-time analysis of basal respiration, oxygen consumption, ATP turnover, coupling efficiency, proton leak, maximum respiration rate, respiratory control ratio, spare respiratory capacity, and non-mitochondrial respiratory parameters of cells can be determined by the sequential addition of specific electron transport system inhibitors (oligomycin, carbonyl cyanide-4-(trifluoromethoxy)phenylhydrazone, rotenone, and antimycin A) [99].

Luminometric assays has remarkable feature of being able to produce persistent and stable glow-type signal after reagent addition. Cellular adenosine triphosphate (ATP), the most important energy reservoir is one of the most sensitive end-point measurement for cell viability [93]. Cells lose membrane integrity when they’re damaged, hence losing ability to synthetize ATP resulting in reduction of intracellular ATP level. The ATP assay is based on the catalyzed reaction of luciferin to oxyluciferin by enzyme luciferase in the presence of magnesium (Mg^{2+}) yielding a luminescent signal.

Programmed cell death or apoptosis is an important physiologic process that helps in the maintenance of homeostasis of a multicellular organism. Apoptosis may proceed by activation of cysteine proteases known as caspases [100]. Monitoring initiator caspase-3 activity permits comprehensive apoptosis detection in regardless of the apoptotic

pathway. Bioluminescent caspase 3/7 assay is a convenient one step homogenous assay that monitor the apoptosis induction. The conserved recognition sequence for caspases 3 and 7, DEVD; was conjugated to aminoluciferin and N-terminally blocked to produce a proluminescent substrate, Z-DEVD-aminoluciferin, that upon cleavage by caspases 3/7, and combined with thermostable firefly luciferase, formed a "glow-type" luminescent signal that is proportional to caspase-3,7 activity [101].

Real-time systems in combination with end-point measurements assays alleviate the disadvantages posed by each approach alone, providing a more effective means to evaluate drug toxicity and mechanisms of toxicity at the cellular level.

2.3 Metabolism

Metabolism occurs via two steps reactions mainly in the liver: phase I (oxidation, hydrolysis and reduction) and phase II (conjugation) reactions. Phase I reactions comprise a series of chemical processes that result in metabolites that contain new functional groups that are generally more polar and reactive than the parent compound. Phase II reactions consist of different types of reactions in which the parent molecule or its phase I metabolites is conjugated with endogenous molecules, such as glucuronic acid, sulfate, glutathione, glycine, and so on. Phase II metabolites tend to be less toxic than their nonconjugated counterparts and are usually more water soluble, hence facilitating excretion in urine (by the kidneys) and bile (by the liver) [82].

Urine is the matrix of choice for evidence of drug administration in clinical and forensic cases because of the longer window of detection compared to blood or oral fluid, and its non-invasive sample collection method. However, detection of parent NPS in particularly the SCBs are present in extremely low amounts in urine as most of the parent SCBs are extensively metabolized [102-105], making metabolites detection critical for documenting the administration of SCBs. Moreover, some hydroxylated metabolites of SCBs were found to be more toxic than the parent drug [36], further emphasizing the importance of metabolism studies in identifying the structural elucidation of these active metabolites.

As controlled SCBs human administration studies are restricted due to ethical reasons, *in vivo* animal experiments or *in vitro* approaches have been employed to study the metabolism of drugs.

2.3.1 Metabolism models

Various *in vitro* tools have been used to assess human drug metabolism, such as cellular models, subcellular fractions and microbial models.

Primary human hepatocyte cultures are considered the "gold standard" for drug metabolism studies as they possess some intrinsic advantages that make them the closest model to *in vivo*. However, the phenotypic instability and restricted accessibility has greatly hindered the widespread use of primary cultures of human hepatocytes. In contrast to primary cultures, hepatic cell lines have quite stable phenotype, grow continuously with almost an unlimited lifespan, are easily cultured, making easy standardization among laboratories [82]. Human liver microsomes (HLM) is currently the most popular *in vitro* model in the metabolism study of NPS [106, 107]. Fungus *Cunninghamella elegans* (*C. elegans*) have been proven useful when large quantities of metabolites are required for structural characterization [108] and detection of active metabolites [109]. In this study, only HLM and *C. elegans* models will be reviewed.

HLM model are subcellular fractions derived from the endoplasmic reticulum (ER) of hepatic cells and are prepared by homogenization of liver followed by differential centrifugation [110]. They are well established tools for *in vitro* metabolism as it contains the whole spectrum of enzymes located in the ER including cytochrome P450 monooxygenases (CYPs), flavin-monooxygenases (FMOs), and uridine-5'-diphospho(UDP)-glucuronosyltransferases (UGTs) that are involved in the metabolism of drugs [111]. Discrepancies of SCBs major metabolites detected may occur between the HLM and *in vivo* findings especially if the enzymes involved in the biotransformation are not located in the HLM [112]. However, HLM continues to be popular choice for SCBs metabolism, attributed to the relatively low cost when compared to human hepatocytes, its simplicity in handling and the widely availability of HLM for experiments. Inter-individual variations in the activity of HLM are overcome by the application of large pooled human liver microsomes.

Cunninghamella species has the ability to biotransform drugs into both phase I and phase II products that are similar to those identified in humans and other mammals [113]. Hence, fungus in this genus, in particularly the *C. elegans*, has been extensively studied as models of mammalian drug metabolism [114]. Microbial *C. elegans* model is gaining attention as significantly larger quantity of metabolites in cleaner extracts can be

produced by the fungus than other models. This allows for easy detection, isolation, and identification of metabolites. Moreover, the relative ease of handling and its low cost are notable. Phase I metabolites of drugs are generally formed via the oxidative actions of cytochromes P450 (CYPs). Phase II biotransformation of sulfate, glucoside, glucuronide and acetylated metabolites have been isolated from *C. elegans* [115]. Metabolism of SCBs with the *C. elegans* model have been evaluated and found to be promising complementary [108, 116, 117] and independent [118] model to the *in vivo* human model.

The ability to predict *in vivo* metabolism from *in vitro* data or *in vitro-in vivo* extrapolation (IVIVE) is an important challenge in the context of *in vitro* metabolism studies. The easiest way to acquire data on the *in vivo* metabolism of NPS in human would be to analyze human samples such as blood or urine obtained after controlled administration of these drugs. However, this is generally not possible because of ethical reasons. Hence, whenever possible, *in vivo* metabolism data predicted from *in vitro* results should be compared to analytical results of authentic biological samples, obtained from routine drug testing or overdose cases.

2.3.2 Liquid chromatography – mass spectrometry

NPS are often not efficiently detected by traditional immunoassays or routine screening methods, thus requiring alternative methods for detecting its prevalence. Recent scientific literatures recommended the use of MS-based methods for screening and analysis of NPS [119-121]. MS methodologies, coupled to a wide range of separative techniques cum effective sample preparation techniques, provide high levels of sensitivity, selectivity, and versatility needed for reliable broad-spectrum NPS analysis. Mass spectrometry coupled to liquid chromatography is by far the most important tool in identification and elucidation of NPS metabolites structures without the need of derivatization as required for the gas chromatography [22]. It allows determination of the molecular mass of potential metabolites and structural elucidation of metabolites by interpreting fragmentation patterns based on full-scan mass spectra. MS-based methods for NPS analysis can be classified as targeted or untargeted. The first method focuses on predefined sets of analytes and are performed by means of medium- to low-resolution tandem mass spectrometry systems, exploiting multiple reaction monitoring acquisition modes. This approach usually offers high sensitivity and selectivity but do not detect

unknown compounds. On the contrary, the latter untargeted analysis covers all the analytes already included in the considered reference library that can be continuously updated and allows retrospective data mining. High-resolution mass spectrometry (HRMS) data often help in speculating chemical structures, thus are promising strategies for identification of unknown compound [122]. Recent advances in HRMS provides elemental composition of the compound and hence the ability to differentiate and characterize isobaric compounds [123].

2.4 References

1. UNODC (2018) Understanding the synthetic drug market: the NPS factor, *Global SMART Update.* **19**, 1-12.

2. Huestis, M. A., Brandt, S. D., Rana, S., Auwärter, V. & Baumann, M. H. (2017) Impact of Novel Psychoactive Substances on Clinical and Forensic Toxicology and Global Public Health, *Clinical Chemistry.* **63**, 1564-1569.

3. Zawilska, J. B. & Andrzejczak, D. (2015) Next generation of novel psychoactive substances on the horizon – A complex problem to face, *Drug and Alcohol Dependence.* **157**, 1-17.

4. Baumann, M., Solis, E., Watterson, L., Marusich, J., Fantegrossi, W. & Wiley, J. (2014) Bath Salts, Spice, and Related Designer Drugs: The Science Behind the Headlines, *Journal of Neuroscience.* **34**, 15150-15158.

5. Madras, B. K. (2017) The Growing Problem of New Psychoactive Substances (NPS), *Current Topics in Behavioral Neurosciences.* **32**, 1-18.

6. Palamar, J. J., Martins, S. S., Su, M. K. & Ompad, D. C. (2015) Self-reported use of novel psychoactive substances in a US nationally representative survey: Prevalence, correlates, and a call for new survey methods to prevent underreporting, *Drug and alcohol dependence.* **156**, 112-119.

7. Sutherland, R., Peacock, A., Whittaker, E., Roxburgh, A., Lenton, S., Matthews, A., Butler, K., Nelson, M., Burns, L. & Bruno, R. (2016) New psychoactive substance use among regular psychostimulant users in Australia, 2010–2015, *Drug and Alcohol Dependence.* **161**, 110-118.

8. Smith, K. E., Bunting, A. M., Staton, M., Walker, R., Shalash, S., Winston, E. & Pangburn, K. (2017) Examination of Synthetic Cannabinoid and Cathinone Use among a Drug-Using Offender Sample, 2013-2015, *Journal of Psychoactive Drugs.* **49**, 436-445.

9. Zanda, M. T. & Fattore, L. (2017) Chapter 29 - Novel Psychoactive Substances: A New Behavioral and Mental Health Threat in *Addictive Substances and Neurological Disease* (Watson, R. R. & Zibadi, S., eds) pp. 341-353, Academic Press.

10. Corazza, O., Valeriani, G., Bersani, F. S., Corkery, J., Martinotti, G., Bersani, G. & Schifano, F. (2014) "Spice," "Kryptonite," "Black Mamba": An Overview of Brand Names and Marketing Strategies of Novel Psychoactive Substances on the Web, *Journal of Psychoactive Drugs.* **46**, 287-294.

11. Zuba, D. & Byrska, B. (2013) Prevalence and co-existence of active components of 'legal highs': Analysis of 'legal highs' composition, *Drug Testing and Analysis.* **5**, 420-429.

12. UNODC (2020) World Drug Report: Cross-cutting Issues: Evolving Trends and New Challenges, *United Nations publication, Sales No E20XI6.* **Booklet 4**, 1-119.

13. Hondebrink, L., Zwartsen, A. & Westerink, R. H. S. (2018) Effect fingerprinting of new psychoactive substances (NPS): What can we learn from in vitro data?, *Pharmacology and Therapeutics.* **182**, 193-224.

14. Schifano, F., Orsolini, L., Papanti, D. & Corkery, J. (2017) NPS: Medical Consequences Associated with Their Intake, *Curr Top Behav Neurosci.* **32**, 351-380.

15. Monte, A. A., Bronstein, A. C., Cao, D. J., Heard, K. J., Hoppe, J. A., Hoyte, C. O., Iwanicki, J. L. & Lavonas, E. J. (2014) An outbreak of exposure to a novel synthetic cannabinoid, *N Engl J Med.* **370**, 389-390.

16. Trecki, J., Gerona, R. R. & Schwartz, M. D. (2015) Synthetic cannabinoid-related illnesses and death. **373**, 103.

17. Giorgetti, A., Busardò, F. P., Tittarelli, R., Auwärter, V. & Giorgetti, R. (2020) Post-Mortem Toxicology: A Systematic Review of Death Cases Involving Synthetic Cannabinoid Receptor Agonists, *Frontiers in Psychiatry.* **11**.

18. Weinstein, A. M., Rosca, P., Fattore, L. & London, E. D. (2017) Synthetic Cathinone and Cannabinoid Designer Drugs Pose a Major Risk for Public Health, *Frontiers in psychiatry.* **8**, 156-156.

19. Kronstrand R, G. D., Vikingsson S, Wohlfarth A, Gréen H (2018) Fatal Poisonings Associated with New Psychoactive Substances, *Handbook of Experimental Pharmacology.* **252**, 495-541.

20. Kesha, K., Boggs, C. L., Ripple, M. G., Allan, C. H., Levine, B., Jufer-Phipps, R., Doyon, S., Chi, P. & Fowler, D. R. (2013) Methylenedioxypyrovalerone ("Bath Salts"),Related Death: Case Report and Review of the Literature, *Journal of Forensic Sciences.* **58**, 1654-1659.

21. Oliver, C. F., Palamar, J. J., Salomone, A., Simmons, S. J., Philogene-Khalid, H. L., Stokes-McCloskey, N. & Rawls, S. M. (2018) Synthetic cathinone adulteration of illegal drugs, *Psychopharmacology*, 1-11.

22. Ellefsen, K. N., Concheiro, M. & Huestis, M. A. (2016) Synthetic cathinone pharmacokinetics, analytical methods, and toxicological findings from human performance and postmortem cases, *Drug Metabolism Reviews.* **48**, 237-265.

23. Prosser, J. M. & Nelson, L. S. (2012) The Toxicology of Bath Salts: A Review of Synthetic Cathinones, *Journal of Medical Toxicology.* **8**, 33-42.

24. Calinski, D. M., Kisor, D. F. & Sprague, J. E. (2019) A review of the influence of functional group modifications to the core scaffold of synthetic cathinones on drug pharmacokinetics, *Psychopharmacology (Berl).* **236**, 881-890.

25. Protti, M. (2019) Chapter 21 - Review of Bath Salts on Illicit Drug Market in *Critical Issues in Alcohol and Drugs of Abuse Testing (Second Edition)* (Dasgupta, A., ed) pp. 259-271, Academic Press.

26. Forrester, M. B. (2012) Synthetic Cathinone Exposures Reported to Texas Poison Centers, *The American Journal of Drug and Alcohol Abuse.* **38**, 609-615.

27. Karila, L. & Benyamina, A. (2018) The Effects and Risks Associated with Synthetic Cathinones Use in Humans in *Synthetic Cathinones: Novel Addictive and Stimulatory Psychoactive Substances* (Zawilska, J. B., ed) pp. 191-202, Springer International Publishing, Cham.

28. Assi, S., Gulyamova, N., Kneller, P. & Osselton, D. (2017) The effects and toxicity of cathinones from the users' perspectives: A qualitative study, *Human Psychopharmacology: Clinical and Experimental.* **32**, e2610.

29. Gołembiowska, K. & Kamińska, K. (2018) Effects of Synthetic Cathinones on Brain Neurotransmitters in *Synthetic Cathinones: Novel Addictive and Stimulatory Psychoactive Substances* (Zawilska, J. B., ed) pp. 117-124, Springer International Publishing, Cham.

30. Karila, L., Lafaye, G., Scocard, A., Cottencin, O. & Benyamina, A. (2018) MDPV and α-PVP use in humans: The twisted sisters, *Neuropharmacology.* **134**, 65-72.

31. Coppola, M. & Mondola, R. (2012) 3,4-methylenedioxypyrovalerone (MDPV): chemistry, pharmacology and toxicology of a new designer drug of abuse marketed online, *Toxicology letters.* **208**, 12.

32. Palamar, J., Salomone, A., Gerace, E., Di Corcia, D., Vincenti, M. & Cleland, C. (2017) Hair testing to assess both known and unknown use of drugs amongst ecstasy users in the electronic dance music scene, *The International Journal on Drug Policy.* **48**, 91.

33. Salomone, A., Palamar, J. J., Gerace, E., Di Corcia, D. & Vincenti, M. (2017) Hair Testing for Drugs of Abuse and New Psychoactive Substances in a High-Risk Population, *Journal of Analytical Toxicology.* **41**, 376-381.

34. Majchrzak, M., Celiński, R., Kuś, P., Kowalska, T. & Sajewicz, M. (2018) The newest cathinone derivatives as designer drugs: an analytical and toxicological review, *Forensic Toxicology.* **36**, 33-50.

35. Karila, L., Megarbane, B., Cottencin, O. & Lejoyeux, M. (2015) Synthetic Cathinones: A New Public Health Problem, *Current Neuropharmacology.* **13**, 12-20.

36. Tai, S. & Fantegrossi, W. E. (2017) Pharmacological and Toxicological Effects of Synthetic Cannabinoids and Their Metabolites in *Neuropharmacology of New Psychoactive Substances (NPS): The Science Behind the Headlines* (Baumann, M. H., Glennon, R. A. & Wiley, J. L., eds) pp. 249-262, Springer International Publishing, Cham.

37. UNODC (2020) Current NPS Threats, *United Nations publication.* **Volume II**, 1-6.

38. Shevyrin, V., Melkozerov, V., Endres, G. W., Shafran, Y. & Morzherin, Y. (2016) On a New Cannabinoid Classification System: A Sight on the Illegal Market of Novel Psychoactive Substances, *Cannabis and Cannabinoid Research.* **1**, 186-194.

39. Antonides, L. H., Cannaert, A., Norman, C., Vives, L., Harrison, A., Costello, A., Nic Daeid, N., Stove, C. P., Sutcliffe, O. B. & McKenzie, C. (2019) Enantiospecific Synthesis, Chiral Separation, and Biological Activity of Four Indazole-3-Carboxamide-Type Synthetic Cannabinoid Receptor Agonists and Their Detection in Seized Drug Samples, *Frontiers in chemistry.* **7**, 321-321.

40. Cooper, Z. (2016) Adverse Effects of Synthetic Cannabinoids: Management of Acute Toxicity and Withdrawal, *Current Psychiatry Reports.* **18**, 1-10.

41. Banister, S. D., Longworth, M., Kevin, R., Sachdev, S., Santiago, M., Stuart, J., Mack, J. B. C., Glass, M., McGregor, I. S., Connor, M. & Kassiou, M. (2016) Pharmacology of Valinate and tert-Leucinate Synthetic Cannabinoids 5F-AMBICA, 5F-AMB, 5F-ADB, AMB-FUBINACA, MDMB-FUBINACA, MDMB-CHMICA, and Their Analogues, *ACS chemical neuroscience.* **7**, 1241-1254.

42. Naqi, H. A., Pudney, C. R., Husbands, Stephen M. & Blagbrough, I. S. (2019) Analysis of synthetic cannabinoid agonists and their degradation products after combustion in a smoking simulator, *Analytical Methods.* **11**, 3101-3107.

43. Lefever, T. W., Marusich, J. A., Thomas, B. F., Barrus, D. G., Peiper, N. C., Kevin, R. C. & Wiley, J. L. (2017) Vaping Synthetic Cannabinoids: A Novel Preclinical Model of E-Cigarette Use in Mice, *Substance abuse : research and treatment.* **11**.

44. Potts, A. J., Cano, C., Thomas, S. H. L. & Hill, S. L. (2020) Synthetic cannabinoid receptor agonists: classification and nomenclature, *Clinical toxicology (Philadelphia, Pa).* **58**, 82-98.

45. Debruyne, D. & Le Boisselier, R. (2015) Emerging drugs of abuse: current perspectives on synthetic cannabinoids, *Subst Abuse Rehabil.* **6**, 113-129.

46. Arıkan Ölmez, N., Kapucu, H., Çallı Altun, N. & Eren, B. (2018) Identification of the synthetic cannabinoid N-(2-phenyl-propan-2-yl)-1-(4-cyanobutyl)-1H-indazole-3-carboxamide (CUMYL-4CN-BINACA) in a herbal mixture product, *Forensic Toxicology.* **36**, 192-199.

47. Liu, C., Jia, W., Hua, Z. & Qian, Z. (2017) Identification and analytical characterization of six synthetic cannabinoids NNL-3, 5F-NPB-22-7N, 5F-AKB-48-7N, 5F-EDMB-PINACA, EMB-FUBINACA, and EG-018, *Drug Test Anal.* **9**, 1251-1261.

48. Presley, B., Gurney, S., Scott, K., Kacinko, S. & Logan, B. (2016) Metabolism and Toxicological Analysis of Synthetic Cannabinoids in Biological Fluids and Tissues, *Forensic Science Review.* **28**, 103-169.

49. Brents, L. K., Gallus-Zawada, A., Radominska-Pandya, A., Vasiljevik, T., Prisinzano, T. E., Fantegrossi, W. E., Moran, J. H. & Prather, P. L. (2012) Monohydroxylated metabolites of the K2 synthetic cannabinoid JWH-073 retain intermediate to high cannabinoid 1 receptor (CB1R) affinity and exhibit neutral antagonist to partial agonist activity, *Biochemical pharmacology.* **83**, 952-961.

50. Rajasekaran, M., Brents, L. K., Franks, L. N., Moran, J. H. & Prather, P. L. (2013) Human metabolites of synthetic cannabinoids JWH-018 and JWH-073 bind with high affinity and act as potent agonists at cannabinoid type-2 receptors, *Toxicology and applied pharmacology.* **269**, 100-108.

51. Logan, B. K., Mohr, A. L. A., Friscia, M., Krotulski, A. J., Papsun, D. M., Kacinko, S. L., Ropero-Miller, J. D. & Huestis, M. A. (2017) Reports of Adverse Events Associated with Use of Novel Psychoactive Substances, 2013-2016: A Review, *Journal of analytical toxicology.* **41**, 573-610.

52. Gurney, S. M. R., Scott, K. S., Kacinko, S. L., Presley, B. C. & Logan, B. K. (2014) Pharmacology, Toxicology, and Adverse Effects of Synthetic Cannabinoid Drugs, *Forensic science review.* **26**, 53-78.

53. Kemp, A. M., Clark, M. S., Dobbs, T., Galli, R., Sherman, J. & Cox, R. (2016) Top 10 Facts You Need to Know About Synthetic Cannabinoids: Not So Nice Spice, *Am J Med.* **129**, 240-4.e1.

54. Boland, D. M., Reidy, L. J., Seither, J. M., Radtke, J. M. & Lew, E. O. (2020) Forty-Three Fatalities Involving the Synthetic Cannabinoid, 5-Fluoro-ADB: Forensic Pathology and Toxicology Implications, *Journal of Forensic Sciences.* **65**, 170-182.

55. Waugh, J., Najafi, J., Hawkins, L., Hill, S. L., Eddleston, M., Vale, J. A., Thompson, J. P. & Thomas, S. H. (2016) Epidemiology and clinical features of toxicity following recreational use of synthetic cannabinoid receptor agonists: a report from the United Kingdom National Poisons Information Service, *Clin Toxicol (Phila).* **54**, 512-8.

56. Krotulski, A. J., Mohr, A.L.A. & Logan, B.K. (2018) *Trend Report: Q4 2018 Synthetic Cannabinoids in the United States (Detailed)*, https://www.forensicscienceeducation.org/wp-content/uploads/2019/02/Synthetic-Cannabinoid-Trend-Report_Detailed_2018-Q4.pdf (Assessed Aug 1, 2020).

57. Krotulski, A. J., Mohr, A. L. A., Kacinko, S. L., Fogarty, M. F., Shuda, S. A., Diamond, F. X., Kinney, W. A., Menendez, M. J. & Logan, B. K. (2019) 4F-MDMB-BINACA: A New Synthetic Cannabinoid Widely Implicated in Forensic Casework, *Journal of forensic sciences.* **64**, 1451-1461.

58. Krotulski, A. J., Mohr, A.L.A. & Logan, B.K. (2019) *Trend Report: Q1 2019 Synthetic Cannabinoids in the United States (Detailed)*, https://www.forensicscienceeducation.org/wp-content/uploads/2019/04/Synthetic-Cannabinoid-Trend-Report_Detailed_2019-Q1.pdf (Assessed Aug 1, 2020).

59. Krotulski, A. J., Mohr, A.L.A. & Logan, B.K. (2019) *Trend Report: Q2 2019 Synthetic Cannabinoids in the United States (Detailed)*, https://www.npsdiscovery.org/wp-content/uploads/2019/07/Synthetic-Cannabinoid-Trend-Report_Detailed_2019-Q2.pdf (Assessed Aug 1, 2020).

60. Krotulski, A. J., Mohr, A.L.A. & Logan, B.K. (2019) *Trend Report: Q3 2019 Synthetic Cannabinoids in the United States (Detailed)*, https://www.npsdiscovery.org/wp-content/uploads/2019/11/Synthetic-Cannabinoid-Trend-Report_Detailed_2019-Q3.pdf (Accessed Aug 1, 2020).

61. Deavall, D. G., Martin, E. A., Horner, J. M. & Roberts, R. (2012) Drug-Induced Oxidative Stress and Toxicity, *Journal of Toxicology.* **2012**, 645460.

62. Zhang, Y. (2018) Cell toxicity mechanism and biomarker, *Clin Transl Med.* **7**, 34-34.

63. Guo, C., Sun, L., Chen, X. & Zhang, D. (2013) Oxidative stress, mitochondrial damage and neurodegenerative diseases, *Neural regeneration research.* **8**, 2003-2014.

64. Shukla, S. J., Huang, R., Austin, C. P. & Xia, M. (2010) The future of toxicity testing: a focus on in vitro methods using a quantitative high-throughput screening platform, *Drug discovery today.* **15**, 997-1007.

65. Choudhuri, S., Patton, G. W., Chanderbhan, R. F., Mattia, A. & Klaassen, C. D. (2018) From Classical Toxicology to Tox21: Some Critical Conceptual and Technological Advances in the Molecular Understanding of the Toxic Response Beginning From the Last Quarter of the 20th Century, *Toxicological Sciences.* **161**, 5-22.

66. Cook, D., Brown, D., Alexander, R., March, R., Morgan, P., Satterthwaite, G. & Pangalos, M. N. (2014) Lessons learned from the fate of AstraZeneca's drug pipeline: a five-dimensional framework, *Nature Reviews Drug Discovery.* **13**, 419-431.

67. Aarde, S. M. & Taffe, M. A. (2017) Predicting the Abuse Liability of Entactogen-Class, New and Emerging Psychoactive Substances via Preclinical Models of Drug Self-administration, *Curr Top Behav Neurosci.* **32**, 145-164.

68. Kapałczyńska, M., Kolenda, T., Przybyła, W., Zajączkowska, M., Teresiak, A., Filas, V., Ibbs, M., Bliźniak, R., Łuczewski, Ł. & Lamperska, K. (2018) 2D and 3D cell cultures - a comparison of different types of cancer cell cultures, *Arch Med Sci.* **14**, 910-919.

69. Biedler, J. L., Roffler-Tarlov, S., Schachner, M. & Freedman, L. S. (1978) Multiple neurotransmitter synthesis by human neuroblastoma cell lines and clones, *Cancer research.* **38**, 3751.

70. Xicoy, H., Wieringa, B. & Martens, G. J. M. (2017) The SH-SY5Y cell line in Parkinsons disease research: a systematic review, *Molecular Neurodegeneration* **12**, 10.

71. Moratalla, R., Khairnar, A., Simola, N., Granado, N., Garcia-Montes, J. R., Porceddu, P. F., Tizabi, Y., Costa, G. & Morelli, M. (2017) Amphetamine-related drugs neurotoxicity in humans and in experimental animals: Main mechanisms, *Progress in Neurobiology* **155**, 149-170.

72. Valente, M. J., Bastos, M. D. L., Fernandes, E., Carvalho, F., Guedes De Pinho, P. & Carvalho, M. (2017) Neurotoxicity of β-Keto Amphetamines: Deathly Mechanisms

Elicited by Methylone and MDPV in Human Dopaminergic SH-SY5Y Cells, *ACS Chemical Neuroscience.* **8**, 850-859.

73. Valente, M. J., Amaral, C., Correia-da-Silva, G., Duarte, J. A., Bastos, M. D. L., Carvalho, F., Guedes de Pinho, P. & Carvalho, M. (2017) Methylone and MDPV activate autophagy in human dopaminergic SH-SY5Y cells: a new insight into the context of β-keto amphetamines-related neurotoxicity, *Archives of Toxicology*, 1-14.

74. Huey Sze, L., Morgan, P., Martin, S., Paul Kenneth, W. & Shanlin, F. (2020) Synthetic Cathinones Induce Cell Death in Dopaminergic SH-SY5Y Cells via Stimulating Mitochondrial Dysfunction, *International journal of molecular sciences.* **21**, 1370.

75. Soares, J., Costa, V. M., Bronze, S., Gaspar, H., Santos, S., Bastos, M. L., Carvalho, F. & Capela, J. (2016) Neurotoxicity of synthetic cathinones on differentiated SH-SY5Y human dopaminergic cells, *Toxicology Letters.* **258**, S181.

76. Soares, J., Costa, V., Bronze, S., Gaspar, H., Santos, S., Bastos, M. D. L., Carvalho, F. & Capela, J. (2018) Clorgyline and N-acetyl-L-cysteine provide partial protection against the toxicity of synthetic cathinones and methamphetamine on SH-SY5Y humans cells, *Toxicology Letters.* **295**, S274.

77. Coccini, T., Vecchio, S., Crevani, M. & Simone, U. D. (2018) Cytotoxic Effects of 3,4-Catechol-PV (One Major MDPV Metabolite) on Human Dopaminergic SH-SY5Y Cells, *Neurotoxicity research*, 1-14.

78. Ferreira, P. S., Nogueira, T. B., Costa, V. M., Branco, P. S., Ferreira, L. M., Fernandes, E., Bastos, M. L., Meisel, A., Carvalho, F. & Capela, J. P. (2013) Neurotoxicity of "ecstasy" and its metabolites in human dopaminergic differentiated SH-SY5Y cells, *Toxicology letters.* **216**, 159.

79. Presgraves, S. P., Ahmed, T., Borwege, S. & Joyce, J. N. (2004) Terminally differentiated SH-SY5Y cells provide a model system for studying neuroprotective effects of dopamine agonists, *Neurotoxicity research.* **5**, 579.

80. Ares-Santos, S., Granado, N. & Moratalla, R. (2013) The role of dopamine receptors in the neurotoxicity of methamphetamine, *Journal of Internal Medicine.* **273**, 437-453.

81. Sassa, S., Sugita, O., Galbraith, R. A. & Kappas, A. (1987) Drug metabolism by the human hepatoma cell, Hep G2, *Biochemical and biophysical research communications.* **143**, 52-57.

82. Castell, J. V., Jover, R., Martnez-Jimnez, C. P. & Gmez-Lechn, M. J. (2006) Hepatocyte cell lines: their use, scope and limitations in drug metabolism studies, *Expert Opinion on Drug Metabolism & Toxicology.* **2**, 183-212.

83. Luethi, D., Liechti, M. E. & Krahenbuhl, S. (2017) Mechanisms of hepatocellular toxicity associated with new psychoactive synthetic cathinones, *Toxicology.* **387**, 57-66.

84. Richter, L. H. J., Flockerzi, V., Maurer, H. H. & Meyer, M. R. (2017) Pooled human liver preparations, HepaRG, or HepG2 cell lines for metabolism studies of new psychoactive substances? A study using MDMA, MDBD, butylone, MDPPP, MDPV, MDPB, 5-MAPB, and 5-API as examples, *Journal of Pharmaceutical and Biomedical Analysis.* **143**, 32-42.

85. Gaspar, H., Bronze, S., Oliveira, C., Victor, B. L., Machuqueiro, M., Pacheco, R., Caldeira, M. J. & Santos, S. (2018) Proactive response to tackle the threat of emerging drugs: Synthesis and toxicity evaluation of new cathinones, *Forensic Science International.* **290**, 146-156.

86. Richter, L. H. J., Beck, A., Flockerzi, V., Maurer, H. H. & Meyer, M. R. (2019) Cytotoxicity of new psychoactive substances and other drugs of abuse studied in human HepG2 cells using an adopted high content screening assay, *Toxicology Letters.* **301**, 79-89.

87. O'Brien, P. J. & Edvardsson, A. (2017) Validation of a Multiparametric, High-Content-Screening Assay for Predictive/Investigative Cytotoxicity: Evidence from Technology Transfer Studies and Literature Review, *Chemical research in toxicology.* **30**, 804-829.

88. Aslantürk, Ö. (2018) In Vitro Cytotoxicity and Cell Viability Assays: Principles, Advantages, and Disadvantages in *Genotoxicity - A Predictable Risk to Our Actual World*.

89. Strober, W. (2001) Trypan blue exclusion test of cell viability, *Curr Protoc Immunol.* **111**, A3.B.1-A3.B.3.

90. Louis, K. S., Siegel, A. C. (2011) Cell viability analysis using trypan blue: manual and automated methods. Mammalian cell viability: methods and protocols, *Methods Mol Biol.* **740**, 7–12.

91. Scudiero, D. A., Shoemaker, R. H., Paull, K. D., Monks, A., Tierney, S., Nofziger, T. H., Currens, M. J., Seniff, D. & Boyd, M. R. (1988) Evaluation of a soluble

tetrazolium/formazan assay for cell growth and drug sensitivity in culture using human and other tumor cell lines, *Cancer research.* **48**, 4827-4833.

92. Decker, T. & Lohmann-Matthes, M.-L. (1988) A quick and simple method for the quantitation of lactate dehydrogenase release in measurements of cellular cytotoxicity and tumor necrosis factor (TNF) activity, *Journal of Immunological Methods.* **115**, 61-69.

93. Terry L.R., R. A. M., Andrew L.N, Sarah D, Hélène A.B, Tracy J.W, and Lisa M (2016) Cell Viability Assays, *Assay Guidance Manual*, 1-31.

94. Perry, S. W., Norman, J. P., Barbieri, J., Brown, E. B. & Gelbard, H. A. (2011) Mitochondrial membrane potential probes and the proton gradient: a practical usage guide, *Biotechniques.* **50**, 98-115.

95. Wardman, P. (2007) Fluorescent and luminescent probes for measurement of oxidative and nitrosative species in cells and tissues: progress, pitfalls, and prospects, *Free Radic Biol Med.* **43**, 995-1022.

96. Kalyanaraman, B., Darley-Usmar, V., Davies, K. J. A., Dennery, P. A., Forman, H. J., Grisham, M. B., Mann, G. E., Moore, K., Roberts, L. J., 2nd & Ischiropoulos, H. (2012) Measuring reactive oxygen and nitrogen species with fluorescent probes: challenges and limitations, *Free radical biology & medicine.* **52**, 1-6.

97. Lock, J. T., Parker, I. & Smith, I. F. (2015) A comparison of fluorescent Ca2+ indicators for imaging local Ca2+ signals in cultured cells, *Cell Calcium.* **58**, 638-648.

98. Tada, M., Takeuchi, A., Hashizume, M., Kitamura, K. & Kano, M. (2014) A highly sensitive fluorescent indicator dye for calcium imaging of neural activity in vitro and in vivo, *Eur J Neurosci.* **39**, 1720-1728.

99. Horan, M. P., Pichaud, N. & Ballard, J. W. O. (2012) Review: Quantifying Mitochondrial Dysfunction in Complex Diseases of Aging, *The Journals of Gerontology: Series A.* **67**, 1022-1035.

100. Budihardjo, I., Oliver, H., Lutter, M., Luo, X. & Wang, X. (1999) Biochemical pathways of caspase activation during apoptosis, *Annu Rev Cell Dev Biol.* **15**, 269-90.

101. O'Brien, M. A., Daily, W. J., Hesselberth, P. E., Moravec, R. A., Scurria, M. A., Klaubert, D. H., Bulleit, R. F. & Wood, K. V. (2005) Homogeneous, bioluminescent protease assays: caspase-3 as a model, *J Biomol Screen.* **10**, 137-48.

102. Carlier, J., Diao, X., Scheidweiler, K. B. & Huestis, M. A. (2017) Distinguishing Intake of New Synthetic Cannabinoids ADB-PINACA and 5F-ADB-PINACA with

Human Hepatocyte Metabolites and High-Resolution Mass Spectrometry.(Drug Monitoring and Toxicology), *Clinical Chemistry.* **63**, 1008.

103. Yeter, O. & Öztürk, Y. E. (2019) Metabolic profiling of synthetic cannabinoid 5F-ADB by human liver microsome incubations and urine samples using high-resolution mass spectrometry, *Drug Testing and Analysis.* **11**, 847-858.

104. Watanabe, S., Vikingsson, S., Åstrand, A., Gréen, H. & Kronstrand, R. (2019) Biotransformation of the New Synthetic Cannabinoid with an Alkene, MDMB-4en-PINACA, by Human Hepatocytes, Human Liver Microsomes, and Human Urine and Blood, *The AAPS journal.* **22**, 13.

105. Wagmann, L., Frankenfeld, F., Park, Y. M., Herrmann, J., Fischmann, S., Westphal, F., Müller, R., Flockerzi, V. & Meyer, M. R. (2020) How to Study the Metabolism of New Psychoactive Substances for the Purpose of Toxicological Screenings—A Follow-Up Study Comparing Pooled Human Liver S9, HepaRG Cells, and Zebrafish Larvae, *Frontiers in Chemistry.* **8**, 539.

106. Diao, X. & Huestis, M. A. (2019) New Synthetic Cannabinoids Metabolism and Strategies to Best Identify Optimal Marker Metabolites, *Frontiers in Chemistry.* **7**, 109.

107. Richter, L. H. J., Maurer, H. H. & Meyer, M. R. (2017) New psychoactive substances: Studies on the metabolism of XLR-11, AB-PINACA, FUB-PB-22, 4-methoxy-α-PVP, 25-I-NBOMe, and meclonazepam using human liver preparations in comparison to primary human hepatocytes, and human urine, *Toxicology Letters.* **280**, 142-150.

108. Watanabe, S., Kuzhiumparambil, U., Nguyen, M., Cameron, J. & Fu, S. (2017) Metabolic Profile of Synthetic Cannabinoids 5F-PB-22, PB-22, XLR-11 and UR-144 by Cunninghamella elegans, *The AAPS Journal.* **19**, 1148-1162.

109. Rydevik, A., Hansson, A., Hellqvist, A., Bondesson, U. & Hedeland, M. (2015) A novel trapping system for the detection of reactive drug metabolites using the fungus Cunninghamella elegans and high resolution mass spectrometry, *Drug Testing and Analysis.* **7**, 626-633.

110. Asha, S. & Vidyavathi, M. (2010) Role of Human Liver Microsomes in In Vitro Metabolism of Drugs—A Review, *Applied Biochemistry and Biotechnology.* **160**, 1699-1722.

111. Peters, F. T. & Meyer, M. R. (2011) In vitro approaches to studying the metabolism of new psychoactive compounds in (Kicman, A. T. & King, L. A., eds) pp. 483-495, John Wiley & Sons, Ltd., Chichester, UK.

112. Diao, X. & Huestis, M. A. (2017) Approaches, Challenges, and Advances in Metabolism of New Synthetic Cannabinoids and Identification of Optimal Urinary Marker Metabolites, *Clin Pharmacol Ther.* **101**, 239-253.

113. Murphy, C. (2015) Drug metabolism in microorganisms, *Biotechnology Letters.* **37**, 19-28.

114. Asha, S. & Vidyavathi, M. (2009) Cunninghamella – A microbial model for drug metabolism studies – A review, *Biotechnology Advances.* **27**, 16-29.

115. Zhang, D., Yang, Y., Leakey, J. E. & Cerniglia, C. E. (1996) Phase I and phase II enzymes produced by Cunninghamella elegans for the metabolism of xenobiotics, *FEMS microbiology letters.* **138**, 221-226.

116. Watanabe, S., Kuzhiumparambil, U., Winiarski, Z. & Fu, S. (2016) Biotransformation of synthetic cannabinoids JWH-018, JWH-073 and AM2201 by Cunninghamella elegans, *Forensic Science International.* **261**, 33-42.

117. Watanabe, S., Kuzhiumparambil, U. & Fu, S. (2018) In vitro metabolism of synthetic cannabinoid AM1220 by human liver microsomes and Cunninghamella elegans using liquid chromatography coupled with high resolution mass spectrometry, *Forensic toxicology.* **36**, 435-446.

118. Gaunitz, F., Dahm, P., Mogler, L., Thomas, A., Thevis, M. & Mercer-Chalmers-Bender, K. (2019) In vitro metabolic profiling of synthetic cannabinoids by pooled human liver microsomes, cytochrome P450 isoenzymes, and Cunninghamella elegans and their detection in urine samples, *Analytical and Bioanalytical Chemistry.* **411**, 3561-3579.

119. Mercolini, L. & Protti, M. (2016) Biosampling strategies for emerging drugs of abuse: towards the future of toxicological and forensic analysis, *J Pharm Biomed Anal.* **130**, 202-219.

120. Meyer, M. R. & Maurer, H. H. (2016) Review: LC coupled to low- and high-resolution mass spectrometry for new psychoactive substance screening in biological matrices - Where do we stand today?, *Anal Chim Acta.* **927**, 13-20.

121. Sundström, M., Pelander, A. & Ojanperä, I. (2015) Comparison between drug screening by immunoassay and ultra-high performance liquid chromatography/high-

resolution time-of-flight mass spectrometry in post-mortem urine, *Drug Test Anal.* **7**, 420-7.

122. Mercolini, L. (2019) Chapter 20 - New Psychoactive Substances: An Overview in *Critical Issues in Alcohol and Drugs of Abuse Testing (Second Edition)* (Dasgupta, A., ed) pp. 247-258, Academic Press.

123. Maurer, H. H. & Meyer, M. R. (2016) High-resolution mass spectrometry in toxicology: current status and future perspectives, *Arch Toxicol.* **90**, 2161-2172.

Chapter 3

Synthetic cathinones induce cell death in dopaminergic SH-SY5Y cells via stimulating mitochondrial dysfunction

3.1 Foreword

The following manuscript was published in *International Journal of Molecular Sciences* and details the cytotoxicity potential and toxicity mechanistic pathways of butylone, pentylone and MDPV in dopaminergic SH-SY5Y cells. The publication was authored by Ms Huey Sze Leong (H.S.L.)[1,2], Dr Morgan Philp (M.P.)[1], Mr Martin Simone (M.S.)[2], Professor Paul Kenneth Witting (P.K.W.)[2,*] and Professor Shanlin Fu (S.F.)[2,*].

[1] Centre for Forensic Science, School of Mathematical and Physical Sciences, University of Technology Sydney, Ultimo NSW 2007, Australia.
[2] Discipline of Pathology, Charles Perkins Centre, School of Medical Sciences, Faculty of Medicine and Health, The University of Sydney, Camperdown NSW 2006, Australia.
*Correspondence author

Author Contributions: Conceptualization: H.S.L., P.K.W., and S.F.; Methodology: H.S.L., M.S., and M.P.; Software: H.S.L., M.S., and P.K.W.; Validation: H.S.L., M.S., and M.P; Formal analysis: H.S.L., M.S., and P.K.W.; Investigation: H.S.L.; Resources: H.S.L., M.S., M.P., P.K.W., and S.F.; Data curation: H.S.L., P.K.W., and S.F.; Writing - original draft preparation: H.S.L.; Writing - review and editing: H.S.L., M.P., M.S., P.K.W., and S.F.; Visualization: H.S.L. and P.K.W.; Supervision: P.K.W. and S.F.; Project administration: H.S.L.; Funding acquisition: H.S.L., P.K.W., and S.F.

All authors have read and agreed to the published version of the manuscript.

3.2 Abstract

Increasing reports of neurological and psychiatric complications due to psychostimulant synthetic cathinones (SCs) have recently raised public concern. However, the precise mechanism of SCs toxicity is unclear. This paucity of understanding highlights the need to investigate the *in vitro* toxicity and mechanistic pathways of three SCs: butylone, pentylone, and 3,4-Methylenedioxypyrovalerone (MDPV). Human neuronal cells of SH-SY5Y were cultured in supplemented DMEM/F12 media and differentiated to a neuronal phenotype using retinoic acid (10 μM) and 12-*O*-tetradecanoylphorbol-13-acetate (81 nM). Trypan blue and lactate dehydrogenase assays were utilized to assess the neurotoxicity potential and potency of these three SCs. To investigate the underlying neurotoxicity mechanisms, measurements included markers of oxidative stress, mitochondrial bioenergetics, and intracellular calcium (Ca^{2+}), and cell death pathways were evaluated at two doses (EC_{15} and EC_{40}), for each drug tested. Following 24 h of treatment, all three SCs exhibited a dose-dependent neurotoxicity, characterized by a significant ($p < 0.0001$ vs. control) production of reactive oxygen species, decreased mitochondrial bioenergetics, and increased intracellular Ca^{2+} concentrations. The activation of caspases 3 and 7 implicated the orchestration of mitochondrial-mediated neurotoxicity mechanisms for these SCs. Identifying novel therapeutic agents to enhance an altered mitochondrial function may help in the treatment of acute-neurological complications arising from the illicit use of these SCs.

Keywords: Mitochondrial dysfunction; calcium dysregulation; apoptosis; synthetic cathinones; SH-SY5Y

3.3 Introduction

Synthetic cathinones (SCs) have emerged as popular supplements to "traditional" drugs of abuse, such as cocaine, 3, 4-methylenedioxymethamphetamine (MDMA, Ecstasy or "Molly"), and methamphetamine (meth), due to their psychostimulant and entactogenic effects [1]. These illicit psychostimulants, often labelled as "not for human consumption", are also marketed as "legal highs", "bath salts", "plant food", and "research chemicals" to evade scrutiny and detection by law enforcement agencies. Their relatively low cost, ease of internet purchases, and the lack of control over clandestine drug manufacturers have greatly contributed to the explosion of these drugs in the recreational drug scene [2].

3,4-Methylenedioxypyrovalerone (MDPV) (chemical structure shown in Figure 3.1) is one of the most prevalent SCs found on the illegal drug market [3], with butylone and pentylone (Figure 3.1) being identified as substitute drugs among the "legal highs" [4-9]. Powders, pills, and tablets sold as "Molly" to electronic dance music attendees have also been found to be adulterated with butylone and pentylone [10-12].

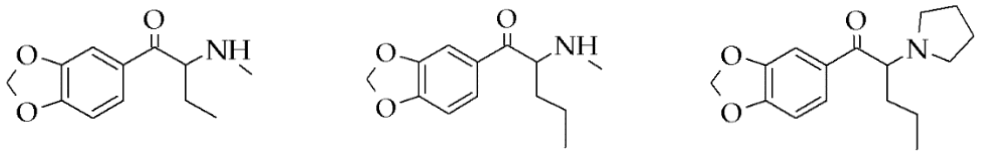

A B C

	pKa	Calculated XLogP3-AA	MW (Da)	PSA ($Å^2$)	HBD
A	8.12	1.9	221.256	47.6	1
B	8.14	2.3	235.283	47.6	1
C	7.31	3.3	275.348	38.8	0

Figure 3.1 Chemical structures of three synthetic cathinones (SCs): (A) butylone, (B) pentylone, and (C) 3,4-Methylenedioxypyrovalerone (MDPV). Table: Estimated pKa values (measure of ionization) calculated using MarvinSketch software (https://chemicalize.com/), XLogP3-AA (measure of lipophilicity), molecular weight (MW), polar surface area (PSA), and hydrogen bond donors (HBD) of (A) butylone, (B) pentylone, and (C) MDPV. Data were obtained from the PubChem Compound. Database

(https://www.ncbi.nlm.nih.gov/pccompound/56843046; 60208608; 20111961). Optimal penetration of BBB: XLogP3-AA ranged from 1 to 4, MW < 450 Da, PSA < 90 Å2, and HBD < 3

SCs act as central nervous stimulants via escalating neurotransmitters' concentration. Butylone and pentylone display hybrid transporter activity, characterized by inhibition effects at the dopamine transporter, DAT (more potent for pentylone), but substrate effects at the serotonin transporter, SERT (more potent for butylone) [13]. MDPV, on the other hand, is known for its potent inhibition effects at DAT and NET, but not as a substrate releaser [14]. SCs are readily self-administered, with pentylone and MDPV exhibiting a higher reinforcing efficacy, suggesting considerable potential for compulsive use [15, 16].

The abuse of SCs poses serious public health concerns due to their high addiction potential and increasing number of fatalities [17, 18]. Severe intoxications and death cases have been linked to the usage of butylone, pentylone, and MDPV [19-25], and the majority of cases have been connected to neuropsychiatric and neurological complications associated with SCs toxicity [26, 27]. In addition to the direct SCs neurotoxicity effects, potential interactions, such as hyperthermia, toxic metabolites, excitotoxicity, and neuroinflammation, may also contribute to SC-induced neurotoxicity [28]. In this study, the primary focus will be on the direct neurotoxicity effects that are potentiated by dopaminergic neuron signalling. Preclinical studies have suggested the potential neuronal damage induced by SCs [29]. Studies have also documented neurotoxic effects of synthetic cathinones in utero and early life exposure [30, 31]. More recently, the repeated binge-like administration of MDPV in rats showed evidence of neurodegeneration [32]. Previous *in vitro* studies have revealed the neurotoxic potential of several SCs [33-38], but the neurotoxicity potential of butylone and pentylone has remained unexplored. In recent years, oxidative stress and mitochondrial dysfunction mechanisms have been identified as significant contributors to SC-induced neurotoxicity [36, 37, 39, 40]. However, the role of neuronal calcium signalling in mitochondrial dysfunction and the induction of neurotoxic cascades for SCs is scarce. The paucity of scientific research and understanding of neurotoxic mechanisms determined the aims of the study.

The present study aimed to evaluate the neurotoxicity potential and potency of butylone and pentylone in relation to MDPV using the well-established SH-SY5Y cell line that can be differentiated into a dopaminergic neuronal phenotype [41]. It also aimed to define the role of these SCs in promoting oxidative stress and mitochondrial dysfunction and altering calcium (Ca^{2+}) levels as a plausible mechanistic pathway of neurotoxicity in cultured neurons.

3.4 Materials and Methods

3.4.1 Chemical Synthesis

Hydrochloride salts of butylone, pentylone, and MDPV were synthesized in-house with a purity greater than 98 %. The synthesis of salts involved a multiple-step reaction sequence: Grignard reaction of piperonal, oxidation, α-bromination, and nucleophilic substitution with methylamine (for butylone and pentylone HCl) and pyrrolidine (for MDPV HCl). The final product salt was obtained following extraction and HCl work-up. The salts were fully characterised by proton (^{1}H-NMR) and carbon (^{13}C-NMR) nuclear magnetic resonance spectroscopy, gas chromatography-mass spectrometry (GC/MS), Fourier-transform infrared (FTIR) spectroscopy, and ultraviolet (UV) spectroscopy. Detailed synthetic routes and NMR spectra were provided in Appendix A and Appendix B, respectively. Butylone HCl: ^{1}H-NMR (500 MHz, D_2O) δ, ppm: 7.705–7.686 (dd, ^3JHH = 8.25 Hz, 4JHH = 1.25 Hz, 1H), 7.481–7.478 (d, ^4JHH = 1.5 Hz, 1H), 7.045–7.028 (d, ^3JHH = 8.5 Hz, 1H), 6.134–6.130 (d, ^2JHH = 2.0 Hz, 2H), 5.025–5.003 (t, ^3JHH = 5.5 Hz, 1H), 2.741 (s, 3H), 2.131–2.040 (m, 2H), 0.889–0.859 (t, ^3JHH = 7.5 Hz, 3H); ^{13}C–NMR (125 MHz, CD_3OD) δ, ppm: 194.114, 153.006, 148.401, 128.603, 125.986, 108.719, 107.987, 102.687, 62.641, 31.494, 23.187, 8.385; EI (*m/z,* %): 221(M^+,0), 219(2), 149(11), 121(7), 72(100), 70(30); FTIR (ATR) ν_{max}, cm^{-1}: 2909 (C-H stretch), 2689 and 2475 (asym. and sym. NH_2^+ stretches), 1674 (C=O stretch), 1602 and 1452 (C=C stretch), 1252 (C-C=O stretch), 1035 (C-O stretch), 880 and 802 (1,2,4-trisubstituted benzene); UV (H_2O) λ_{max}, nm: 236, 282, 321. Pentylone HCl: ^{1}H-NMR (500 MHz, D_2O) δ, ppm: 7.696–7.679 (d, ^3JHH = 7.5 Hz, 1H), 7.467 (s, 1H), 7.040–7.023 (d, ^3JHH = 8.5 Hz, 1H), 6.129 (s, 2H), 5.024–5.002 (t, ^3JHH = 5.5 Hz, 1H), 2.734 (s, 3H),

2.031–1.916 (m, 2H), 1.365–1.218 (m, 2H), 0.874–0.845 (t, ^{3}JHH = 7.25 Hz, 3H); ^{13}C-NMR (125 MHz, CD_3OD) δ, ppm: 194.334, 153.024, 148.416, 128.728, 126.008, 108.726, 107.979, 102.706, 61.799, 32.142, 31.566, 17.295, 13.855; EI (*m/z,* %): 235(M^+,0), 192(24), 164(8), 149(100), 121(20), 91(4), 65(9); FTIR (ATR) ν_{max}, cm^{-1}: 2963 (C-H stretch), 2744 and 2481 (asym. and sym. NH_2^+ stretches), 1675 (C=O stretch), 1603 and 1453 (C=C stretch), 1256 (C-C=O stretch), 1033 (C-O stretch), 863 and 806 (1,2,4-trisubstituted benzene); UV (H_2O) λ_{max}, nm: 236, 282, 321. MDPV HCl: ^{1}H-NMR (500 MHz, D_2O) δ, ppm: 7.725–7.709 (d, ^{3}JHH= 8.0 Hz, 1H), 7.496 (s, 1H), 7.061–7.044 (d, ^{3}JHH = 8.5 Hz, 1H), 6.148–6.142 (d, ^{4}JHH = 3.0 Hz, 2H), 5.122 (br. s, 1H), 3.455–3.284 (m, 4H), 2.128–1.999 (m, 6H), 1.248–1.147 (m, 2H), 0.850–0.821 (t, ^{3}JHH = 7.25 Hz, 3H); ^{13}C-NMR (125 MHz, CD_3OD) δ, ppm: 194.334, 153.024, 148.416, 128.728, 126.008, 108.726, 107.979, 102.706, 61.799, 32.142, 31.566, 24.389, 17.295, 13.855; EI (*m/z,*%): 275(M^+,0), 149(5), 126(100), 96(4), 55(5); FTIR (ATR) ν_{max}, cm^{-1}: 2969 (C-H stretch), 2610 (NH^+ stretch), 1684 (C=O stretch), 1609 and 1435 (C=C stretch), 1253 (C-C=O stretch), 1033 (C-O), 867 and 807 (1,2,4-trisubstituted benzene); UV (H_2O) λ_{max}, nm: 237, 285, 324.

3.4.2 Cellular Studies

The Countess™ cell counting chamber slide and Trypan Blue (TB) Stain 0.4 % w/v were purchased from Invitrogen (Eugene, OR, USA). The lactate dehydrogenase (LDH) cytotoxicity assay kit was purchased from Cayman Chemical (Ann Arbor, MI, USA). The DCFDA/H2DCFDA (2′, 7′-dichlorofluorescin diacetate) - Cellular reactive oxygen species (ROS) detection assay kit and Cal-520 AM were purchased from Abcam (Cambridge, UK). Seahorse Extracellular Flux (XF) 96 cell culture microplates, the XF 96 assay kit, the Cell Mito Stress Test Kit, XF calibrant, XF Base Medium, and the XF96 Analyzer were obtained from Seahorse Bioscience (North Billerica, MA, USA). The ATPlite luminescence assay system was purchased from Perkin Elmer (Waltham, MA, USA). The Caspase-Glo® 3/7 assay was purchased from Promega (Madison, WI, USA). T75 tissue culture flasks, and 96-well and 6-well cell culture plates were purchased from Corning (Corning, NY, USA). Milli-Q water (18.2 $M\Omega cm^{-1}$) was obtained from Sartorius (Göttingen, Germany). The phosphate buffered saline (PBS) tablet, copper (II) sulfate

solution (CuSO4, 4 % *w*/*v*), bicinchoninic acid (BCA), phorbolester 12-*O*-tetradecanoylphorbol-13-acetate (TPA), retinoic acid (RA), and all cell culture materials were purchased from Sigma-Aldrich (St. Louis, MO, USA). The Countess™ II automated cell counter was purchased from Thermo Fisher Scientific (Waltham, MA, USA). The Axio Vert.A1 inverted microscope was purchased from Zeiss (Jena, Germany). Centrifuge 5415 R and 5810 R were purchased from Eppendorf (Hamburg, Germany). The Orbit P4 digital microtube and microplate orbital shaker was obtained from Labnet (Edison, NJ, USA). The IncuCyte® system was purchased from Essen BioScience (Ann Arbor, MI, USA). The Infinite® M200 Pro plate reader was purchased from Tecan (Männedorf, Switzerland).

3.4.3 Cell Culture

The human neuroblastoma SH-SY5Y cell line (ATCC, Manassas, VA, USA) was grown in a T75 tissue culture flask containing Dulbecco's Modified Eagle's Medium (DMEM)/F-12 Ham mixtures supplemented with 10 % heat-inactivated fetal bovine serum (HI-FBS), L-glutamine (2 mM), a mixture of penicillin/streptomycin (100 U/mL/100 µg/mL), and non-essential amino acid solution (NEAA, 1x). Cells were cultured at 37 °C in a humidified atmosphere incubator containing 95 % air and 5 % CO_2, until 75 % – 80 % confluence. Media was changed every 2 to 3 days. Where required, cells were harvested by subculture with media containing trypsin/EDTA (0.12 % trypsin/ 0.02 % EDTA *w*/*v*). The cells were passaged over 8 passages (Passage 6 – 13) and counted under TB staining using an automated cell counter. Cells were seeded in full media (10 % HI-FBS) onto multi-well plates overnight at the required density. Cells were differentiated to a dopaminergic neuronal phenotype by a previously reported method, with slight modification [42], using 10 µM RA media (2.5 % HI-FBS) for 3 days, followed by a mixture of 10 µM RA and 81 nM TPA (2.5 % HI-FBS) for another 3 days. General cell morphology was monitored at regular intervals using phase contrast inverted microscopy.

3.4.4 Cytotoxicity Assays

Cells were sub-cultured and seeded at a density of 25,000 cells/cm^2. Cells were then treated with butylone, pentylone, and MDPV individually for 24 h at 37 °C. This exposure time was identical to those used for other *in vitro* studies involving similar SCs doses [36, 40, 43-45]. Dose-response curves for these SCs (1 to 10 mM) were determined using TB and LDH assays. The effective concentrations of EC_{15}, EC_{40}, and EC_{50}, that is, the concentration that induces 15 %, 40 %, and 50 % cell death, respectively, for each drug were determined from the dose-response curves. The calculated mean EC_{15} and EC_{40} of butylone, pentylone, and MDPV (refer to tabulated data in Figure 3.2) were then used for subsequent experiments.

3.4.5 TB Assay

Upon treatment, drug media containing non-adherent cells was transferred from the 6-well plate into a 1.5 mL tube and centrifuged (200 relative centrifugal force, *r.c.f.*; 6 min). Adherent cells were harvested as described above and resuspended into the pellet cells obtained from the media fraction. The total number of cells were then counted using an automated cell counter. Data were obtained from three independent experiments. Background subtraction (untreated control) was performed for all wells. Finally, the % cytotoxicity was calculated as the percentage of the ratio of non-viable cells to the total number of cells.

3.4.6 LDH Assay

Upon treatment, a 96-well plate was centrifuged (400 *r.c.f.*, 5 min). Next, 100 µL of the isolated supernatant was transferred to another 96-well plate and each well was treated with 100 µL of reaction mixture containing nicotinamide adenine dinucleotide (NAD^+), lactic acid, iodonitrotetrazolium salt (INT), and reconstituted diaphorase, prepared according to the manufacturer's instruction. Treated samples were incubated at 37 °C with shaking on an orbital shaker. After 30 min, absorbance was measured at 490 nm with a Tecan plate reader. Data were obtained from four independent experiments with background subtraction (media only) prior to determination of the % cytotoxicity, as follows (Equation 1 below):

$$\% \text{ Cytotoxicity of sample} = (A_{sample} - A_{assay\ buffer}) / (A_{Triton\ X\text{-}100} - A_{assay\ buffer}) \times 100 \quad (1)$$

3.4.7 Measurement of Intracellular ROS

Levels of intracellular ROS were determined using a commercial kit, as per the manufacturer's instruction. Briefly, cells were seeded at a density of 50,000 cells/cm^2 onto a 96-well black, clear-bottom plate. Cells were rinsed with 1x buffer (provided in the kit) and incubated with 100 µL DCFDA (25 µM) at 37 °C for 45 min in the dark. Cells were rinsed with 1x buffer before being treated with each drug individually. Fluorescence was measured at Ex/Em: 485/535 nm with a Tecan plate reader at different time points (2, 4, 6, and 24 h). Background subtraction (media only) was performed for all wells. Data were obtained from four independent experiments and the data was expressed as a % fold-change relative to the control.

3.4.8 Measurement of Mitochondrial Respiration

Cells were seeded at a density of 20,000 cells/80 µL well onto XF 96-well cell culture microplates. Upon the individual treatment of each drug, media was replaced with XF base media with added glucose (10 mM), sodium pyruvate (1 mM), and L-glutamine (2 mM), and kept in a non-CO_2 incubator at 37 °C for 1 h. Analysis of oxygen consumption rate (OCR) was performed in a Seahorse XF96 analyser, according to the manufacturer's instructions. Mitochondrial respiration kinetics using the Seahorse analyser was employed to provide valuable information regarding the extent of mitochondrial dysfunction in response to butylone, pentylone, and MDPV. The measurement of OCR using the Seahorse analyser has been proven to be the most widely used technique in determining mitochondrial bioenergetics dysfunction in cells [78]. OCR was measured in a basal condition and following the injection of each compound: ATP synthase inhibitor oligomycin (1 µM), the mitochondrial uncoupler carbonyl cyanide 4-(trifluoromethoxy)phenylhydrazone, FCCP (0.5 µM), and a mixture of complex I + II inhibitors rotenone with antimycin A (1 µM + 1 µM). The mixture was incubated for 3 min, followed by a 3 min lag-time for each cycle. Three measurements were taken for

each condition. Data were obtained from at least four independent experiments and normalized to % confluence using the IncuCyte® system and standard software.

3.4.9 Measurement of Intracellular ATP

Levels of intracellular adenosine triphosphate (ATP) were determined using a commercial kit, as per the manufacturer's instructions. Briefly, cells were seeded at a density of 25,000 cells/cm^2 onto a 96-well plate. Following individual drug treatment, media was replaced with a mixture of 100 µL of PBS (0.01 M, pH 7.5) and 50 µL of mammalian cell lysis solution (provided in the kit). The mixture was mixed in an orbital shaker (700 revolutions per min, *r.p.m.*; 5 min). In the dark, 50 µL of substrate, luciferase-lucerin (provided in the kit), was added and shaken for another 5 min at 700 *r.p.m.* The plate was left in the dark (10 min; 22 °C) and luminescence was measured with a Tecan plate reader. Intracellular ATP levels were determined with a calibration curve that was obtained in parallel on the same plate using a 10 mM stock solution of reconstituted lyophilized ATP standard prepared in Milli-Q water. Data were obtained from three independent experiments and normalized to the total protein using the BCA assay method. Briefly, protein levels in the cell lysates were measured with 190 µL of CuSO4/BCA solution (0.02 % v/v) added to each well containing 10 µL of BSA standards or treated samples (5 µL of Milli-Q water was added to 5 µL of sample). The mixture was incubated (37 °C; 25 min) and absorbance was measured at 562 nm with a Tecan plate reader. Values were standardized against a BSA protein standard curve generated on the same plate.

3.4.10 Measurement Real-Time Imaging and Measurement of Intracellular Ca^{2+}

Cells were seeded at a density of 25,000 cells/cm^2 onto a 96-well black, clear-bottom plate. Cells were incubated with 100 µL of Cal-520 AM (5 µM) at 37 °C for 1 h and then allowed to equilibrate to 22 °C for a further 30 min before treatment of the cells with individual drugs. Fluorescence was measured at Ex/Em: 490/525 nm with a Tecan plate reader. Background subtraction (media only) was performed for all wells. Data were obtained from four independent experiments and the data was expressed as a % fold-

change relative to the control. Phase contrast and fluorescence images of cellular Ca^{2+} were also acquired using a real-time imaging IncuCyte® system at different time points (8, 12, and 22 h). Cal-520 AM was excited with a 440–490 nm filter and emitted fluorescence was collected with a 504–544 nm filter (green channel). Images were captured using a 10x objective.

3.4.11 Measurement of Caspase 3 and 7 Activity

Cells were seeded at a density of 25,000 cells/cm^2 onto 96-well white, clear-bottom plates. Upon the individual treatment of each drug, media was replaced with 100 µL of 2.5 % HI-FBS media. The plate was allowed to equilibrate at 22 °C and 100 µL of Caspase-Glo® 3/7 reagent was then added, and the plate was incubated in the dark. The mixture was mixed in an orbital shaker (500 *r.p.m.*; 30 s) and further incubated at 22 °C for 1.5 h. Luminescence was measured with a Tecan plate reader. Background subtraction (media only) was performed for all wells. Data were obtained from four independent experiments and normalized to % confluence using the IncuCyte® system employing standard software.

3.4.12 Data Analysis

Data was expressed as the mean ± standard deviation from at least three independent experiments. For comparisons, data were analysed using one-way analysis of variance (ANOVA) followed by Tukey's test using Graph Pad Prism 7 (San Diego, CA, USA). Statistical significance was set at $p < 0.05$. EC_{50} values were obtained from the dose-response curve. EC_{15} and EC_{40} values were calculated using Graph Pad QuickCalcs. The XF mito stress test report generator automatically calculated the XF cell mito stress test parameters from wave data that were exported to Excel.

3.5 Results

3.5.1 Butylone, Pentylone, and MDPV Elicited Neurotoxicity with Different Potencies

After 24 h of drug treatment, all of the SCs displayed a dose-dependent toxicity, whereby increasing the drugs' dosage increased the percentage of cell death of dopaminergic neuronal SH-SY5Y cells (Figure 3.2). Both the TB assay and LDH assay produced similar dose-response curves and EC_{50} values for all SCs. Butylone and pentylone had higher EC_{50} values when compared to MDPV. In order to elucidate the possible mechanisms underlying the SCs-elicited neurotoxicity, EC_{15} and EC_{40} doses were chosen for subsequent studies.

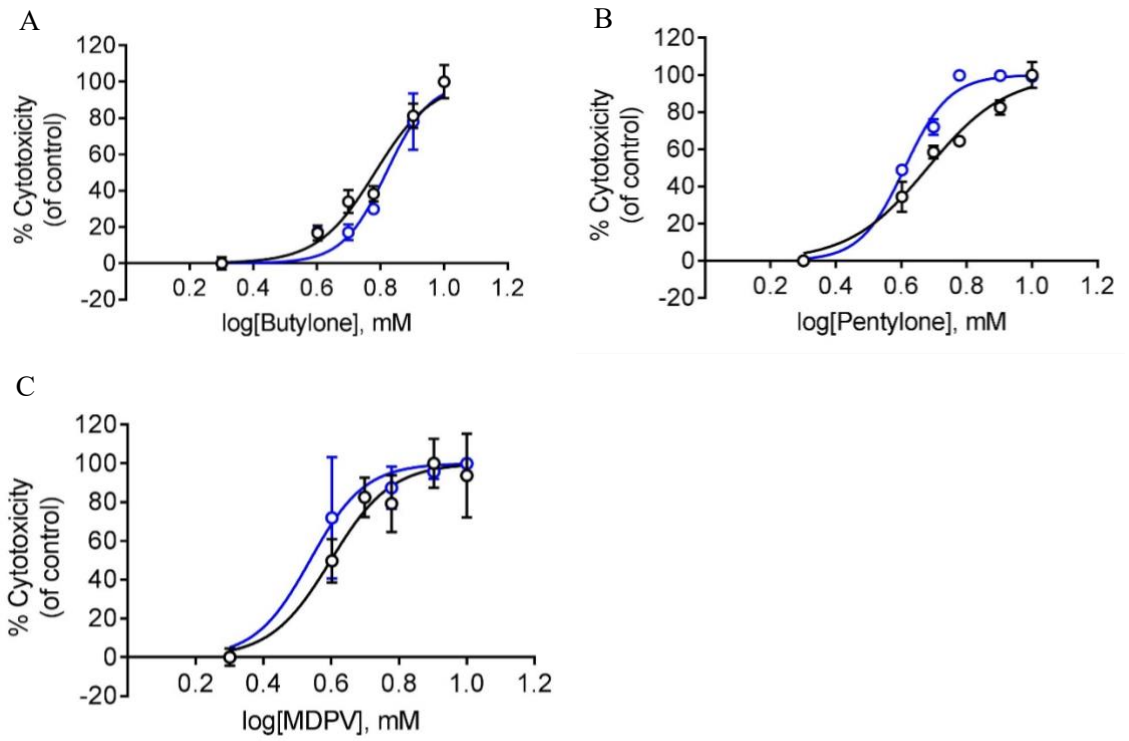

EC values (mM)	EC_{15}	EC_{40}	EC_{50}
Butylone	4.67	5.91	6.39
Pentylone	3.05	4.06	4.44
MDPV	2.60	3.43	3.61

Figure 3.2 Dose-response curves after the treatment of (A) butylone, (B) pentylone, and (C) MDPV for 24 h; lactate dehydrogenase (LDH) (black) and trypan blue (TB) assay (blue). Data are Mean ± SD obtained from three independent experiments for the TB assay and four independent experiments for the LDH assay. Table: Mean EC_{15}, EC_{40}, and

EC_{50} values after 24 h of treatment of butylone, pentylone, and MDPV, obtained from both TB and LDH assays

3.5.2 Butylone, Pentylone, and MDPV Triggered Oxidative Stress

To determine the role of oxidative stress in SCs-induced neurotoxicity, the effect of butylone, pentylone, and MDPV on the production of intracellular ROS was examined at different time points (2, 4, 6, and 24 h). All the SCs demonstrated a time-dependent increased ROS production starting as early as 2 h post drug treatment. At 24 h, both EC_{15} and EC_{40} doses of butylone, pentylone, and MDPV induced approximately a two-fold increase of ROS production (Figure 3.3).

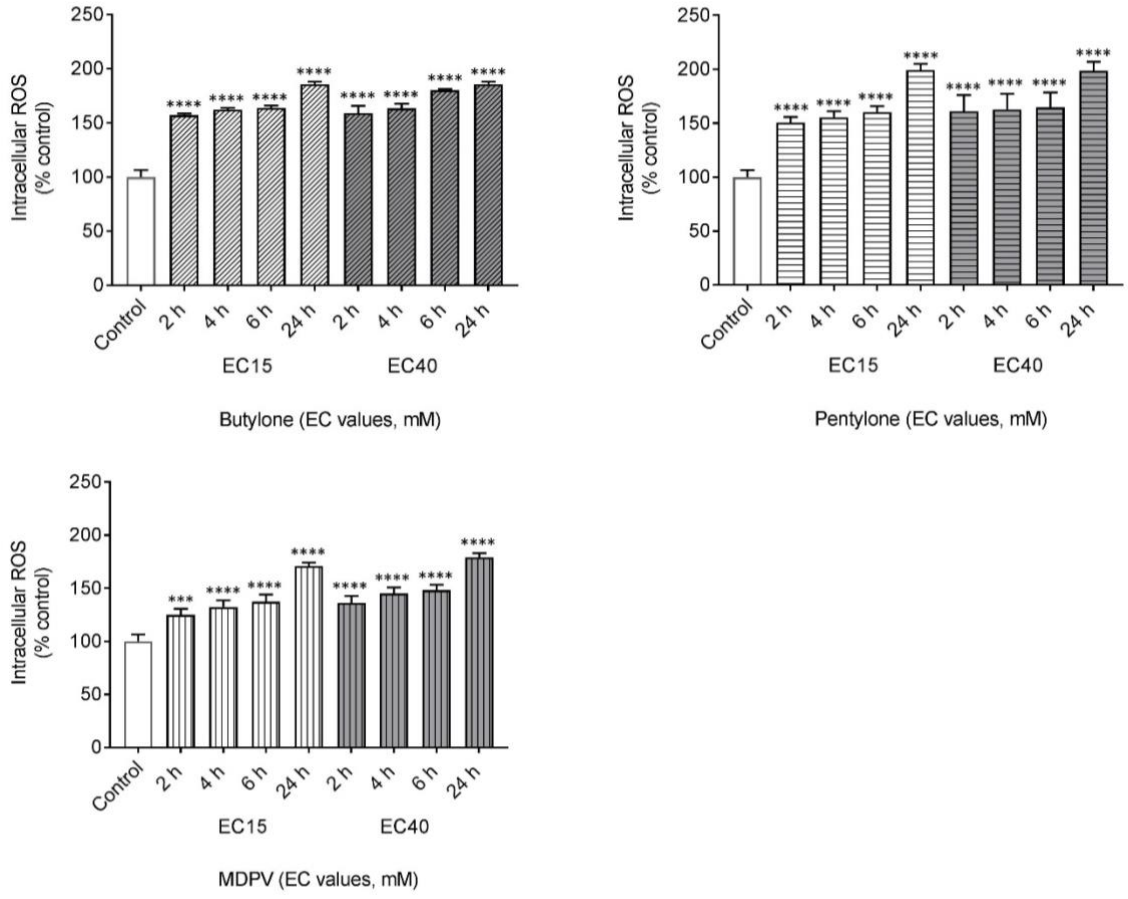

Figure 3.3 Intracellular levels of reactive oxygen species (ROS) after 2, 4, 6, and 24 h treatment of EC_{15} and EC_{40} for (A) butylone, (B) pentylone, and (C) MDPV. Data are Mean ± SD obtained from three independent experiments. Different to the control; **** $p < 0.0001$ and *** $p < 0.001$

3.5.3 Butylone, Pentylone, and MDPV Compromised Mitochondrial Bioenergetics

The production of ROS is often linked to mitochondrial respiratory chain dysfunction. The optimized Seahorse Mito Stress assay was used to assess key parameters of mitochondrial bioenergetics by measuring the oxygen consumption rate (OCR) of cells. This was performed by sequential compound injections that targeted components of the electron transport chain (ETC) in the mitochondria. All of the SCs reduced mitochondrial respiration (expressed by OCR) and increased mitochondrial stress levels in cultured SH-SY5Y cells relative to the control at both doses EC_{15} and EC_{40} after 24 h of drug treatment (Figure 3.4 A–F). The OCR for basal and maximal respiration decreased markedly (****$p < 0.0001$ vs. control) and the decreased OCR was found to be dose-dependent for pentylone and MDPV. The OCR for proton leak and non-mitochondrial respiration was also found to decrease significantly when cultured SH-SY5Y cells were treated with the EC_{40} dose (****$p < 0.0001$ vs. control). Furthermore, the OCR for the spare respiratory capacity reduced markedly at the EC_{40} dose (****$p < 0.0001$ vs. control) and was dose-dependent for pentylone and MDPV. Collectively, these findings show that all three SCs at EC_{40} doses profoundly impaired the mitochondrial function by the disruption of respiration in dopaminergic neuronal SH-SY5Y cells.

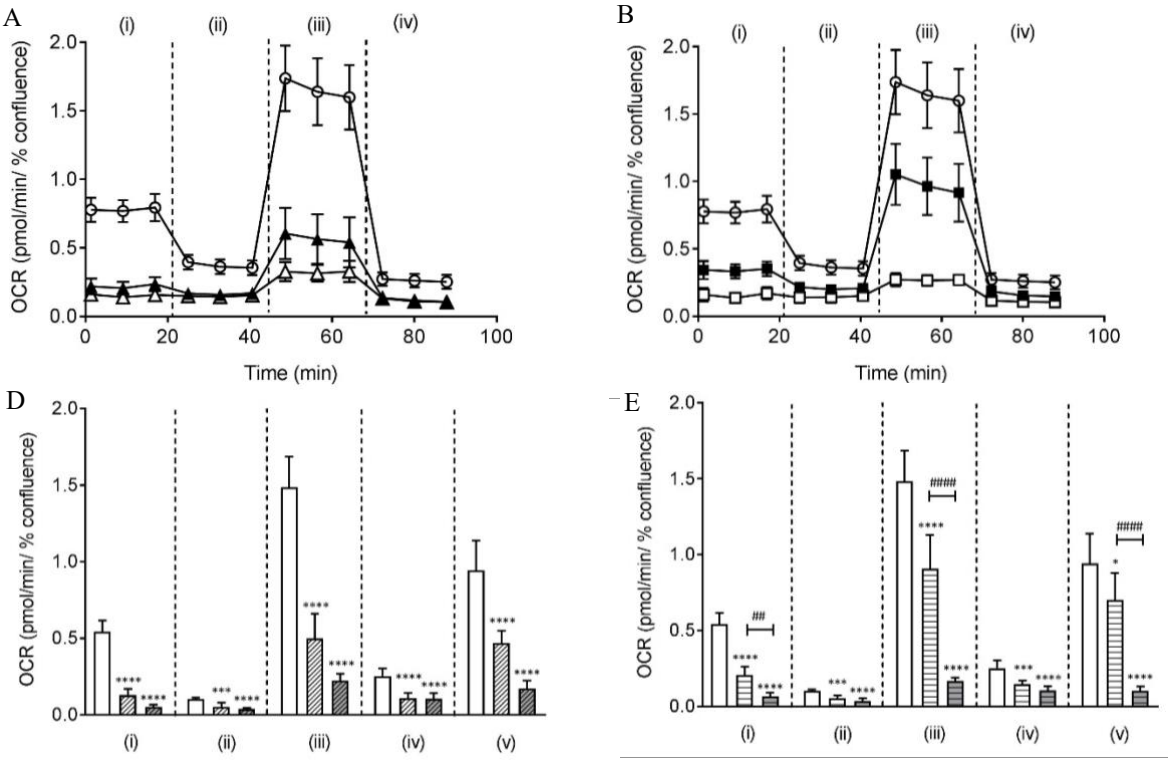

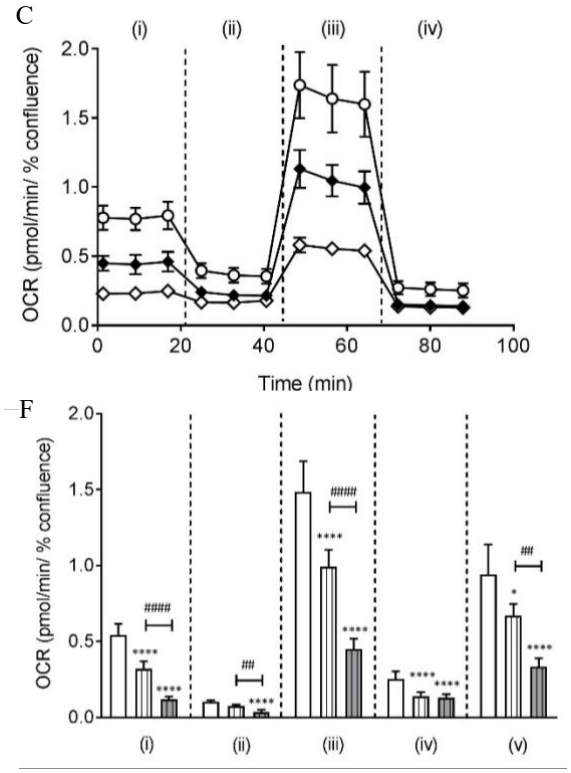

Figure 3.4 Oxygen consumption rate (OCR) measurement over time after 24 h of treatment of EC_{15} and EC_{40} for (A) butylone (filled and empty triangle, respectively), (B) pentylone (filled and empty square, respectively), and (C) MDPV (filled and empty diamond, respectively) with control (empty circle). Individual mitochondrial function parameters of EC_{15} and EC_{40} for (D) butylone (clear and grey diagonal bars, respectively), (E) pentylone (clear and grey horizontal bars, respectively), and (F) MDPV (clear and grey vertical bars, respectively): (i) basal respiration ($^{\#\#}p < 0.01$ vs. EC_{15} pentylone, and $^{\#\#\#\#}p < 0.0001$ vs. EC_{15} MDPV), (ii) proton leak ($^{\#\#}p < 0.01$ vs. EC_{15} MDPV), (iii) maximal respiration ($^{\#\#\#\#}p < 0.0001$ vs. EC_{15} pentylone and EC_{15} MDPV), (iv) non-mitochondrial respiration, and (v) spare respiratory capacity ($^{\#\#\#\#}p < 0.0001$ vs. EC_{15} pentylone, and $^{\#\#}p < 0.01$ vs. EC_{15} MDPV). The spare respiratory capacity was calculated from the difference between maximal and basal respiration. Data are Mean ± SD obtained from at least four independent experiments normalized to the % confluence of cells. Different to the control; * $p < 0.1$, *** $p < 0.001$ and **** $p < 0.0001$

Impairment of the mitochondrial ETC function often leads to a subsequently compromised bioenergetics balance. To further confirm that butylone-, pentylone-, and

MDPV-induced mitochondrial inhibition cause the impairment of cellular bioenergetics, a highly sensitive luminescence-based assay was employed to assess the intracellular adenosine triphosphate (ATP) levels in cells. After 24 h of drug treatment, all of the SCs stimulated significant intracellular ATP depletion when cells were exposed to SCs at both EC_{15} and EC_{40} doses (all values significantly decreased relative to the control; 100 % value corresponding to 11.4 mM/mg protein, Figure 3.5). Therefore, the residual ATP levels in cultured SH-SY5Y cells determined for butylone, pentylone, and MDPV (administered at their corresponding EC_{15} doses) were 23.5 ± 10.0 %, 15.8 ± 15.5 %, and 23.0 ± 22.5 %, respectively. ATP levels were further reduced to 8.5 ± 16.5 %, 6.2 ± 17.8 %, and 9.5 ± 12.9 % at EC_{40} doses for butylone, pentylone, and MDPV, respectively.

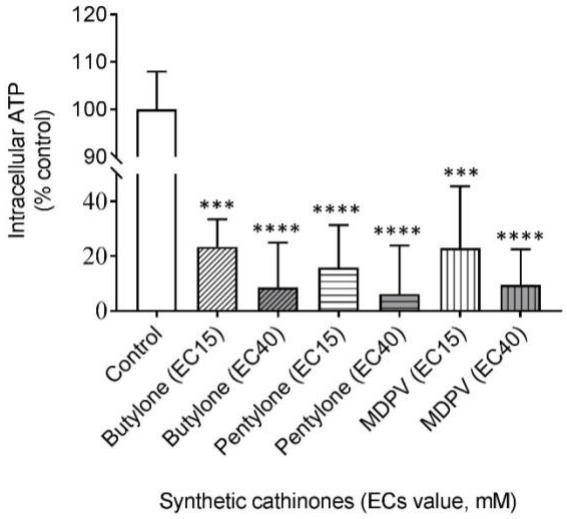

Figure 3.5 Intracellular levels of adenosine triphosphate (ATP) after 24 h of treatment of EC_{15} and EC_{40} for butylone, pentylone, and MDPV. Data are Mean ± SD obtained from three independent experiments normalized to total protein. Different to the control; *** $p < 0.001$ and **** $p < 0.0001$

3.5.4 Butylone, Pentylone, and MDPV Altered Neuronal Ca^{2+} Homeostasis

Direct imaging and measurement of Ca^{2+} provides important insights into the regulation of intracellular Ca^{2+} in neurons. Treatment with drugs for 24 h significantly changed the neuronal phenotype of branched dendrites (triangular arrowhead, Figure 3.6 A) to that of rounded shaped cells with neurite retraction (Figure 3.6 B-D). In the controls (no drug

treatment), a focal distribution of Ca^{2+} fluorescence was detected (filled arrow, Figure 3.6 A), while a mixture of a focal and dispersed cytoplasmic Ca^{2+} distribution (broken arrow) was detected in cells treated with SCs at EC_{15} concentrations (Figure 3.6 B–D). The dispersion of Ca^{2+} fluorescence was observed as early as 8 h after drug treatment, with an increasing Ca^{2+} fluorescence intensity occurring in a time-dependent manner and reaching a steady state between 12 and 22 h.

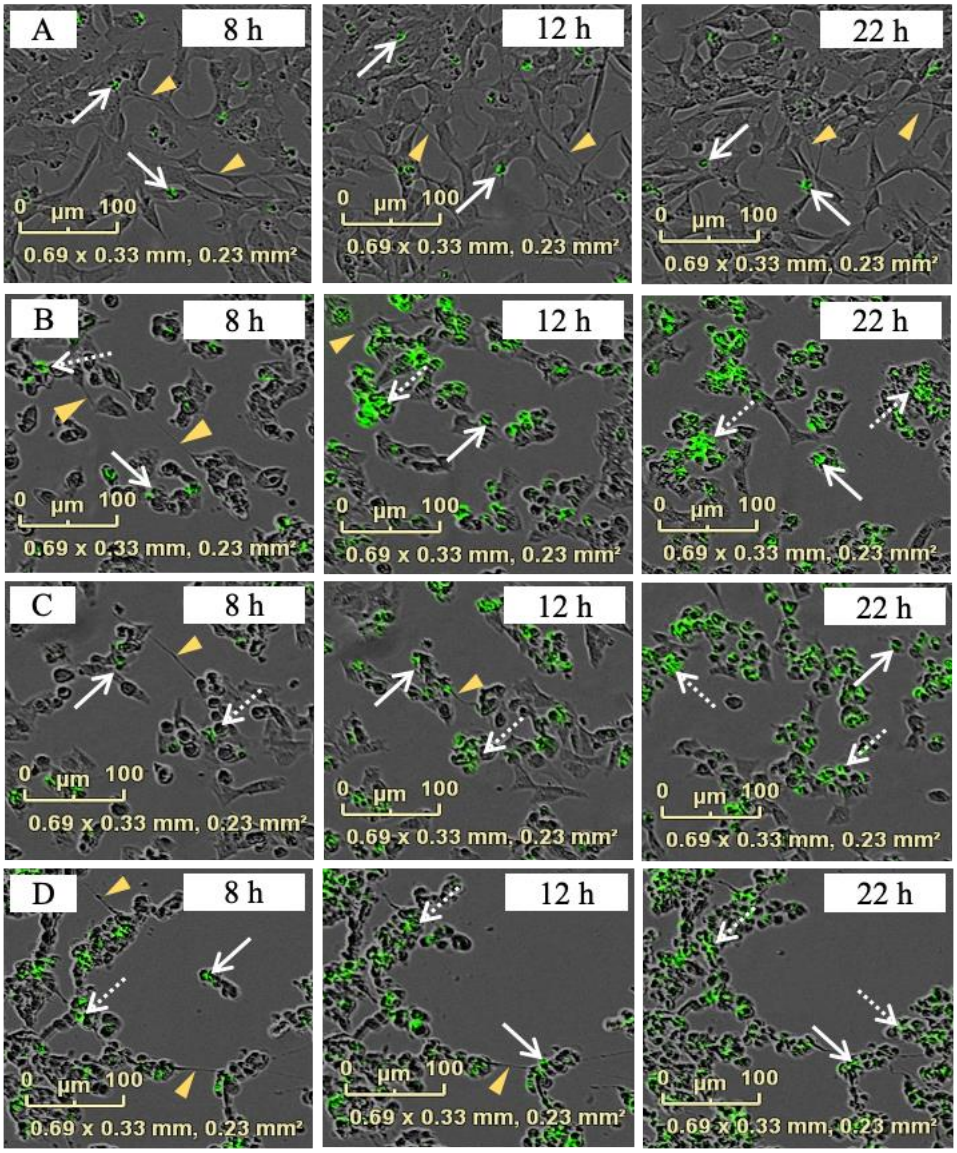

E

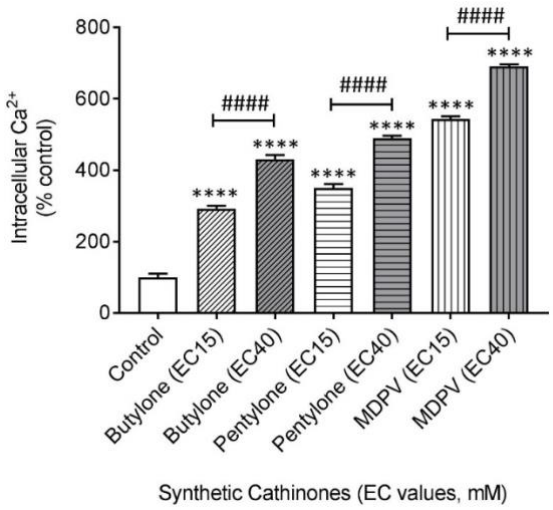

Figure 3.6 Representative merged images of Cal-520AM staining in (A) the control, (B) EC_{15} butylone, (C) EC_{15} pentylone, and (D) EC_{15} MDPV using the IncuCyte® live-cell imaging system (scale bar: 100 μm) at different time points (8, 12, and 22 h) after drug treatments. Triangular arrowhead shows cell axons, the filled arrow shows the focal distribution, and the broken arrow shows the dispersed distribution of Cal-520 AM staining. (E) Quantification of Cal-520 AM fluorescence after 24 h of treatment of EC_{15} and EC_{40} for butylone, pentylone, and MDPV. Data shown in panel E are Mean ± SD obtained from four independent experiments. $^{\#\#\#\#}p < 0.0001$ vs. EC_{15} butylone, EC_{15} pentylone and EC_{15} MDPV. Different to the control; $^{****}p < 0.0001$

The quantification of intracellular Ca^{2+} showed that the intracellular Ca^{2+} levels increased significantly 24 h after drug treatment (Figure 3.6 E). Intracellular Ca^{2+} levels in cells exposed to butylone, pentylone, and MDPV (administered at corresponding EC_{15} doses) were 292.3 ± 8.5 %, 350.1 ± 11.0 %, and 543.2 ± 7.6 %, respectively. Intracellular Ca^{2+} was further increased to 430.7 ± 11.5 %, 489.5 ± 6.8 %, and 690.9 ± 5.9 % at EC_{40} doses for butylone, pentylone, and MDPV, respectively. The increased intracellular Ca^{2+} concentrations were dose-dependent for all SCs ($^{\#\#\#\#}p < 0.0001$ vs. EC_{15}).

3.5.5 Butylone, Pentylone, and MDPV Induce an Apoptotic Cell Death Pathway

To investigate whether SCs neurotoxicity leads to mitochondrial programmed cell death, measurement of the apoptosis executioner caspases 3 and 7 was performed. Caspase cleavage of the proluminescent substrate liberates free aminoluciferin that is consumed by luciferase to generate a glow-type luminescent signal. The signal produced is proportional to the caspase 3 and 7 activity. The administration of butylone, pentylone, and MDPV promoted caspase 3 and 7 activation in cultured SH-SY5Y cells 24 h after treatment (Figure 3.7). Caspase activation values in cells exposed to butylone, pentylone, and MDPV (administered at their corresponding EC_{15} doses) were 392.0 ± 6.2 %, 372.0 ± 6.8 %, and 253.1 ± 10.8 % vs. the control, respectively. Caspase activation was further increased to 468.4 ± 16.7 % and 342.0 ± 13.5 % in cells treated with EC_{40} doses for butylone and MDPV, respectively, but decreased to 200.0 ± 20.5 % at EC_{40} doses for pentylone. Both butylone and MDPV stimulated a dose-dependent increase in caspase activity ($^{\#\#\#\#}p < 0.0001$ vs. EC_{15}).

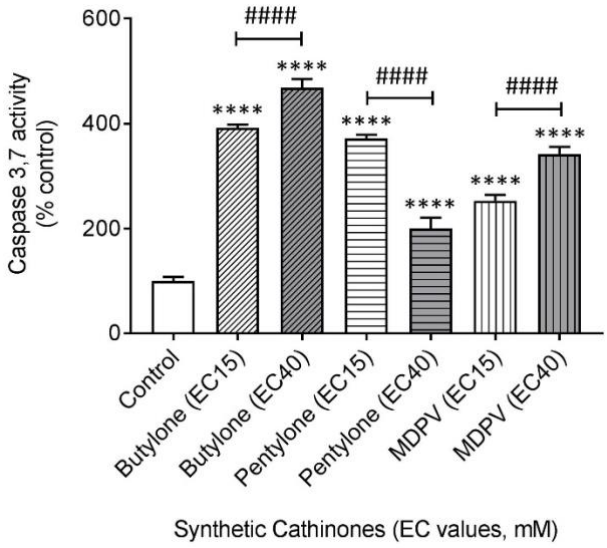

Figure 3.7 Effect elicited by EC_{15} and EC_{40} for butylone, pentylone, and MDPV in the activation of caspase 3 and 7 after 24 h of treatment. Data are Mean ± SD obtained from four independent experiments normalized to the % confluence of cells. $^{\#\#\#\#}p < 0.0001$ vs. EC_{15}. Different to the control; **** $p < 0.0001$

3.6 Discussion

The present findings highlight the potential neurotoxicity potency associated with the abuse of butylone, pentylone, and MDPV. The neurotoxicity of these SCs resulted in a raft of cellular and molecular level effects, including the accumulation of ROS production, mitochondrial dysfunction, and the alteration of Ca^{2+} homeostasis that finally led to apoptotic cell death. The increased incidence of neurological and psychiatric changes involving cognitive impairments and mental illnesses after SCs use further demonstrated their neurotoxicity [46]. A growing number of studies have suggested that SCs induce neurocognitive dysfunction among acute and long-term users [32]. Currently, there is no antidote for acute intoxications of SCs, although behavioural-based and lifestyle interventions, together with seemingly promising pharmacotherapy drug treatment, are gaining more attention.

Our study demonstrates that SCs exert significant neurotoxic effects on cultured dopaminergic neuronal SH-SY5Y cells. The dose-dependent neurotoxicity pattern demonstrated showed the detrimental impact of these SCs upon exposure when administered. Overall, butylone appeared to be less potent when compared to pentylone and MDPV (EC_{50}: butylone 6.39, pentylone 4.44, and MDPV 3.61 mM). The orders of drug potency determined by both TB and LDH assays were similar (MDPV ≈ pentylone > butylone). These results were consistent with previous studies conducted, where an increasing cytotoxicity was documented for drugs with longer alkyl side-chain. Such elongation is thought to increase the lipophilicity (XLogP3-AA values, Figure 3.1: butylone 1.9, pentylone 2.3, and MDPV 3.3) and hence its ability to penetrate the cell membrane, in order to facilitate cell death [47, 48]. Drug potency is also influenced by drug permeability to the blood–brain barrier (BBB). All the SCs' physicochemical properties were within the optimal ranges (Figure 3.1), suggesting the ease with which these SCs can cross the BBB [49-51] and reach the neurons, their pharmacological site of actions. Some other factors that might affect drug potency includes the pharmacokinetic-pharmacodynamic properties of the SCs [52], changes in the plasma membrane fluidity [48], alterations in monoaminergic systems that resulted in loss of dopamine functions [53], and the generation of metabolites and reactive species during enzymatic breakdown [33]. The relative neurotoxic potencies (demonstrated by the difference in EC_{50} values)

shown did not correlate with the values of previously reported DAT inhibition potencies [54, 55], indicating that the neurotoxicity of butylone, pentylone, and MDPV seemed to be independent of DAT-mediated uptake. These findings are in agreement with an independent study conducted by Valente et al., whereby no protective effect of the GBR 12909 DAT inhibitor was observed for MDPV-induced neurotoxicity [36]. It is not known whether these SCs gain entry into cells via other carrier-mediated uptake or by diffusion, demonstrating that the precise underpinnings of cellular uptake are not fully understood and require future investigation.

Psychostimulant SCs exposure induce a substantial accumulation of monoamines in the presynaptic terminal or extracellular space resulting excess dopamine metabolism that leads to the formation of cell-damaging reactive species such as reactive oxygen (ROS) and nitrogen species (RNS). The formation of toxic ROS and RNS has been implicated in the promotion of neuronal cell death. Recently, there has been increasing evidence that ROS are responsible for SCs-related neuronal damage. In this study, the rapid and time-dependent production of intracellular ROS (Figure 3.3) was observed, indicative of a central role for oxidative stress involvement in the neurotoxicity mediated by butylone, pentylone, and MDPV. ROS production following this SCs exposure might be an early biochemical indicator that precedes neuronal cell death. It is unclear why ROS production under these experimental conditions showed a time-dependent, but not dose-dependent, increment for these SCs. However, the findings from this study are in agreement with recent *in vitro* studies whereby oxidative stress was found to be involved in the mechanism of action of the SCs 4-Methylmethcathinone (4-MMC), 3,4-Methylenedioxymethcathinone (MDMC), α-Pyrrolidinooctanophenone (α-POP), α-Pyrrolidinononanophenone (α-PNP), methylone, 3-Fluoromethcathinone (3-FMC), and MDPV [36, 37, 39, 40, 47, 56, 57]. Although the mechanism underlying ROS production remains to be elucidated, it is clear that intracellular ROS promote oxidative stress and potentiate mitochondrial dysfunction in neuronal cells.

Mitochondria, the major regulators of cellular energy metabolism, have been recognised as the primary source of intracellular ROS and the key player in amphetamine-induced stress [58]. They act as energy generators in cells via oxidative phosphorylation and ATP production. Mitochondrial respiration impairment has been implicated in neuronal death and several neurodegenerative diseases. In the basal state, mitochondrial

oxygen consumption is mainly driven by ATP synthase. Drug treatment at an EC_{15} dosage of butylone, pentylone, and MDPV led to a 41 % – 76 % inhibition of basal OCR in comparison to the control, suggesting significantly altered ATP consumption, even at low doses of SCs. Following the addition of oligomycin when evaluating the mitochondrial coupling, the OCR decreased, and the remaining mitochondrial oxygen consumption was predominantly driven by the proton leak across the inner membrane. A substantial reduction of proton leak at EC_{40} doses (63 % – 67 % from the control), indicated that mitochondria were severely damaged and uncoupled. The addition of FCCP dissipated the proton gradient across the mitochondrial inner membrane, uncoupling electron transport from oxidative phosphorylation and hence facilitating measurement of the maximal OCR. A significant reduction of the maximal respiration capacity (33 % – 66 % from the control) signified dysfunction in the respiratory complexes and depletion of the mitochondrial membrane potential, which is crucial for the functional integrity of mitochondrial ETC. The final addition of rotenone and antimycin A shut down the mitochondrial ETC function, enabling the measurement of nonmitochondrial oxygen consumption. A significant reduction of non-mitochondrial oxygen consumption at both doses (41 % – 58 % from the control) implied an overall slowing down of cell metabolism due to energy stress. The spare respiratory capacity, the major determinant of the cells' survival under the maximal physiological or pathophysiological condition, is a critical factor in maintaining the ATP-generating capacity reserve. At the EC_{40} dose, the level of OCR, a surrogate for the spare respiratory capacity, was reduced significantly (64 % – 89 % from the control), further confirming the inhibition of ETC by these SCs. Generally, the reduction of mitochondrial respiration demonstrated by the significantly decreased OCR of the individual parameters at EC_{40} doses (Figure 3.4 A-F) compared to controls, indicated that butylone, pentylone, and MDPV may inhibit multiple components of the ETC, resulting in the impairment of mitochondria. Mitochondrial impairment upon MDPV exposure has been reported in SH-SY5Y cells using end-point measurement, such as mitochondrial membrane depolarisation [36]. Up to now, there is only one other respiration kinetic study that has described the involvement of the mitochondrial inhibition of complexes within the ETC for SCs-induced neurotoxicity [39]. In this study, the effects of butylone, pentylone, and MDPV were identified and quantified for impairment of the mitochondrial ETC function, leading to the mitochondrial dysfunction

of dopaminergic neuronal SH-SY5Y cells. Although the molecular mechanisms by which these SCs impair the ETC are still not clear, inhibition of mitochondrial ETC function may result from either direct inhibition of protein subunit of one (or more) the enzyme complexes by these SCs, and/or by uncoupling the activity of the ETC from ATP synthesis [59].

The inhibition of mitochondrial ETC complexes' activity by these SCs might be the key player in the neurotoxicity, oxidative stress, and consequent disruption of the mitochondrial bioenergetics balance. Impaired energy metabolism that results in ATP depletion as a consequence of mitochondrial dysfunction has been associated with SCs-induced toxicities [36, 60, 61]. The significantly decreased residual intracellular ATP content relative to the control (Figure 3.5) in this study supports the fact that butylone, pentylone, and MDPV treatment induced severe cellular energy deficits resulting from mitochondrial impairment in dopaminergic neuronal SH-SY5Y cells. The mechanisms by which these SCs may cause energy impairment remained to be identified. Overall, these data support that a decreased mitochondrial function, specifically the impairment of oxidative phosphorylation through the depletion of energy stores, is critically linked with butylone-, pentylone-, and MDPV-induced neurotoxicity.

Mitochondria also participate in Ca^{2+} buffering, together with the endoplasmic reticulum, in maintaining Ca^{2+} homeostasis. A time- (Figure 3.6 B–D) and dose-dependent (Figure 3.6 E) increase of intracellular Ca^{2+} induced by butylone, pentylone, and MDPV after treatment verified the alteration of intracellular Ca^{2+} regulation. Dysregulated Ca^{2+} release from intracellular reservoirs combined with influx from the extracellular domain could lead to a sustained increase in intracellular Ca^{2+} over time. The amount of intracellular Ca^{2+} detected depends on the regulated openings of Ca^{2+}-permeable channels expressed in the plasma membrane and in different organelles upon SCs exposure [62]. Meth-mediated neuronal damage involving the disruption of Ca^{2+} homeostasis has been reported [63], but studies on how Ca^{2+} is linked to SCs-induced neurotoxicity are scarce. Our work extends the link to SCs disrupting neuronal Ca^{2+} homeostasis that is linked downstream to mitochondrial dysfunction. Although the intracellular Ca^{2+} concentrations observed between the SCs groups seemed to correlate with the order of drug potency (butylone < pentylone < MDPV) as determined by end-point measurements based upon cell membrane integrity, further investigation of the

exact mechanisms explaining how these SCs contribute to the dysregulation of Ca^{2+} homeostasis, including the identity of protein transporters that are affected, is warranted.

Calcium is involved in many aspects of neuronal physiology, as well as pathophysiology. It is well established that cross-talk between Ca^{2+} and redox signals plays a key role in physiological functions in the brain. Ca^{2+} homeostasis disruption triggered the initiation of the intrinsic apoptotic cell death pathway via increased generation of ROS, which in turn trigger mitochondrial oxidative damage and dysfunction. [64]. The activation of both intrinsic and extrinsic apoptotic pathways has been previously reported for MDPV [36, 61], but the death mechanism has remained unknown for both butylone and pentylone. The data obtained in this study indicated that all of the SCs stimulated an apoptotic cell death pathway through the activation of effector caspases 3 and 7. Regardless of the type of activation, the signal sources ultimately activated the common downstream mechanisms, specifically the apoptosis executioner caspase 3 and 7 cascade (Figure 3.7). The present findings demonstrated that mitochondrial dysfunction, oxidative stress and calcium dysregulation, play a role in SCs-induced neurotoxicity, ultimately leading to cell death by apoptosis.

Although the EC_{15} and EC_{40} SCs concentrations used in this study are much higher than commonly reported concentrations found in blood (up to 0.09 mM) of post-mortem (PM) cases [19, 20, 23], they are in good agreement with previously conducted mechanistic *in vitro* studies using neuronal cell lines. For example, other researchers have employed ~1.2 and 1.7 mM MDPV in SH-SY5Y cells [36], 1–4 mM 3-FMC in HT22 cells [40], 0.25–20 mM for a series of 13 synthetic cathinones in SH-SY5Y cells [65], and 0.01–2.5 mM MDPV in SH-SY5Y cells [43]. Moreover, PM blood concentrations are usually lower than the peak concentrations expected after the initial drug intake, so are not a useful measure of the maximal drug concentration. Furthermore, it is worth considering that these SCs can accumulate in the intracellular compartment. Hence, it can be assumed that the PM blood levels reported likely underestimate the circulating and intracellular concentrations of SCs. Interestingly, PM findings have shown that the tissue levels of the drug MDMA can be up to 30 times higher in the human brain [66], consistent with the notion that these drugs can traverse the blood–brain barrier (BBB) and accumulate in the brain. Precise prediction of the SCs concentration in the brain is unclear and complicated due to the different administration routes and BBB permeabilities of

these drugs (which may or may not be compromised in abusers), as well as possible PM SCs redistribution [67] and/or metabolism [68]. Moreover, it is important to note that the immortalised dopaminergic neuronal cell line SH-SY5Y can be more resistant to the cytotoxicity of added drugs. One possibility of the more resistant differentiated SH-SY5Y cellular phenotype may be linked to the up-regulated expression of Nrf2 proteins that provide an enhanced capacity to buffer the oxidative insults [69]. Hence, the pathophysiological outcomes from this study are tempered by the drug dose required to elicit responses in this cell culture model. While it is unclear precisely how the actual dose of SCs used in this study is pharmacologically or even clinically relevant, or indeed whether the dose range employed in this work can be translated to the human usage of recreational SCs, particularly at the time of administration, it remains important to understand the type of damage elicited in different cell types that may be vulnerable to these drugs. This, in turn, may provide some understanding on the potential for similar doses in humans (if achievable) to cause neuronal cell damage via mechanisms that involve mitochondrial dysfunction leading to a decreased cell viability. For the above reasons, the neurotoxicity findings observed in this *in vitro* system should be repeated in cultures of primary neuronal cell cultures and *in vivo* models to ascertain the sensitivity to a lower SCs dose as a further model of neuronal toxicity for these drugs.

The chronic use of psychostimulants has been associated with cognitive dysfunction and various neuropsychological consequences, such as impaired impulse control, working memory, decision making, attention, and motor coordination [32, 70, 71]. In addition, meth use has been linked to an increased risk of developing neurodegeneration diseases, such as Parkinson's disease (PD) [72]. Repeated long-term acute exposure of meth has been associated with the neurodegeneration of dopaminergic neurons, reflecting the degeneration pattern observed in PD patients [73]. These epidemiological findings suggest that only a very small proportion of meth users are subsequently diagnosed with PD and the usage of dopamine substitution therapy among meth users is still in a premature investigational stage [74]. Given the chemical structure similarities of the SCs to meth, it is reasonable to postulate that long-term high-dosage exposure of these SCs might also result in Parkinson-like development. Reports have shown that SCs users have also been associated with homelessness [75] or lower socioeconomic areas [76], where a greater risk of poor health with a poor antioxidant

system further enhanced their susceptibility to SCs toxicity. Behavioural factors such as physical exercise [77] and healthy dietary lifestyle measures via an increased anti-oxidative capacity have been shown to be a promising approach in the management of psychostimulant addiction [78]. There is currently no remedy for SCs intoxication, except for supportive care [79]. Evidence that SCs exert neurotoxic effects, likely via oxidative stress and/or apoptotic mechanisms suggest the possibility of efficacious antioxidant pharmacotherapies for attenuating SCs-induced ROS production [80]. Incubation of neuronal cells with antioxidants such as *N*-acetyl-L-cysteine or ascorbic acid [37, 56, 65] were shown to attenuate the SCs-induced ROS production and apoptosis, further underscoring a critical role of oxidative stress in these neurotoxic effects. Considering that mitochondrial dysfunction plays a critical part in SCs-induced neurotoxicity, the enhancement of mitochondrial function [81] and mitochondrial transplantation [82] have received attention as strategies that might ameliorate the associated mitochondrial neurodegeneration. Moreover, the development of therapeutic strategies that stabilize neuronal Ca^{2+} homeostasis by targeting the calcium channels may also be capable of preventing neurotoxicity induced by these SCs [83].

3.7 Conclusion

The present study sheds light on the cellular and molecular mechanisms underlying the neurotoxicity potency of butylone, pentylone, and MDPV. The apoptotic cell death pathway implicated the orchestration of mitochondrial-mediated toxicity mechanisms via oxidative stress, a compromised bioenergetics balance, and changes in Ca^{2+} homeostasis. Understanding the mechanisms underlying these neurotoxic actions and related clinical manifestation is imperative in the management and treatment of acute-neurological complications arising from SCs addiction. The potential clinical relevance of this study includes the demonstration that butylone, pentylone, and MDPV (i) trigger neuronal apoptosis and stimulate (ii) increased intracellular Ca^{2+} and (iii) mitochondrial dysfunction, leading to a loss in ATP, which is information that may be useful in understanding the detrimental impact of these drugs. The findings in this study should be viewed as a model for understanding the neurotoxic mechanisms that may play a role in the response of the human central nervous system to SCs exposure. Substantial work

remains before safe and novel therapeutic agents may be developed and translated for human use in the prevention of the devastating neurotoxic effects associated with the abuse of these drugs.

3.8 References

1. German, C. L., Fleckenstein, A. E. & Hanson, G. R. (2014) Bath salts and synthetic cathinones: an emerging designer drug phenomenon, *Life sciences.* **97**, 2-8.

2. Huestis, M. A., Brandt, S. D., Rana, S., Auwärter, V. & Baumann, M. H. (2017) Impact of Novel Psychoactive Substances on Clinical and Forensic Toxicology and Global Public Health, *Clinical Chemistry.* **63**, 1564-1569.

3. Giannotti, G., Canazza, I., Caffino, L., Bilel, S., Ossato, A., Fumagalli, F. & Marti, M. (2017) The Cathinones MDPV and α-PVP Elicit Different Behavioral and Molecular Effects Following Acute Exposure, *Neurotoxicity Research.* **32**, 594-602.

4. Brandt, S. D., Freeman, S., Sumnall, H. R., Measham, F. & Cole, J. (2011) Analysis of NRG 'legal highs' in the UK: identification and formation of novel cathinones, *Drug Testing and Analysis.* **3**, 569-575.

5. Leffler, A. M., Smith, P. B., de Armas, A. & Dorman, F. L. (2014) The analytical investigation of synthetic street drugs containing cathinone analogs, *Forensic Science International.* **234**, 50-56.

6. Zuba, D. & Byrska, B. (2013) Prevalence and co-existence of active components of 'legal highs': Analysis of 'legal highs' composition, *Drug Testing and Analysis.* **5**, 420-429.

7. Reitzel, L. A., Dalsgaard, P. W., Müller, I. B. & Cornett, C. (2012) Identification of ten new designer drugs by GC-MS, UPLC-QTOF-MS, and NMR as part of a police investigation of a Danish Internet company, *Drug Testing and Analysis.* **4**, 342-354.

8. Westphal, F., Junge, T., Girreser, U., Greibl, W. & Doering, C. (2012) Mass, NMR and IR spectroscopic characterization of pentedrone and pentylone and identification of their isocathinone by-products, *Forensic Science International.* **217**, 157-167.

9. Majchrzak, M., Celiński, R., Kuś, P., Kowalska, T. & Sajewicz, M. (2018) The newest cathinone derivatives as designer drugs: an analytical and toxicological review, *Forensic Toxicology.* **36**, 33-50.

10. Palamar, J., Salomone, A., Gerace, E., Di Corcia, D., Vincenti, M. & Cleland, C. (2017) Hair testing to assess both known and unknown use of drugs amongst ecstasy users in the electronic dance music scene, *The International Journal on Drug Policy.* **48**, 91.

11. Salomone, A., Palamar, J. J., Gerace, E., Di Corcia, D. & Vincenti, M. (2017) Hair Testing for Drugs of Abuse and New Psychoactive Substances in a High-Risk Population, *Journal of Analytical Toxicology.* **41**, 376-381.

12. Mohr, A. L. A., Friscia, M., Yeakel, J. K. & Logan, B. K. (2018) Use of synthetic stimulants and hallucinogens in a cohort of electronic dance music festival attendees, *Forensic Science International.* **282**, 168-178.

13. Saha, K., Li, Y., Holy, M., Lehner, K. R., Bukhari, M. O., Partilla, J. S., Sandtner, W., Sitte, H. H. & Baumann, M. H. (2018) The synthetic cathinones, butylone and pentylone, are stimulants that act as dopamine transporter blockers but 5-HT transporter substrates, *Psychopharmacology*.

14. Karila, L., Lafaye, G., Scocard, A., Cottencin, O. & Benyamina, A. (2018) MDPV and α-PVP use in humans: The twisted sisters, *Neuropharmacology.* **134**, 65-72.

15. Dolan, S. B., Chen, Z., Huang, R. & Gatch, M. B. (2018) "Ecstasy" to addiction: Mechanisms and reinforcing effects of three synthetic cathinone analogs of MDMA, *Neuropharmacology.* **133**, 171-180.

16. Simmons, S. J., Gregg, R. A., Tran, F. H., Mo, L., Weltin, E., Barker, D. J., Gentile, T. A., Watterson, L. R., Rawls, S. M. & Muschamp, J. W. (2018) Comparing rewarding and reinforcing properties between 'bath salt' 3,4-methylenedioxypyrovalerone (MDPV) and cocaine using ultrasonic vocalizations in rats, *Addiction Biology.* **23**, 102-110.

17. Zawilska, J. B. & Wojcieszak, J. (2018) Novel Psychoactive Substances: Classification and General Information in *Synthetic Cathinones: Novel Addictive and Stimulatory Psychoactive Substances* (Zawilska, J. B., ed) pp. 11-24, Springer International Publishing, Cham.

18. Weinstein, A. M., Rosca, P., Fattore, L. & London, E. D. (2017) Synthetic Cathinone and Cannabinoid Designer Drugs Pose a Major Risk for Public Health, *Frontiers in psychiatry.* **8**, 156-156.

19. Elliott, S. & Evans, J. (2014) A 3-year review of new psychoactive substances in casework, *Forensic science international.* **243**, 55-60.

20. Rojek, S., Klys, M., Strona, M., Maciow, M. & Kula, K. (2012) "Legal highs"-Toxicity in the clinical and medico-legal aspect as exemplified by suicide with bk-MBDB administration, *Forensic Science International.* **222**, E1-E6.

21. Marinetti, L. J. & Antonides, H. M. (2013) Analysis of Synthetic Cathinones Commonly Found in Bath Salts in Human Performance and Postmortem Toxicology: Method Development, Drug Distribution and Interpretation of Results, *Journal of Analytical Toxicology.* **37**, 135-146.

22. Kesha, K., Boggs, C. L., Ripple, M. G., Allan, C. H., Levine, B., Jufer-Phipps, R., Doyon, S., Chi, P. & Fowler, D. R. (2013) Methylenedioxypyrovalerone ("Bath Salts"),Related Death: Case Report and Review of the Literature, *Journal of Forensic Sciences.* **58**, 1654-1659.

23. Kriikku, P., Wilhelm, L., Schwarz, O. & Rintatalo, J. (2011) New designer drug of abuse: 3,4-Methylenedioxypyrovalerone (MDPV). Findings from apprehended drivers in Finland, *Forensic Science International.* **210**, 195-200.

24. Froberg, B. A., Levine, M., Beuhler, M. C., Judge, B. S., Moore, P. W., Engebretsen, K. M., McKeown, N. J., Rosenbaum, C. D., Young, A. C., Rusyniak, D. E., Consortium, A. T. I. & On behalf of the, A. T. I. C. (2015) Acute Methylenedioxypyrovalerone Toxicity, *Journal of Medical Toxicology.* **11**, 185-194.

25. Krotulski, A. J., Papsun, D. M., De Martinis, B. S., Mohr, A. L. A. & Logan, B. K. (2018) N-Ethyl Pentylone (Ephylone) Intoxications: Quantitative Confirmation and Metabolite Identification in Authentic Human Biological Specimens, *JOURNAL OF ANALYTICAL TOXICOLOGY.* **42**, 467-475.

26. Assi, S., Gulyamova, N., Kneller, P. & Osselton, D. (2017) The effects and toxicity of cathinones from the users' perspectives: A qualitative study, *Human Psychopharmacology: Clinical and Experimental.* **32**, e2610.

27. Archer, T. & Kostrzewa, R. M. (2018) Synthetic Cathinones: Neurotoxic Health Hazards and Potential for Abuse in *Synthetic Cathinones: Novel Addictive and Stimulatory Psychoactive Substances* (Zawilska, J. B., ed) pp. 1-10, Springer International Publishing, Cham.

28. Leyrer-Jackson, J. M., Nagy, E. K. & Olive, M. F. (2018) Cognitive deficits and neurotoxicity induced by synthetic cathinones: is there a role for neuroinflammation? in pp. 1-17, Springer Science & Business Media, Heidelberg.

29. Costa, G., De Luca, M. A., Piras, G., Marongiu, J., Fattore, L. & Simola, N. (2020) Neuronal and peripheral damages induced by synthetic psychoactive substances: an update of recent findings from human and animal studies, *Neural regeneration research.* **15**, 802-816.

30. Ádám, Á., Gerecsei, L. I., Lepesi, N. & Csillag, A. (2014) Apoptotic effects of the 'designer drug' methylenedioxypyrovalerone (MDPV) on the neonatal mouse brain, *Neurotoxicology.* **44**, 231-236.

31. Naseri, G., Fazel, A., Golalipour, M. J., Haghir, H., Sadeghian, H., Mojarrad, M., Hosseini, M., Shahrokhi Sabzevar, S., Beheshti, F. & Ghorbani, A. (2018) Exposure to mephedrone during gestation increases the risk of stillbirth and induces hippocampal neurotoxicity in mice offspring, *Neurotoxicology and Teratology.* **67**, 10-17.

32. Sewalia, K., Watterson, L. R., Hryciw, A., Belloc, A., Ortiz, J. B. & Olive, M. F. (2018) Neurocognitive dysfunction following repeated binge-like self-administration of the synthetic cathinone 3,4-methylenedioxypyrovalerone (MDPV), *Neuropharmacology.* **134**, 36-45.

33. Wojcieszak, J., Andrzejczak, D., Woldan-Tambor, A. & Zawilska, J. B. (2016) Cytotoxic Activity of Pyrovalerone Derivatives, an Emerging Group of Psychostimulant Designer Cathinones, *Neurotoxicity Research.* **30**, 239-250.

34. Den Hollander, B., Sundström, M., Pelander, A., Ojanperä, I., Mervaala, E., Korpi, E. R. & Kankuri, E. (2014) Keto amphetamine toxicity-focus on the redox reactivity of the cathinone

designer drug mephedrone, *Toxicological sciences : an official journal of the Society of Toxicology.* **141**, 120-131.

35. Siedlecka-Kroplewska, K., Szczerba, A., Lipinska, A., Slebioda, T. & Kmiec, Z. (2014) 3-Fluoromethcathinone, a structural analog of mephedrone, inhibits growth and induces cell cycle arrest in HT22 mouse hippocampal cells *Journal of Physiology and Pharmacology* **65**, 241-246.

36. Valente, M. J., Bastos, M. D. L., Fernandes, E., Carvalho, F., Guedes De Pinho, P. & Carvalho, M. (2017) Neurotoxicity of β-Keto Amphetamines: Deathly Mechanisms Elicited by Methylone and MDPV in Human Dopaminergic SH-SY5Y Cells, *ACS Chemical Neuroscience.* **8**, 850-859.

37. Matsunaga, T., Morikawa, Y., Kamata, K., Shibata, A., Miyazono, H., Sasajima, Y., Suenami, K., Sato, K., Takekoshi, Y., Endo, S., El-Kabbani, O. & Ikari, A. (2017) α-Pyrrolidinononanophenone provokes apoptosis of neuronal cells through alterations in antioxidant properties, *Toxicology.* **386**, 93-102.

38. Soares, J., Costa, V. M., Bronze, S., Gaspar, H., Santos, S., Bastos, M. L., Carvalho, F. & Capela, J. (2016) Neurotoxicity of synthetic cathinones on differentiated SH-SY5Y human dopaminergic cells, *Toxicology Letters.* **258**, S181-S181.

39. Den Hollander, B., Sundström, M., Pelander, A., Siltanen, A., Ojanperä, I., Mervaala, E., Korpi, E. R. & Kankuri, E. (2015) Mitochondrial respiratory dysfunction due to the conversion of substituted cathinones to methylbenzamides in SH-SY5Y cells, *Scientific Reports.* **5**, 14924.

40. Siedlecka-Kroplewska, K., Wrońska, A., Stasiłojć, G. & Kmieć, Z. (2018) The Designer Drug 3-Fluoromethcathinone Induces Oxidative Stress and Activates Autophagy in HT22 Neuronal Cells, *Neurotoxicity research*, 1-13.

41. Presgraves, S. P., Ahmed, T., Borwege, S. & Joyce, J. N. (2004) Terminally differentiated SH-SY5Y cells provide a model system for studying neuroprotective effects of dopamine agonists, *Neurotoxicity research.* **5**, 579.

42. Barbosa, D. J., Capela, J. P., Silva, R., Vilas-Boas, V., Ferreira, L. M., Branco, P. S., Fernandes, E., Bastos, M. d. L. & Carvalho, F. (2014) The mixture of "ecstasy" and its metabolites is toxic to human SH-SY5Y differentiated cells at in vivo relevant concentrations, *Archives of toxicology.* **88**, 455.

43. Rosas-Hernandez, H., Cuevas, E., Lantz, S. M., Imam, S. Z., Rice, K. C., Gannon, B. M., Fantegrossi, W. E., Paule, M. G. & Ali, S. F. (2016) 3,4-methylenedioxypyrovalerone (MDPV) induces cytotoxic effects on human dopaminergic SH-SY5Y cells, *Journal of Drug and Alcohol Research.* **2016**.

44. Lantz, S. M., Rosas-Hernandez, H., Cuevas, E., Robinson, B., Rice, K. C., Fantegrossi, W. E., Imam, S. Z., Paule, M. G. & Ali, S. F. (2017) Monoaminergic toxicity induced by cathinone phthalimide: An in vitro study, *Neuroscience Letters.* **655**, 76-81.

45. Rosas-Hernandez, H., Cuevas, E., Lantz, S. M., Rice, K. C., Gannon, B. M., Fantegrossi, W. E., Gonzalez, C., Paule, M. G. & Ali, S. F. (2016) Methamphetamine, 3,4-methylenedioxymethamphetamine (MDMA) and 3,4-methylenedioxypyrovalerone (MDPV) induce differential cytotoxic effects in bovine brain microvessel endothelial cells, *Neuroscience letters.* **629**, 125-130.

46. Moszczynska, A. & Callan, S. P. (2017) Molecular, Behavioral, and Physiological Consequences of Methamphetamine Neurotoxicity: Implications for Treatment, *Journal of Pharmacology and Experimental Therapeutics* **362**, 474-488.

47. Matsunaga, T., Morikawa, Y., Tanigawa, M., Kamata, K., Shibata, A., Sasajima, Y., Suenami, K., Sato, K., Takekoshi, Y., Endo, S., El-Kabbani, O. & Ikari, A. (2017) Structure-activity relationship for toxicity of α-pyrrolidinophenones in human aortic endothelial cells, *Forensic Toxicology.* **35**, 309-316.

48. Wojcieszak, J., Andrzejczak, D., Kedzierska, M., Milowska, K. & Zawilska, J. B. (2018) Cytotoxicity of α-Pyrrolidinophenones: an Impact of α-Aliphatic Side-chain Length and Changes in the Plasma Membrane Fluidity, *Neurotoxicity Research.* **34**, 613-626.

49. Van de Waterbeemd, H., Camenisch, G., Folkers, G., Chretien, J. R. & Raevsky, O. A. (1998) Estimation of Blood-Brain Barrier Crossing of Drugs Using Molecular Size and Shape, and H-Bonding Descriptors, *Journal of Drug Targeting.* **6**, 151-165.

50. Hitchcock, S. A. & Pennington, L. D. (2006) Structure-brain exposure relationships, *Journal of Medicinal Chemistry.* **49**, 7559-7583.

51. Ibáñez, D. F. S. M. B. M. X. C. F. H. F. M. G. M. V. C. P. S. J. V. S. M. (2020) Understanding the pharmacokinetics of synthetic cathinones: Evaluation of the blood-brain barrier permeability of 13 related compounds in rats, *Addiction biology*, e12979-e12979.

52. Grecco, G. G., Kisor, D. F., Magura, J. S. & Sprague, J. E. (2017) Impact of common clandestine structural modifications on synthetic cathinone “bath salt” pharmacokinetics, *Toxicology and Applied Pharmacology.* **328**, 18-24.

53. Angoa-Pérez, M., Anneken, J. H. & Kuhn, D. M. (2017) Neurotoxicology of Synthetic Cathinone Analogs, *Current topics in behavioral neurosciences.* **32**, 209-230.

54. Simmler, L. D., Buser, T. A., Donzelli, M., Schramm, Y., Dieu, L. H., Huwyler, J., Chaboz, S., Hoener, M. C. & Liechti, M. E. (2013) Pharmacological characterization of designer cathinones in vitro, *British Journal of Pharmacology.* **168**, 458-470.

55. Simmler, L. D., Rickli, A., Hoener, M. C. & Liechti, M. E. (2014) Monoamine transporter and receptor interaction profiles of a new series of designer cathinones, *Neuropharmacology* **79**, 152-160.

56. Valente, M. J., Amaral, C., Correia-da-Silva, G., Duarte, J. A., Bastos, M. D. L., Carvalho, F., Guedes de Pinho, P. & Carvalho, M. (2017) Methylone and MDPV activate autophagy in human dopaminergic SH-SY5Y cells: a new insight into the context of β-keto amphetamines-related neurotoxicity, *Archives of Toxicology*, 1-14.

57. Soares, J., Costa, V., Bronze, S., Gaspar, H., Santos, S., Bastos, M. D. L., Carvalho, F. & Capela, J. (2018) Clorgyline and N-acetyl-L-cysteine provide partial protection against the toxicity of synthetic cathinones and methamphetamine on SH-SY5Y humans cells, *Toxicology Letters.* **295**, S274.

58. Barbosa, D. J., Capela, J. P., Feio-Azevedo, R., Teixeira-Gomes, A., Bastos, M. d. L. & Carvalho, F. (2015) Mitochondria: key players in the neurotoxic effects of amphetamines, *Archives of Toxicology.* **89**, 1695-1725.

59. Zhou, X., Luethi, D., Sanvee, G. M., Bouitbir, J., Liechti, M. E. & Krähenbühl, S. (2019) Molecular Toxicological Mechanisms of Synthetic Cathinones on C2C12 Myoblasts, *International journal of molecular sciences.* **20**, 1561.

60. Luethi, D., Liechti, M. E. & Krahenbuhl, S. (2017) Mechanisms of hepatocellular toxicity associated with new psychoactive synthetic cathinones, *Toxicology.* **387**, 57-66.

61. Valente, M. J., Araújo, A. M., Silva, R., Bastos, M. d. L., Carvalho, F., Guedes de Pinho, P. & Carvalho, M. (2016) 3,4-Methylenedioxypyrovalerone (MDPV): in vitro mechanisms of hepatotoxicity under normothermic and hyperthermic conditions, *Archives of Toxicology.* **90**, 1959-1973.

62. Daily, N. J., Santos, R., Vecchi, J., Kemanli, P. & Wakatsuki, T. (2017) Calcium Transient Assays for Compound Screening with Human iPSC-derived Cardiomyocytes: Evaluating New Tools, *J Evol Stem Cell Res.* **1**, 1-11.

63. Chen, X., Xing, J., Jiang, L., Qian, W., Wang, Y., Sun, H., Wang, Y., Xiao, H., Wang, J. & Zhang, J. (2016) Involvement of calcium/calmodulin-dependent protein kinase II in methamphetamine-induced neural damage: Methamphetamine induces neural damage through Ca2+signaling, *Journal of Applied Toxicology.* **36**, 1460-1467.

64. Pandya, J. D., Nukala, V. N. & Sullivan, P. G. (2013) Concentration dependent effect of calcium on brain mitochondrial bioenergetics and oxidative stress parameters, *Frontiers in neuroenergetics.* **5**, 10-10.

65. Soares, J., Costa, V., Gaspar, H., Santos, S., Bastos, M., Carvalho, F. & Capela, J. (2019) Structure-cytotoxicity relationship profile of 13 synthetic cathinones in differentiated human SH-SY5Y neuronal cells, *Neurotoxicology.* **75**, 158.

66. García-Repetto, R., Moreno, E., Soriano, T., Jurado, C., Giménez, M. P. & Menéndez, M. (2003) Tissue concentrations of MDMA and its metabolite MDA in three fatal cases of overdose, *Forensic Science International.* **135**, 110-114.

67. Glicksberg, L., Winecker, R., Miller, C. & Kerrigan, S. (2018) Postmortem distribution and redistribution of synthetic cathinones, *Forensic Toxicology.* **36**, 291-303.

68. Coccini, T., Vecchio, S., Crevani, M. & Simone, U. D. (2018) Cytotoxic Effects of 3,4-Catechol-PV (One Major MDPV Metabolite) on Human Dopaminergic SH-SY5Y Cells, *Neurotoxicity research*, 1-14.

69. Zhao, F., Wu, T., Lau, A., Jiang, T., Huang, Z., Wang, X.-J., Chen, W., Wong, P. K. & Zhang, D. D. (2009) Nrf2 promotes neuronal cell differentiation, *Free Radical Biology and Medicine.* **47**, 867-879.

70. Colon-Perez, L. M., Tran, K., Thompson, K., Pace, M. C., Blum, K., Goldberger, B. A., Gold, M. S., Bruijnzeel, A. W., Setlow, B. & Febo, M. (2016) The psychoactive designer drug and bath salt constituent MDPV causes widespread disruption of brain functional connectivity, *Neuropsychopharmacology.* **41**, 2352-2365.

71. Bernheim, A., See, R. E. & Reichel, C. M. (2016) Chronic methamphetamine self-administration disrupts cortical control of cognition, *Neuroscience and Biobehavioral Reviews.* **69**, 36-48.

72. Curtin, K., Fleckenstein, A. E., Robison, R. J., Crookston, M. J., Smith, K. R. & Hanson, G. R. (2014) Methamphetamine/amphetamine abuse and risk of Parkinson's disease in Utah: A population-based assessment, *Drug and Alcohol Dependence.* **146**, 30-38.

73. Granado, N., Ares-Santos, S. & Moratalla, R. (2013) Methamphetamine and parkinson's disease, *Parkinson's Disease.* **2013**, 308052-10.

74. Kish, S. J., Boileau, I., Callaghan, R. C., Tong, J. & Bolam, P. (2017) Brain dopamine neurone 'damage': methamphetamine users vs. Parkinson's disease – a critical assessment of the evidence, *European Journal of Neuroscience.* **45**, 58-66.

75. Smith, K. E., Bunting, A. M., Staton, M., Walker, R., Shalash, S., Winston, E. & Pangburn, K. (2017) Examination of Synthetic Cannabinoid and Cathinone Use among a Drug-Using Offender Sample, 2013-2015, *Journal of Psychoactive Drugs.* **49**, 436-445.

76. AIHW (2017) National Drug Strategy Household Survey. Detailed Findings, *Australian Institute of Health and Welfare, Australia's health 2016*, 1-168.

77. Toborek, M., Seelbach, M. J., Rashid, C. S., András, I. E., Chen, L., Park, M. & Esser, K. A. (2013) Voluntary exercise protects against methamphetamine-induced oxidative stress in brain microvasculature and disruption of the blood-brain barrier, *Molecular Neurodegeneration.* **8**, 22-22.

78. Cichello, S. (2013) Herbal treatment for hepatotoxicity associated with high fat diet, methamphetamine use and anxiety: A case study, *Australian Journal of Herbal Medicine.* **25**, 202-204.

79. Pourmand, A., Mazer-Amirshahi, M., Chistov, S., Li, A. & Park, M. (2018) Designer drugs: Review and implications for emergency management, *Human & Experimental Toxicology.* **37**, 94-101.

80. Yang, X., Wang, Y., Li, Q. Y., Zhong, Y. X., Chen, L. P., Du, Y. J., He, J., Liao, L. S., Xiong, K., Yi, C. X. & Yan, J. (2018) The Main Molecular Mechanisms Underlying Methamphetamine-Induced Neurotoxicity and Implications for Pharmacological Treatment, *Frontiers in Molecular Neuroscience* **11**, 186.

81. Dawson, T. M. & Dawson, V. L. (2017) Mitochondrial Mechanisms of Neuronal Cell Death: Potential Therapeutics, *Annual Review of Pharmacology and Toxicology.* **57**, 437-454.

82. Chang, C.-Y., Liang, M.-Z. & Chen, L. (2019) Current progress of mitochondrial transplantation that promotes neuronal regeneration, *Translational Neurodegeneration.* **8**.

83. Zündorf, G. & Reiser, G. (2011) Calcium Dysregulation and Homeostasis of Neural Calcium in the Molecular Mechanisms of Neurodegenerative Diseases Provide Multiple Targets for Neuroprotection, *Antioxidants & Redox Signaling.* **14**, 1275-1288.

Chapter 4

Monitoring metabolism of synthetic cannabinoid 4F-MDMB-BINACA via high-resolution mass spectrometry assessed in cultured hepatoma cell line, fungus, liver microsomes and confirmed using urine samples

4.1 Foreword

The following manuscript was submitted for a peer-reviewed publication and details the investigation of the metabolism pathway of 4F-MDMB-BINACA using three different *in vitro* models: cell-based (HepG2 hepatoma cell line), microbial (fungus *Cunninghamella* elegans) and subcellular fractions (human liver microsomes) and to propose suitable urinary marker(s). The manuscript was authored by Ms Huey Sze Leong (H.S.L.)[1,2], Dr Shimpei Watanabe (S.W.)[3,4,#], Dr Unnikrishnan Kuzhiumparambil (U.K.)[5], Ms Ching Yee Fong (C.Y.F.)[6], Ms Hooi Yan Moy (H.Y.M.)[6], Dr Yi Ju Yao (Y.J.Y.)[6], Professor Paul Kenneth Witting (P.K.W.)[2] and Professor Shanlin Fu (S.F.)[1,*].

[1] Centre for Forensic Science, School of Mathematical and Physical Sciences, University of Technology Sydney, Australia

[2] Discipline of Pathology, Faculty of Medicine and Health, The Charles Perkins Centre, The University of Sydney, Australia

[3] Division of drug Research, Department of Biomedical and Clinical Sciences, Linköping University, Linköping, Sweden

[4] Deparment of Forensic Genetics and Forensic Toxicology, National Board of Forensic Medicine, Linköping, Sweden

[5] Climate Change Cluster, University of Technology Sydney, Australia

[6] Analytical Toxicology Laboratory, Applied Sciences Group, Health Sciences Authority, Singapore

[#] Present address: Forensic Science Group, Photon Science Research Division, RIKEN SPring-8 Center, Japan

* Corresponding author

Author Contributions: Conceptualization: H.S.L., S.W., and S.F.; Methodology: H.S.L., S.W., U.K., and C.Y.F.; Software: H.S.L., and C.Y.F.; Validation: H.S.L., and C.Y.F.; Formal analysis: H.S.L., and S.W.; Investigation: H.S.L. and C.Y.F.; Resources: H.S.L., U.K., Y.J.Y., P.K.W., and S.F.; Data curation: H.S.L., and C.Y.F.; Writing - original draft preparation: H.S.L.; Writing - review and editing: H.S.L., S.W., U.K., C.Y.F., H.Y.M., Y.J.Y., P.K.W., and S.F.; Visualization: H.S.L. S.W., and Y.J.Y.; Supervision: H.Y.M., Y.J.Y., P.K.W. and S.F.; Project administration: H.S.L.; Funding acquisition: H.S.L., and P.K.W.

All authors have read and agreed to the version of the manuscript.

4.2 Abstract

Synthetic cannabinoids (SCBs) *tert*-leucinate derivative, methyl (2S)-2-([1-(4-fluorobutyl)-1H-indazole-3-carbonyl]amino)-3,3-dimethylbutanoate (4F-MDMB-BINACA) is known to adversely impact health. This study aimed to evaluate the suitability of three different modes of monitoring metabolism: HepG2 liver cells, fungus *Cunninghamella elegans* (*C. elegans*) and pooled human liver microsomes (HLM) for comparison with human *in vivo* metabolism in identifying suitable urinary marker/s for 4F-MDMB-BINACA intake.

Tentative structure elucidation of *in vitro* metabolites was performed on HepG2, *C. elegans* and HLM using liquid chromatography–tandem mass spectrometry and high-resolution mass spectrometry analysis. *In vivo* metabolites obtained from twenty authentic human urine samples were analysed using liquid chromatography-orbitrap mass spectrometry. Incubation with HepG2, *C. elegans* and HLM yielded nine, twenty-two and seventeen metabolites of 4F-MDMB-BINACA, respectively, formed via ester hydrolysis, hydroxylation, carboxylation, dehydrogenation, oxidative defluorination, carbonylation or reaction combinations. Phase II metabolites of glucosidation and sulfation were also exclusively identified using *C. elegans* model. Eight *in vivo* metabolites tentatively identified were mainly products of ester hydrolysis with or without additional dehydrogenation, N-dealkylation, monohydroxylation and oxidative defluorination with further oxidation to butanoic acid. Metabolites with intact terminal methyl ester moiety, i.e., oxidative defluorination with further oxidation to butanoic acid, were also tentatively identified.

The *in vitro* models presented proved useful in the exhaustive metabolism studies. Despite limitations, HepG2 identified the major 4F-MDMB-BINACA ester hydrolysis metabolite and *C. elegans* demonstrated the capacity to produce a wide variety of metabolites. Both *C. elegans* and HLM produced all the *in vivo* metabolites. Ester hydrolysis and ester hydrolysis dehydrogenation 4F-MDMB-BINACA metabolites were recommended as urinary markers for 4F-MDMB-BINACA intake.

Keywords: 4F-MDMB-BINACA, metabolism, HepG2, *Cunninghamella elegans*, human liver microsomes

4.3 Introduction

Synthetic cannabinoids (SCBs) are agonists at cannabinoid receptor type 1 (CB_1) and type 2 (CB_2) where it elicits its main effects. Due to their similar physiological effects to principal psychoactive component of cannabis, delta-9-tetrahydrocannabinol (Δ^9-THC), SCBs are gaining popularity and are often abused as recreational drugs. However, most of the SCBs are full agonists at CB_1 and CB_2 receptors, having higher risk of undesirable side effects when compared to Δ^9-THC which is a partial agonist [1]. Methyl (2S)-2-([1-(4-fluorobutyl)-1H-indazole-3-carbonyl]amino)-3,3-dimethylbutanoate (4F-MDMB-BINACA), found in numerous SCBs products seizures, has been reported by various law enforcement since 2018 [2]. The *tert*-leucine derived indazole-3-carboxamide analogue, 4F-MDMB-BINACA is postulated to be a potent agonist of the CB_1 receptor based upon its structural similarity to methyl-2-([1-(5-fluoropentyl)-1H-indazole-3-carbonyl]amino)-3,3-dimethylbutanoate (5F-MDMB-PINACA) [3, 4], has significant abuse potential and causes central nervous system depression. Death involving these drugs have been reported [5-9], and this raises public health and social concerns. Moreover, 4F-MDMB-BINACA has been listed in Schedule II of the Convention on Psychotropic Substances of 1971 recently.

Proliferation of SCBs has become a global challenge as new compounds are rapidly introduced into the illegal drug market to evade existing drug laws. Identifying SCBs intake and its correlating specific adverse effects requires rapid elucidation of these SCBs. Since most SCBs are extensively metabolized in urine, the identification of metabolites is of vital importance for forensic and clinical toxicologists. Furthermore, some hydroxylated urinary metabolites have been found to be active and more toxic than the parent SCBs themselves, emphasizing the importance of metabolism study in identifying potential toxic metabolites [10, 11].

Traditional *in vivo* metabolism studies to generate human metabolites of drugs relied heavily on the use of whole animal model systems which are expensive, limited by drug administration amount, influenced by species variation and faced many ethical issues. *In vitro* metabolism studies are generally used to complement these data using perfused organs, tissue or cell cultures and microsomal preparations. Amongst which pooled human liver microsomes (HLM) has been frequently used to elucidate metabolism

of SCBs [12-16]. The hepatic cell line HepG2 is often used as an initial screen as it is known to produce high reproducibility experiments with relatively stable enzyme concentration, although they are limited by the low-level expression of several metabolizing enzymes, including the cytochrome P450 (CYP) class of proteins [17, 18]. The metabolic competence of HepG2 was described to be sufficient for *in vitro* studies after an incubation time of at least 72 h [19]. An alternative to these was the use of microbial model with phase I and II metabolite-generating capabilities such as the zygomycete fungus, *Cunninghamella* elegans (*C. elegans*). *C. elegans* has the advantage of more closely mimicking mammalian metabolism [20] and has been used as a complementary model in metabolism studies of new psychoactive substances, in particularly the SCBs [21-26]. This class of fungi has enzymatic activity to facilitate phase I and II metabolism including hydroxylation, carboxylation, dihydrodiol formation, oxidative defluorination, N-dealkylation, glucuronidation, glucosidation and sulfation [23, 27]. The advantages offered by the microbial transformation over other approaches include the low setting up cost, reliability and reproducibility as well as possible economical scale up affording both phase I and II metabolites in higher yield. This scaled production is useful for further characterization of metabolites that required to be distinguished from its isomeric species and in the identification of potentially toxic metabolites [28].

Although there were reports on the metabolism of 4F-MDMB-BINACA using *in vivo* and various *in vitro* models, studies were either conducted using small *in vivo* sample size such as 1 to 4 biological samples [5, 29], or in closed environments such as forensic psychiatric wards and prisons [30]. In our study, twenty *in vivo* urine samples screened positive for 4F-MDMB-BINACA intake were employed and the findings were compared to those obtained via HepG2, *C. elegans* and HLM *in vitro* models. The aim of this study was to assess the suitability of these *in vitro* models in the *in vitro – in vivo* extrapolations and to suggest suitable urinary marker(s) for 4F-MDMB-BINACA intake.

4.4 Materials and Methods

4.4.1 Chemicals and reagents

4F-MDMB-BINACA was provided by Health Sciences Authority (Singapore). 4F-MDMB-BINACA 3,3-dimethylbutanoic acid metabolite was purchased from Cayman Chemical (Ann Arbor, MI, USA).

In vitro metabolism study: Hundred and fifty (mixed gender) - donor HLM pool, NADPH system solution A and NADPH system solution B, T75 tissue culture flasks, and 96-well cell culture plates were purchased from Corning (Corning, NY, USA). *C. elegans* ATCC 10028b was from Cryosite Ltd. (South Granville, NSW, Australia). HepG2 cell line was purchased from CellBank (Sydney, NSW, Australia). Minimum Essential Medium – Eagle with Earle's BSS (MEM Eagle EBSS) was purchased from Lonza (Basel, Switzerland). Liquid chromatography–mass spectrometry (LC–MS) grade acetonitrile (ACN) was obtained from Honeywell (Muskegon, MI, USA). Reagent grade dichloromethane (CH_2Cl_2) and sodium chloride (NaCl) were purchased from Chem-supply (Gilman, SA, Australia). LC–MS grade formic acid was obtained from Sigma-Aldrich (St. Louis, MO, USA). Glycerol, potassium dihydrogen phosphate (KH_2PO_4) and dipotassium hydrogen phosphate (K_2HPO_4) were from Ajax Chemicals (Auburn, NSW, Australia). Potato dextrose agar, glucose, peptone, and yeast extract were purchased from Oxoid Australia (Adelaide, SA, Australia).

In vivo metabolism study: Chemicals for preparing reagents and buffers were obtained from Fluka, Sigma-Aldrich (Saint Louis, Missouri, USA). Optima LC-MS grade ACN was purchased from ThermoFisher Scientific (Fair Lawn, NJ, USA). Purified water was used, and all solvents used were of LC-MS grade or better. The enzyme, β-glucuronidase from abalone (*Haliotis rufescens*) was obtained from KURA Biotec (Rancho Dominguez, CA, USA). Clean Screen FASt® filter tubes (3 mL packed with 200 mg solid phase sorbent) were purchased from UCT, Inc (Bristol, PA, USA).

4.4.2 Monitoring *in vitro* metabolism

HepG2 liver cells

Cryofrozen HepG2 cells were thawed and sub-cultured (up to passage 7) in a T75 tissue culture flask containing MEM Eagle EBSS media supplemented with 10 % heat-inactivated fetal bovine serum (HI-FBS), L-glutamine (2 mM), penicillin:streptomycin (100 U/mL:100 µg/mL) and non-essential amino acid solution (NEAA, 1x). Cells were cultured at 37 °C in a humidified atmosphere incubator containing 95 % air and 5 % CO_2, until about 80 % confluent. The media was changed every 2 days and when required, cells were harvested by subculture with media containing trypsin/EDTA (0.12 % trypsin/ 0.02 % EDTA w/v). The following method was adopted [31] with slight modifications: Cells were seeded at a density of 9600 cells/well onto 96-well plates overnight. Cells were treated with 120 µM of 4F-MDMB-BINACA media solution (100 µL) in triplicates for 72 h. Supernatant (60 µL) was transferred into a 0.5 mL capped tube containing ice-cold ACN (60 µL). The mixture was vortex-mixed and cooled for another 15 min at - 30 °C before centrifuging at 10,000 g for 5 min. The filtered sample (0.22 µm, 100 µL) was diluted with ACN (500 µL) and 10 µL was injected into liquid chromatography-quadrupole time-of-flight mass spectrometry (LC–QTOF-MS). 2 µL was also injected into liquid chromatography–triple quadrupole mass spectrometer (LC–MS/MS). A control without HepG2 and/or without 4F-MDMB-BINACA were also treated in identical fashion.

Fungus C. elegans

C. elegans was cultured on potato dextrose agar plates at 27 °C for 5 days. The mycelia of the fungus were mixed in sterile physiological saline solution (1 plate of mycelia/ 10 mL). Growth medium consisting of NaCl:KH_2PO_4:Yeast extract:Peptone:Glucose (1:1:1:1:2 v/v/v/v), water and glycerol was prepared as previously described [32] and autoclaved (121 °C, 15 min) before use. 1.5 mL of the homogenate were inoculated into 100 mL of growth medium in a conical flask. The culture was incubated for 48 h at 26 °C and 180 rpm on an Infors HT Multitron rotary shaker. 4F-MDMB-BINACA (1 mg in 0.5 mL ACN) was added to the conical flask in triplicate and incubated for another 72 h. The solution was filtered in a Buchner funnel, extracted with CH_2Cl_2 (3 × 50 mL). The

combined extracts were evaporated to dryness using a rotary evaporator followed by a vacuum pump. The sample was reconstituted in 2 mL ACN, filtered using a 0.22 µm filter and was further diluted in ACN tenfold before injected (5 µL) into LC–QTOF-MS. An aliquot of the filtrate (100 µL) was diluted in 900 µL water/ACN (90:10, v/v) and 2 µL was also injected into LC-MS/MS. Control samples in the absence of *C. elegans* and/or 4F-MDMB-BINACA were also treated in identical fashion.

Pooled human liver microsomes (HLM)

The incubation mixture using 4F-MDMB-BINACA solution in ACN/phosphate buffer (25 µL, final concentration 1.7 µM in 0.03 % ACN), phosphate buffer (0.1 M, pH 7.4, 855 µL), NADPH-A (50 µL) and NADPH-B (20 µL) were mixed in a 2 mL capped tube, to which HLM (50 µL = 1 mg protein) was added. The mixture was vortexed mixed and incubated in triplicate at 37 °C in a shaking water bath (100 r.p.m.) for 1 h. The reaction was quenched by adding ice-cold ACN (1 mL) to the mixture, vortex mixed and then centrifuged at 13,000 g for 10 min. The sample was filtered (0.22 µm) and 5 µL was injected into LC–QTOF-MS. 100 µL of the filtrate was diluted in 900 µL water/ACN (90:10, v/v) and 2 µL was also injected into LC-MS/MS. Controls samples without HLM and/or without 4F-MDMB-BINACA were also incubated and subsequently worked up under identical conditions.

LC-QTOF-MS

Chromatographic separation was performed on an Agilent 1290 LC system with Poroshell 120 EC-C18 analytical column (2.7 µm, 75 mm x 2.1 mm; Agilent Technologies, Santa Clara, CA, USA). The mobile phase consisted of 0.1 % formic acid in water (A) and 0.1 % formic acid in acetonitrile (B). The gradient elution was as follows: 10 % B until 2 min, increased to 40 % B until 4 min, ramped to 60 % B until 15 min, and further increased to 80 % B at 18 min and ramped down to 10 % B until 19 min and held until 21 min. The flow rate was 0.3 mL/min and the column temperature was kept at 35 °C. High resolution quadrupole time-of-flight mass spectrometry data were acquired on an Agilent 6510 Accurate Mass QTOF mass spectrometer (Agilent Technologies) equipped with dual electrospray ionization (ESI) source operated both positive and negative ion mode, in order to determine accurate masses of the metabolites. The

parameters were as follows: scanning mass range, *m/z* 100 – 700 (MS), *m/z* 100 – 600 (MS/MS); capillary voltage, 3500 V; nebulizer pressure, 40 psi.; gas temperature, 310 °C; drying gas flow, 13 L/ min; fragmentor voltage, 160 V; collision energy (CE) for product ion scan analysis, 10, 20 and 40 eV; skimmer voltage, 65 V. Mass calibration was performed with the mixture provided by the manufacturer. Real-time mass calibration was enabled using the following reference masses: *m/z* 118.086255 and 322.048121 (positive ion mode); 112.985587 and 301.998139 (negative ion mode). Extracted ion chromatograms and mass spectra were analysed using Agilent MassHunter Workstation Software Qualitative Analysis (version B.06.00). The criteria for metabolites elucidation were as follows: mass error of the precursor ion ≤ 5.00 ppm, mass error of product ions ≤ 20.00 ppm, consistent fragmentation pattern with proposed structure, reasonable retention time and absence of the specific peak in controls.

LC-MS/MS

Chromatographic equipment and conditions were the same as described above. MS was run in multiple reaction monitoring (MRM) mode on an Agilent 6490 Triple Quadrupole mass spectrometer with electrospray ionisation (ESI) source in positive ion mode (Agilent Technologies). An optimized CE 8-40 eV was applied for each individual MRM transition. The source parameters were as follows: The capillary and nozzle voltage, 3500 and 1500 V, respectively; The sheath gas temperature and flow were set to 400 °C and 12 L/min, respectively; nebulizer pressure, 40 psi.; gas temperature, 290 °C; drying gas flow, 12 L/min; fragmentor voltage, 380 V. Mass calibration was routinely performed via check tune before analysis. Extracted ion chromatograms and MRM mass spectra were analysed using Agilent MassHunter Workstation Software Qualitative Analysis (version B.06.00). Percentage (%) peak area ratios were obtained by dividing the peak area of detected metabolite by the peak area of the most abundant metabolite in the same sample. Major metabolites were defined as those with greater than 10 % average peak area ratios.

4.4.3 *In vivo* metabolism

Authentic human urine samples

Antemortem urine samples from routine toxicology cases (n = 20) confirmed with the 4F-MDMB-BINACA ester hydrolysis metabolite (4F-MDMB-BINACA 3,3-dimethylbutanoic acid metabolite) were processed and analysed for *in vivo* metabolites in collaboration with the *in vitro* metabolism findings. Urine sample (500 µL) was incubated with 250 µL of pH 5 acetate buffer and 50 µL β-glucuronidase (10,000 Fisherman units/mL) for 1 h at 60 °C. After incubation, the mixture was cooled at room temperature and 150 µL of purified water was added. The mixture was vortex-mixed and 500 µL of this mixture and 500 µL of methanol were loaded onto a Clean Screen FASt tube. About 10-20 bar pressure was applied on the tube using a positive pressure manifold to allow all the samples to flow through the tube. The eluent was collected in a 2 mL sample vial for analysis.

LC-Orbitrap-MS

Chromatographic separation was achieved on a Kinetex XB-C18 column (2.6 µm, 100 mm x 2.1 mm, Phenomenex, Torrance, CA, USA) with an identically packed defender guard cartridge (2.6 µm, 10 mm x 2.1 mm). The mobile phase consisted of 10 mM ammonium formate, pH 3 (A) and 0.1 % formic acid in acetonitrile (B). The gradient elution was as follows: 5 % B until 1 min, increased to 95 % B until 10 min, ramped to 99 % B at 10.1 min and held until 11.5 min, ramped down to 5 % B at 11.6 min and held until 13.0 min. The flow rate was 0.5 mL/min for the whole run except from 10.1 to 11.5 min which was set at 0.8 mL/min. The identification of the metabolites was performed using a liquid chromatography coupled with Thermo Scientific Q-Exactive hybrid quadrupole - orbitrap mass spectrometer (Thermo Scientific, Fremont, CA, USA) equipped with heated electrospray ionization source (HESI-II) operated in positive ionization with full MS and data dependent MS^2 (FS-ddMS^2) acquisition mode. The parameters were as follows: scanning mass range, *m/z* 120–1000 (MS), sheath gas flow rate, 40 (all flow rates as per manufacturer's unit); auxiliary gas flow rate, 10; sweep gas flow rate, 1; spray voltage, 3.5 kV; capillary temperature, 270 °C; heater temperature, 425 °C. The *in vitro* metabolites elucidated from the cultured HepG2 cells, *C. elegans* and HLM were added to the

compound database. Data obtained from the twenty urine samples were retrospectively analysed and processed using TraceFinder software based on the identification criteria of mass error less than ± 5 ppm for full MS peak and MS/MS peak from the theoretical mass and matching of MS/MS spectral. Percentage (%) peak area ratios of the metabolites were similarly calculated as the *in vitro* metabolism study.

4.5 Results

A total of 25 different metabolites (B1 – B25) were tentatively identified and listed in Table 4.1 in the order of retention time (RT) with postulated biotransformation. 4F-MDMB-BINACA was eluted at 12.0 min whilst the metabolites eluted between 5.5 to 9.6 min. Metabolites were identified according to their precursor ions, product ions and fragmentation pattern (Figure 4.1). The proposed biotransformation pathways of 4F-MDMB-BINACA was presented in Figure 4.2.

4.5.1 *In vitro* metabolism

Twenty-two, seventeen and nine metabolites were tentatively identified after incubation of 4F-MDMB-BINACA with *C. elegans*, HLM and HepG2 cells, respectively.

Ester hydrolysis of 4F-MDMB-BINACA generated 4F-MDMB-BINACA ester hydrolysis metabolite, 4F-MDMB-BINACA 3,3-dimethylbutanoic acid (B22) with further dehydrogenation (B20), monohydroxylation (B8, B9, B13) with further dehydrogenation (B5/B6, B14), oxidative defluorination (B2) with subsequent oxidation to butanoic acid (B4) and N-dealkylation (B1). Other metabolites retained the terminal methyl ester moiety and their biotransformation tentatively identified included: monohydroxylation (B19/B21, B23/B25) with further carbonylation (B24), dihydroxylation (B10, B12/B15), oxidative defluorination (B18) and further oxidation to butanoic acid (B17) and N-dealkylation (B16). Phase II glucosidation (B7) and sulfation (B11) metabolites were only detected in the *C. elegans* model. The tentative structure elucidation of these various metabolites from the different models examined were constructed and shown below.

ID	RT (min)	Biotransformation	Formula	Exact Mass $[M+H]^+$	U	F	M	H
B1	5.30	Ester hydrolysis, N-dealkylation	$C_{14}H_{17}N_3O_3$	276.1343	✓	✓	✓	✓
B2	5.40	Ester hydrolysis, oxidative defluorination	$C_{18}H_{25}N_3O_4$	348.1918	✓	✓	✓	✓
B3	5.40	Ester hydrolysis, oxidative defluorination to butanoic acid, dehydrogenation	$C_{18}H_{21}N_3O_5$	360.1550		✓		
B4	5.45	Ester hydrolysis, oxidative defluorination to butanoic acid	$C_{18}H_{23}N_3O_5$	362.1710	✓	✓	✓	
B5	5.50	Ester hydrolysis, monohydroxylation (butyl), dehydrogenation	$C_{18}H_{22}FN_3O_4$	364.1667		✓		
B6	5.70	Ester hydrolysis, monohydroxylation (butyl), dehydrogenation	$C_{18}H_{22}FN_3O_4$	364.1667		✓	✓	
B7	5.80	Monohydroxylation (indazole), glucosidation	$C_{25}H_{36}FN_3O_9$	542.2508		✓		
B8	5.85	Ester hydrolysis, monohydroxylation (*tert*-leucine)	$C_{18}H_{24}FN_3O_4$	366.1824	✓	✓	✓	✓
B9	6.10	Ester hydrolysis, monohydroxylation (butyl)	$C_{18}H_{24}FN_3O_4$	366.1824		✓	✓	
B10	6.10	Dihydroxylation (butyl)	$C_{19}H_{26}FN_3O_5$	396.1929		✓		
B11	6.40	Monohydroxylation (indazole), sulfation	$C_{19}H_{26}FSN_3O_7$	460.1548		✓		
B12	6.60	Dihydroxylation (indazole, butyl)	$C_{19}H_{26}FN_3O_5$	396.1929		✓		
B13	6.70	Ester hydrolysis, monohydroxylation (indazole)	$C_{18}H_{24}FN_3O_4$	366.1824		✓	✓	✓
B14	6.75	Ester hydrolysis, monohydroxylation (*tert*-leucine), dehydrogenation	$C_{18}H_{22}FN_3O_4$	364.1667		✓	✓	
B15	6.90	Dihydroxylation (indazole, butyl)	$C_{19}H_{26}FN_3O_5$	396.1929		✓		
B16	7.10	N-dealkylation	$C_{15}H_{19}N_3O_3$	290.1499		✓	✓	✓
B17	7.30	Oxidative defluorination to butanoic acid	$C_{19}H_{25}N_3O_5$	376.1867	✓	✓	✓	✓
B18	7.35	Oxidative defluorination	$C_{19}H_{27}N_3O_4$	362.2074	✓	✓	✓	✓
B19	7.70	Monohydroxylation (butyl)	$C_{19}H_{26}FN_3O_4$	380.1980		✓	✓	
B20	7.90	Ester hydrolysis, dehydrogenation	$C_{18}H_{22}FN_3O_3$	348.1718	✓	✓	✓	✓
B21	8.10	Monohydroxylation (butyl)	$C_{19}H_{26}FN_3O_4$	380.1980		✓	✓	
B22	8.30	Ester hydrolysis	$C_{18}H_{24}FN_3O_3$	350.1874	✓	✓	✓	✓
B23	8.50	Monohydroxylation (indazole)	$C_{19}H_{26}FN_3O_4$	380.1980			✓	
B24	9.00	Carbonylation	$C_{19}H_{24}FN_3O_4$	378.1824		✓		
B25	9.60	Monohydroxylation (indazole)	$C_{19}H_{26}FN_3O_4$	380.1980			✓	
B0	12.00	4F-MDMB-BINACA	$C_{19}H_{26}FN_3O_3$	364.2031		✓	✓	✓

Table 4.1 *In vitro* metabolites of 4F-MDMB-BINACA tentatively identified using *C. elegans* (F), human liver microsomes (M) and HepG2 (H) models. Mass error of the precursor ion ≤ 5.00 ppm and mass error of product ions ≤ 20.00 ppm. (U): *In vivo* urine samples

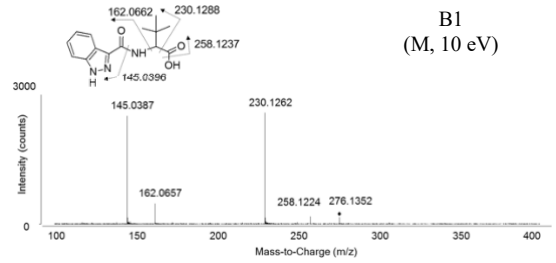
B1
(M, 10 eV)
Intensity (counts)
Mass-to-Charge (m/z)

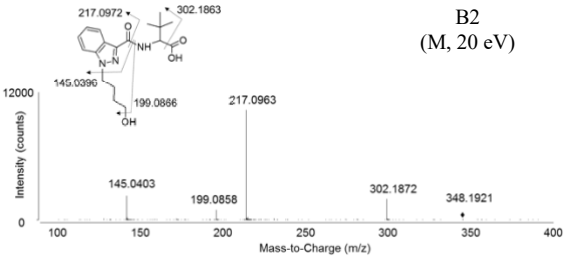
B2
(M, 20 eV)
Intensity (counts)
Mass-to-Charge (m/z)

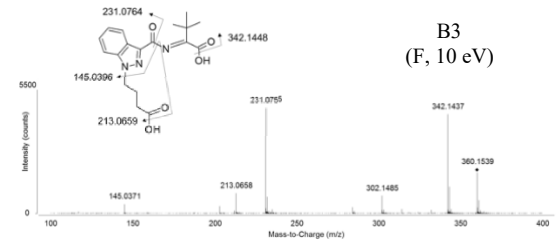
B3
(F, 10 eV)
Intensity (counts)
Mass-to-Charge (m/z)

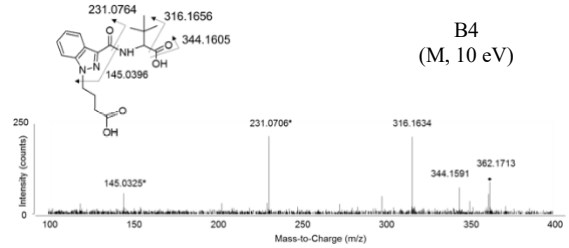
B4
(M, 10 eV)
Intensity (counts)
Mass-to-Charge (m/z)

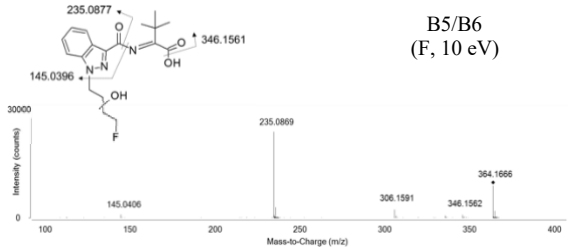
B5/B6
(F, 10 eV)
Intensity (counts)
Mass-to-Charge (m/z)

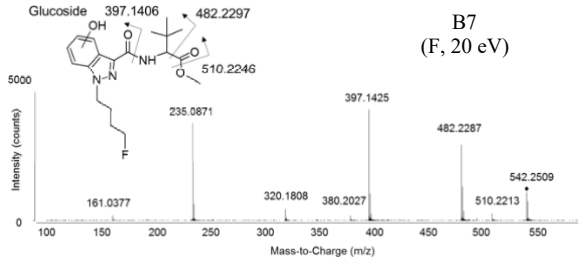
B7
(F, 20 eV)
Glucoside
Intensity (counts)
Mass-to-Charge (m/z)

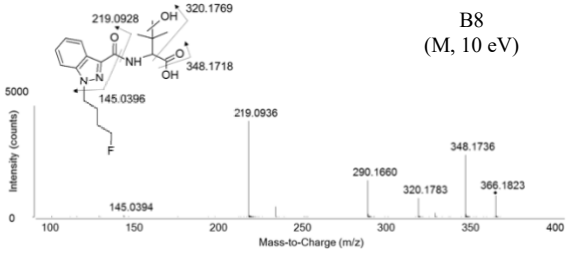
B8
(M, 10 eV)
Intensity (counts)
Mass-to-Charge (m/z)

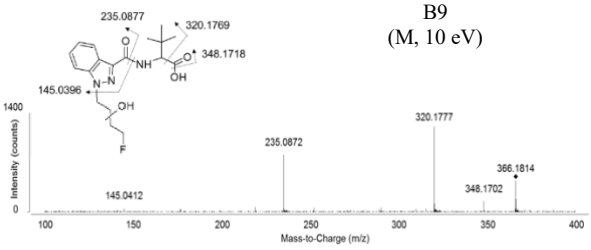
B9
(M, 10 eV)
Intensity (counts)
Mass-to-Charge (m/z)

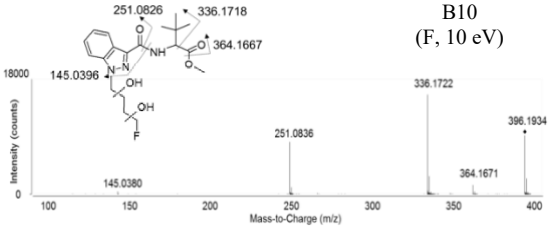
B10
(F, 10 eV)
Intensity (counts)
Mass-to-Charge (m/z)

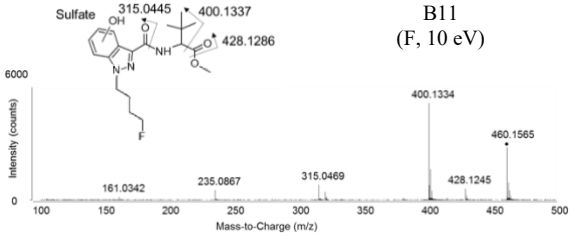
B11
(F, 10 eV)
Sulfate
Intensity (counts)
Mass-to-Charge (m/z)

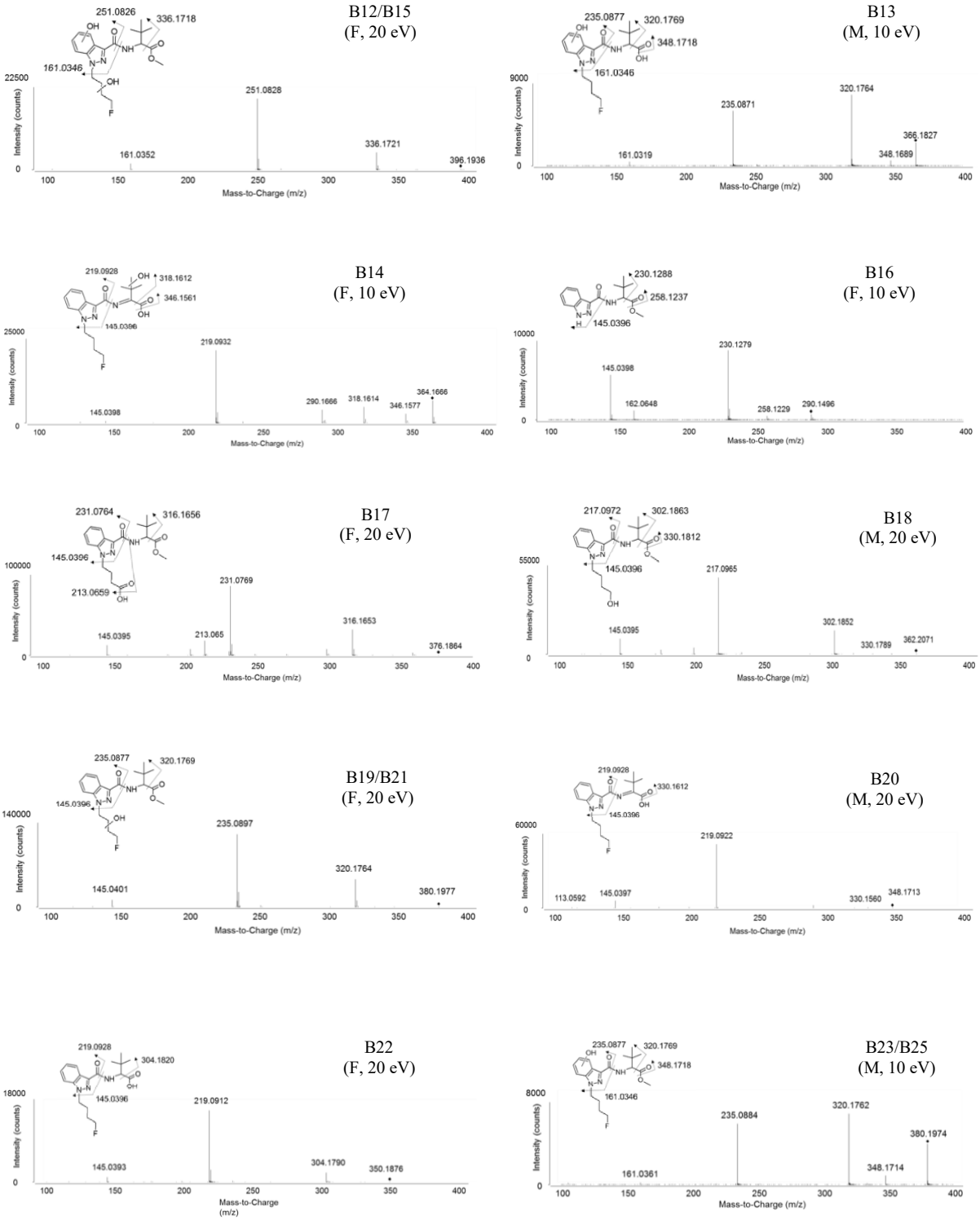
B12/B15
(F, 20 eV)
B13
(M, 10 eV)
B14
(F, 10 eV)
B16
(F, 10 eV)
B17
(F, 20 eV)
B18
(M, 20 eV)
B19/B21
(F, 20 eV)
B20
(M, 20 eV)
B22
(F, 20 eV)
B23/B25
(M, 10 eV)
Intensity (counts)
Mass-to-Charge (m/z)

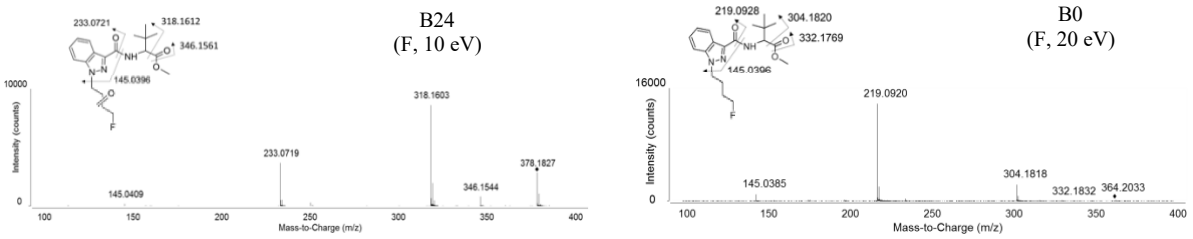

Figure 4.1 Product ion spectra and structures with the suggested fragmentation patterns from the three *in vitro* models: *C. elegans* (F), human liver microsomes (M) and HepG2 (H). Bracket indicates spectra obtained from one of the *in vitro* models with CE 10 or 20 eV. The exact position of the hydroxylation was not determined

4.5.2 Phase I Biotransformation

Ester hydrolysis, dehydrogenation, hydroxylation, oxidation and dealkylation

4F-MDMB-BINACA was hydrolysed via ester hydrolysis forming the 4F-MDMB-BINACA ester hydrolysis metabolite (B22). The product ion spectrum was very similar to 4F-MDMB-BINACA (*m/z* 304, 219, 145). The precursor ion, *m/z* 350 showed a loss of 14 Da explaining the hydrolysis of methyl ester from 4F-MDMB-BINACA. B20 showed similar product ion fragmentation pattern to that of B22 (*m/z*, 219, 145) and additional loss of 2 Da from *m/z* 350, indicating ester hydrolysis and further dehydrogenation at the *tert*-leucine moiety.

Metabolites identified at *m/z* 366 (B8, B9, B13), which was 16 Da higher than the 4F-MDMB-BINACA ester hydrolysis metabolite (B22), confirmed monohydroxylation upon ester hydrolysis. Presence of the ion *m/z* 320, likely formed from a loss of carbon dioxide, indicated monohydroxylation at the *tert*-leucine in B8 (*m/z* 219), butyl side chain in B9 (*m/z* 145) and indazole moiety in B13 (*m/z* 161). Precursor ion, *m/z* 364 (B14, B5/B6) had a loss of 2 Da from *m/z* 366 indicated further dehydrogenation of the ester hydrolysis, monohydroxylated metabolites. Dehydrogenation occurred at the *tert*-leucine moiety for both the butyl side chain (B5/B6) and *tert*-leucine moiety (B14) monohydroxylated metabolites, indicated by the presence of product ions *m/z* 235/346 and *m/z* 219/346, respectively. Similarly, precursor ion identified at *m/z* 380 (B19/B21, B23/B25) was 16 Da higher than the 4F-MDMB-BINACA, indicating

monohydroxylation at the butyl side chain (B19/B21) and indazole (B23/B25) moieties with product ions *m/z* 145 and 161, respectively. Metabolite identified at *m/z* 378 had very similar product ion spectra with B19/B21 except it was 2 Da lower (equating to the loss of 2 hydrogen atoms) while retaining the same product ion *m/z* 145, indicative of carbonylation at the butyl side chain moiety.

Precursor ion *m/z* 396 (B10, B12/B15) was 32 Da higher than the parent drug, 4F-MDMB-BINACA, suggesting the addition of two hydroxy groups. Product ion *m/z* 336 (loss of methyl ester moiety) further confirmed the presence of dihydroxylated metabolites. The presence of product ion *m/z* 251 at B10 and B12/B15 was explained by noting that hydroxylation occurred at the indazole/butyl side chain moieties and not at the *tert*-leucine moiety. B10 showed product ion *m/z* 145 indicating intact indazole moiety and suggested that dihydroxylation occurred at the butyl side chain moiety. The presence of product ion *m/z* 161 in B12/B15, indicated that hydroxylation occurred at the indazole moiety, whilst the second hydroxylation site must be assigned at the butyl side chain moiety by default.

Precursor ion *m/z* 348 and product ion detected at *m/z* 217 (B2) identified was 2 Da less than the 4F-MDMB-BINACA ester hydrolysis metabolite (B22), indicating oxidative defluorination (loss of fluorine with addition of hydroxy group). Product ions detected at *m/z* 302, 217 and 145 confirmed that *tert*-leucine and indazole moieties remained unchanged, leading to structure elucidation of a hydroxy functional group at the 4-position of the butyl side chain by oxidative defluorination. Oxidation of 4'-hydroxybutyl moiety in B2 led to formation of 4'-carboxybutyl metabolite (B4) having a precursor ion of *m/z* 362, which was 14 Da higher than the m/z for B2 (loss of two hydrogen atoms with addition of hydroxy group). Precursor ion *m/z* 360 and product ion detected at *m/z* 342 (B3) identified was 2 Da less than precursor ion at *m/z* 362 (B4) indicated further dehydrogenation at the *tert*-leucine moiety.

The precursor ion at *m/z* 276 (B1) detected was 74 Da lower than that for the 4F-MDMB-BINACA ester hydrolysis metabolite (B22), indicated *N*-dealkylation of B22. The product ion detected at *m/z* 230 was assigned as a neutral loss of HCOOH.

N-Dealkylation

The precursor ion at *m/z* 290 (B16) which was 74 Da lower than the corresponding *m/z* for 4F-MDMB-BINACA, indicated N-dealkylation of 4F-MDMB-BINACA. Product ions *m/z* 258, 230 and 145 showed loss of a single methoxy group, methyl ester and indazole carbonyl fragment, respectively. Taken together these data further confirmed the structure elucidation of B16.

Oxidative defluorination and oxidation

Metabolite B18 with precursor ion at *m/z* 362 and product ions 330, 302, 217 were consecutively 2 Da less than that of the precursor and product ions of 4F-MDMB-BINACA, indicative of oxidative defluorination. Further oxidation of 4'-hydroxybutyl moiety of B18 resulted in 4'-carboxybutyl, B17 *(m/z* 376) having product ions 316, 231 and 213. The product ion identified at ions with *m/z* 316 and 231 were 14 Da higher than that of product ions 302 and 217 respectively, in B18, consistent with the formation of a butanoic acid metabolite.

4.5.3 Phase II Biotransformation

Glucosidation

Precursor ion, *m/z* 542 (B7) resulted from glucosidation of B23/B25. Both have product ions *m/z* 320, 235 and 161. The product ion detected at *m/z* 380 was produced by neutral loss of 162 Da (glucoside).

Sulfation

Precursor ion, *m/z* 460 (B11) detected was a result of sulfation of intermediate metabolite similar to B23/B25. The product ion detected at *m/z* 235 indicating loss of sulfate confirmed the identity of the sulfation metabolite.

4.5.4 Comparison among the *in vitro* models

The major *in vitro* phase I metabolites (> 10 % peak area ratio) tentatively identified were monohydroxylation at the butyl side chain and oxidative defluorination to butanoic acid

for the *C. elegans* model. HLM model produced four major metabolites: ester hydrolysis with/without dehydrogenation, monohydroxylation at indazole moiety and oxidative defluorination. HepG2 model only produced one major metabolite which is the ester hydrolysis of 4F-MDMB-BINACA. Although the metabolite ranking may differ in all the three models, four common metabolites amongst the seven most abundant metabolites were identified (Figure 4.3 A-D): ester hydrolysis (B22, *m/z* 350), ester hydrolysis followed by dehydrogenation (B20, *m/z* 348), oxidative defluorination (B18, *m/z* 362) and further oxidation to butanoic acid (B17, *m/z* 376).

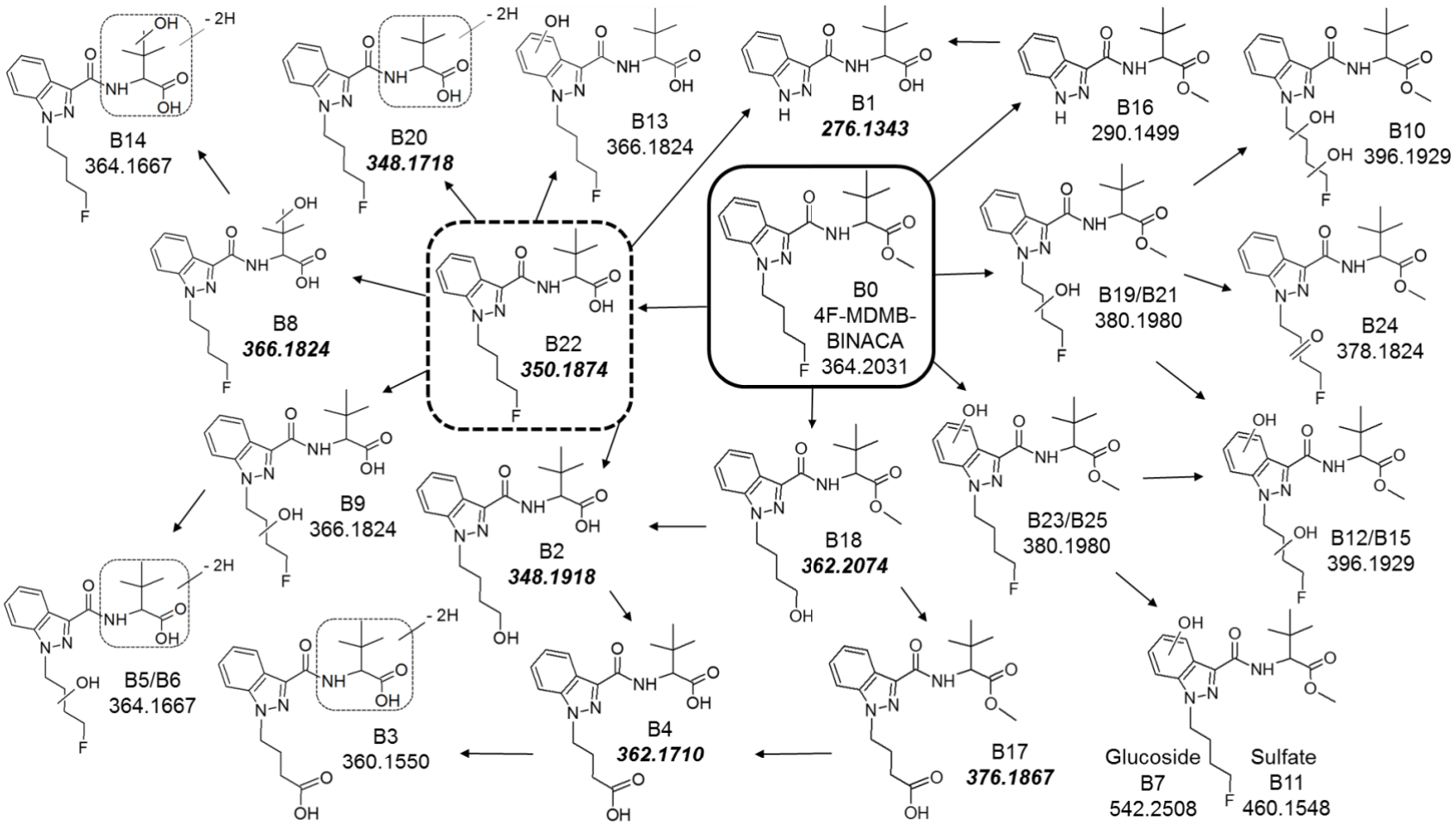

Figure 4.2 Proposed metabolic pathway of 4F-MDMB-BINACA. *In vivo* metabolites were in italics and bold. The exact position of the metabolites with hydroxylation structure were not determined

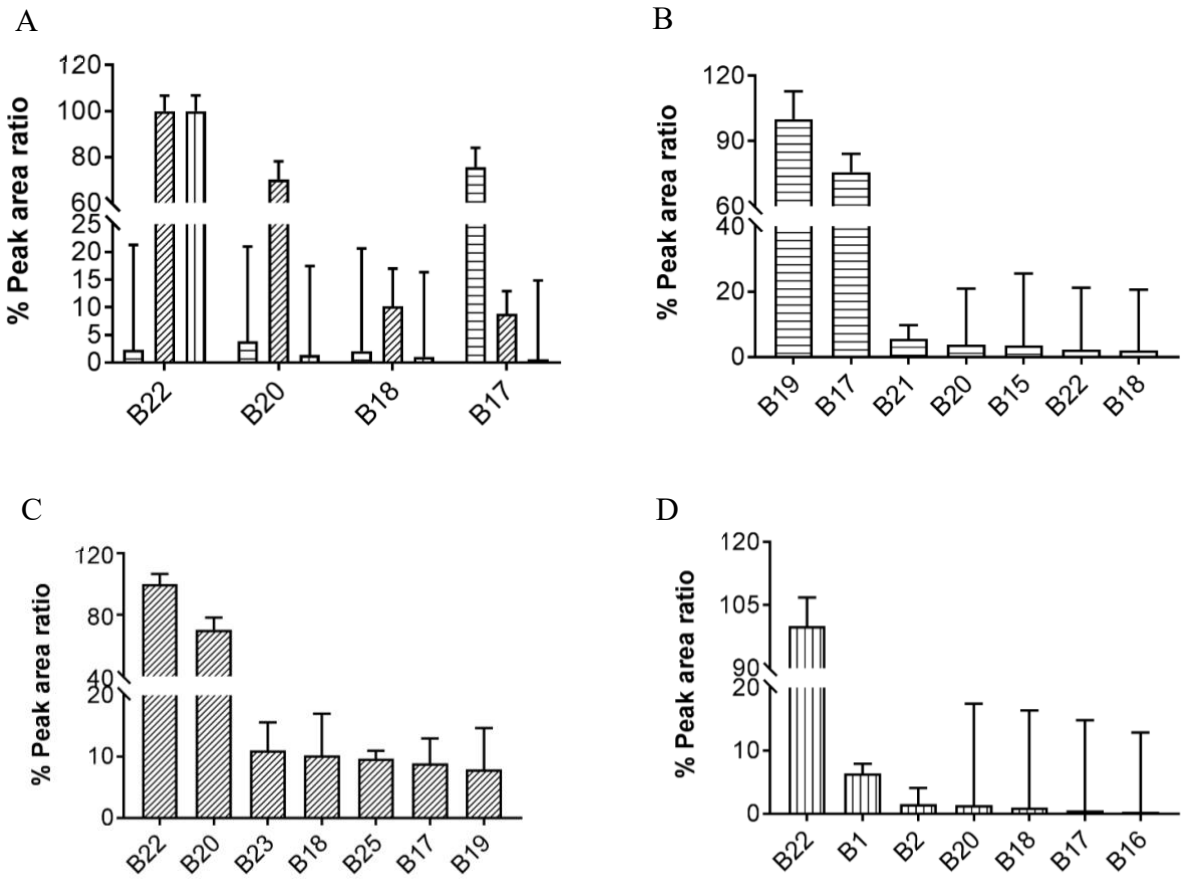

ID	Biotransformation	Exact Mass $[M+H]^+$
B1	Ester hydrolysis, N-dealkylation	276.1343
B2	Ester hydrolysis, oxidative defluorination	348.1918
B15	Dihydroxylation (indazole, butyl)	396.1929
B16	N-dealkylation	290.1499
B17	Oxidative defluorination to butanoic acid	376.1867
B18	Oxidative defluorination	362.2074
B19	Monohydroxylation (butyl)	380.1980
B20	Ester hydrolysis, dehydrogenation	348.1718
B21	Monohydroxylation (butyl)	380.1980
B22	Ester hydrolysis	350.1874
B23	Monohydroxylation (indazole)	380.1980
B25	Monohydroxylation (indazole)	380.1980

Figure 4.3 (A) Common *in vitro* metabolites among the seven most abundant metabolites in (B) *C. elegans* (C) HLM and (D) HepG2 model. *C. elegans*, HLM and HepG2 are represented by horizontal, diagonal and vertical bar lines, respectively. Error bars reflect the relative abundance variation of a specific metabolite within the analysed group (n = 3)

4.5.5 *In vivo* metabolism

A total of eight metabolites were detected in the analysed human urine samples. The average % peak area ratio of the urine metabolites from twenty urine samples were tabulated and compared to that of the *in vitro* metabolites (Table 4.2).

Ester hydrolysis biotransformation constituted the dominant metabolic pathway for the *in vivo* metabolism in human urine samples. The prevalence of the tentative identified metabolites was as follows: 4F-MDMB-BINACA ester hydrolysis metabolite (B22, *m/z* 350, 20/20 samples) followed by further dehydrogenation (B20, *m/z* 348, 18/20 samples). Both ester hydrolysis followed by oxidative defluorination to butanoic acid (B4, *m/z* 362) and monohydroxylation at *tert*-leucine moiety (B8, *m/z* 366) metabolites were found in 16/20 urine samples. Ester hydrolysis followed with *N*-dealkylation (B1, *m/z* 276) metabolite was found in 15/20 urine samples. Oxidative defluorination (B18, *m/z* 362) and ester hydrolysis of oxidative defluorination (B2, *m/z* 348) metabolites were detected in 13/20 and 12/20 urine samples, respectively. Oxidative defluorination to butanoic acid metabolite (B17, *m/z* 376) was detected in the least number of urine samples (7/20 samples). Only 3/20 urine samples were identified with the parent drug, 4F-MDMB-BINACA, highlighting the risk of analysing only parent ion and emphasizing the importance of metabolite identification in the forensic and clinical setting. The metabolite ranking was different for different individual urine samples.

The analysed urine samples (17/20 samples) were also detected with other SCBs such as methyl 2-([1-(5-fluoropentyl)-1H-indole-3-carbonyl]amino)-3,3-dimethylbutanoate (5F-MDMB-PICA), Methyl 3,3-dimethyl-2-[1-(pent-4-en-1-yl)-1H-indazole-3-carboxamido] butanoate (MDMB-4en-PINACA), methyl [1-(4-fluorobenzyl)-1H-indazole-3-carbonyl]valinate (MMB-FUBINACA), Methyl-2-([1-(5-fluoropentyl)-1H-indazole-3-carbonyl]amino)-3,3-dimethylbutanoate (5F-MDMB-PINACA) and other drugs such as methamphetamine, *N*-methyl-1-(3,4-methylenedioxyphenyl)propan-2-amine (MDMA) and ketamine (data not shown). Three out of twenty urine samples were found to contain only metabolites of 4F-MDMB-BINACA (Table 4.3). From these three samples, sample 2 contained only an ester hydrolysis metabolite (m/z 350). Both sample 1 and 3 have similar first four metabolites in terms of % peak area ratio ranking: (1) ester hydrolysis (ion detected at *m/z* 350), (2)

ester hydrolysis, oxidative defluorination to butanoic acid (ion detected at *m/z* 362), (3) ester hydrolysis, monohydroxylation (ion detected at *m/z* 366) and (4) ester hydrolysis, dehydrogenation (ion detected at *m/z* 348).

ID	**Exact Mass $[M+H]^+$**	**Biotransformation**	***In vivo* metabolites % peak area ratio (sample size)**	***In vitro* metabolites % peak area ratio**		
				C. elegans	**HLM**	**HepG2**
B22	350.1874	Ester hydrolysis	100 (20/20)	2.3	***100***	***100***
B20	348.1718	Ester hydrolysis, dehydrogenation	1.7 – 9.4 (18/20)	3.8	***70***	1.4
B4	362.1710	Ester hydrolysis, oxidative defluorination to butanoic acid	1.5 – 27 (16/20)	0.016	0.25	ND
B8	366.1824	Ester hydrolysis, monohydroxylation (*tert*-leucine)	3.7 – 14 (16/20)	0.067	1.9	0.14
B1	276.1343	Ester hydrolysis, N-dealkylation	0.65 – 29 (15/20)	0.003	0.73	6.4
B18	362.2074	Oxidative defluorination	1.4 – 5.4 (13/20)	2.1	***10***	1.0
B2	348.1918	Ester hydrolysis, oxidative defluorination	2.0 – 11 (12/20)	0.005	0.67	1.5
B17	376.1867	Oxidative defluorination to butanoic acid	0.26 – 1.4 (7/20)	***76***	8.9	0.57

ND: Not detected

Table 4.2 Comparison of the *in vitro* metabolites from the three models (n = 3) with the *in vivo* metabolites obtained from authentic human urine samples (n = 20). Major *in vitro* metabolites (> 10 % peak area ratio) are in italics and bold

ID	Exact Mass $[M+H]^+$	Biotransformation	% Peak area ratio (ranking)		
			Sample 1	Sample 2	Sample 3
B22	350.1874	Ester hydrolysis	100 (1)	100 (1)	100 (1)
B20	348.1718	Ester hydrolysis, dehydrogenation	4.9 (4)	ND	4.2 (4)
B4	362.1710	Ester hydrolysis, oxidative defluorination to butanoic acid	12 (2)	ND	6.8 (2)
B8	366.1824	Ester hydrolysis, monohydroxylation (*tert*-leucine)	7.4 (3)	ND	5.2 (3)
B1	276.1343	Ester hydrolysis, *N*-dealkylation	ND	ND	0.81 (7)
B18	362.2074	Oxidative defluorination	2.2 (5)	ND	2.3 (6)
B2	348.1918	Ester hydrolysis, oxidative defluorination	ND	ND	2.7 (5)
B17	376.1867	Oxidative defluorination to butanoic acid	0.55 (6)	ND	ND
B0	364.2031	4F-MDMB-BINACA	0.020	ND	ND

ND: Not detected

Table 4.3 *In vivo* urinary profile of individual urine samples that contain only 4F-MDMB-BINACA metabolites

4.6 Discussion

Glucosides (B7) and sulfate (B11) phase II metabolites of 4F-MDMB-BINACA were tentatively identified in the *C. elegans* model. Glucosides and sulfate metabolites have been reported with other SCBs where *C. elegans* was employed as the *in vitro* model [24]. Sulfate and glucuronide phase II metabolites of 4F-MDMB-BINACA was identified by Wagmann *et al.* [29]. However, glucuronides of 4F-MDMB-BINACA were not observed in the *C. elegans* model, which is consistent with findings from previous studies [23, 24]. Rydevik *et al.* described an easy method to generate endogenous glucuronide conjugates from glucosides using free radical tetramethylpiperidinyl-1-oxy, hence proving *C. elegans*' relevance in mammalian phase II metabolism [33]. Nevertheless, phase I metabolites are usually better marker metabolites compared to phase II metabolites because of its higher mass spectrometry responses and stability over time [34].

The most prevalent and abundant *in vivo* metabolite was that derived from the hydrolysis of metabolically labile terminal methyl ester moiety via a two-step reaction mechanism by the carboxylesterases (CES) [35]. The finding is similar to that obtained by Krotulski *et al.* [5], Haschimi *et al.* [30] and Wagmann *et al.* [29]. This outcome was anticipated since CES-mediated hydrolysis is commonly reported as the major metabolic pathway among the SCBs impacting the terminal ester group [36]. Similar to the *in vivo* findings, 4F-MDMB-BINACA ester hydrolysis (B22) was the major metabolite for both HepG2 and HLM models, consistent with the known hydrolytic activity of CES reported [37]. Wagmann *et al.* established that ester hydrolysis of 4F-MDMB-BINACA is catalysed by the CES1 isoform, in agreement with the preference of CES1 in metabolizing ester substrates that contain a small alcohol group and a bulky acyl group [35]. As CES constitute the major metabolic pathway for the metabolism of 4F-MDMB-BINACA, inter-individual CES1 variability due to genetic polymorphism cannot be overlooked [38].

Ester hydrolysis, dehydrogenation metabolite (B20) was the second most abundant major metabolite in the HLM model, similar to the *in vivo* findings where it is the second most prevalent metabolite detected in 18/20 urine samples. Ester hydrolysis with dehydrogenation formed *in vivo* in this study was also reported among other indazole carboxamide type SCBs with *tert*-leucine methyl ester moiety such as 5F-MDMB-

PINACA [15] and MDMB-4en-PINACA [39, 40]. This biotransformation was reported by both Krotulski *et al.* and Haschimi *et al.* However, it was proposed by Wagmann *et al.* that this metabolite is more likely a lactone product formed after hydroxylation of the *tert*-leucine moiety, with or without former ester hydrolysis of 4F-MDMB-BINACA, based upon the presence of fragments with *m/z* 320 ($C_{17}H_{23}FN_3O_2^+$) and *m/z* 113 ($C_6H_9O_2^+$), a 4,4-dimethyl-2-oxotetrahydrofuran-3-ylium ion in positive ionisation mode, which appear to be more easily formed from lactone, and the absence of these lactone metabolites in negative ionisation mode due to its non-ionizable nature in contrast to ionizable carboxylic acids. Although this proposal sounds plausible, it is not without question. The presence of *m/z* 330 ($C_{18}H_{21}FN_3O_2^+$) in their spectrum of "lactone" indicates loss of H_2O from the precursor ion and similarly the presence of *m/z* 332 ($C_{18}H_{23}FN_3O_2^+$) due to loss of H_2O was observed for ester hydrolysis metabolite, and yet such a H_2O loss fragment ion was not observed for the parent molecule retaining a methyl ester moiety. These results suggest that this compound is more likely to have a carboxylic acid than an ester, which contradicts the aforementioned reasoning by Wagmann *et al.* The same authors also proposed lactone formation for the B3 and B14 metabolites. Careful examination of results in this study showed the presence of the ion at *m/z* 113 in very low signal intensity for B20 but not found for both B3 and B14 product ion spectra. Moreover, B3 and B14 were detected in the negative ESI mode but not for B20 (Table 4.4). Based upon these findings, it appeared that both lactone and dehydrogenation metabolites were present but since mass spectral results can be inconclusive and indeed seemed to be contradictory in this case, further comprehensive structural analysis by nuclear magnetic resonance (NMR) spectroscopy are needed for confirmation.

ID	RT (min)	Biotransformation	Precursor Ion Exact Mass $[M-H]^-$	CE (eV)	Formula	Product Ions Exact Mass $[M^-]$	Product Ions Mass error (ppm)
B3	5.42	Ester hydrolysis, oxidative defluorination to butanoic acid, dehydrogenation	358.1408	10	$C_{14}H_{14}N_3O_3$	272.1041	3.3
					$C_7H_8NO_3$	154.0510	2.6
					$C_7H_5N_2$	117.0458	4.3
B14	6.75	Ester hydrolysis, monohydroxylation (*tert*-leucine), dehydrogenation	362.1522	20	$C_{17}H_{21}FN_3O_2$	318.1623	12
					$C_{12}H_{13}FN_3O$	234.1048	4.3
					$C_{11}H_{12}FN_2$	191.0990	-11
					$C_{11}H_{11}N$	171.0928	-2.3

Table 4.4 Product ion spectra of B3 and B14 metabolites obtained in the negative electrospray ionization (ESI) mode. Mass error of the precursor ion ≤ 5.00 ppm

Oxidative defluorination metabolite (B18), the second major metabolite (% peak area ratio > 10) in HLM model was detected as the third least prevalent metabolite in the *in vivo* samples. Oxidative defluorination with subsequent butanoic acid formation (B17) metabolite, the second major metabolite after monohydroxylation in the *C. elegans* model was the least prevalent metabolite found among the 20 urine samples. Fluoro-substituted SCB at the 5-pentyl position of pentylindole/pentylindazole moiety was found to give rise to predominantly 5-hydroxypentyl and 5-pentanoic acid metabolites [41]. However, oxidative defluorination with (B17) or without further butanoic acid (B18) metabolite were found only in 7 and 13 urines samples, respectively. B18 metabolite was ranked third by Haschimi et al., whilst B17 was ranked second by Krotulski *et al.* in terms of relative peak area abundance. One possible explanation for the differences was that both Haschimi *et al.* and Krotulski *et al.* used relative peak area abundance for the ranking but for this study, the metabolite prevalence in the urine samples was employed instead. The major *in vitro* metabolites discussed above: B22, B20, B18 and B17 (Table 4.2) were also the four common metabolites identified among the seven most abundant metabolites for each model (Figure 4.3 A-D), demonstrating complementary *in vitro* findings that may assist in further streamlining selection of suitable urinary marker(s).

As most of the urine samples obtained in this study was found to contain other SCBs' metabolites and other drugs, the urinary profile of the three individual urine samples that encompass 4F-MDMB-BINACA metabolites exclusively (Table 4.3) is

worth considering when selecting a suitable urinary marker. The four most abundant metabolites identified (B22, B4, B8 and B20) among the three urine samples coincided with the top four most prevalent metabolites found in the 20 urine samples. This indicated that the phase I metabolism of 4F-MDMB-BINACA are unlikely to be affected significantly by polydrug intake. Wagmann *et al.* identified CYP3A5, CYP3A4, CYP1A2, CYP2C8 and CYP2C19 involvement in the phase I metabolism of 4F-MDMB-BINACA also excluded the possibility of single CYP enzyme that may impact the *in vivo* biotransformation of 4F-MDMB-BINACA.

It is difficult to assign a ranking to the *in vivo* metabolites based upon % peak area ratio as wide inter-individual variability were observed among the metabolites. The % peak area abundance ratio of metabolites detected in the urine samples are often affected by numerous factors such as drug intake behaviour (intake route, amount of drug and intake frequency), time from last drug intake [16] and metabolic stability. It should be noted that % peak area abundance ratio do not necessarily reflect absolute concentrations due to differences in ionization capacity and matrix effects bias for each metabolite. Exact ranking of metabolites with respect to their peak area abundance would require further validated quantification of the metabolites. Moreover, genetic makeup, physiological conditions (age, gender and ethnicity), environmental influences (diet) and pathological factors (liver diseases, diabetes, and obesity) would further complicate the metabolism of drugs. Thus, identification of the relevant urinary markers was based primarily upon the prevalence of the *in vivo* metabolites instead of the metabolites ranking that was based upon % peak area abundance ratio. The urinary marker selected would also be preferably found in all the three *in vitro* models especially in the *C. elegans* model where metabolites production could be scaled up to allow isolation and characterization of the metabolites.

Based upon the two criterion and the above findings, suggested relevant *in vivo* urinary markers were ester hydrolysis, *m/z* 350 (B22, in 20/20 samples) and ester hydrolysis followed by dehydrogenation, m/z 348 (B20, in 18/20 samples) metabolites. Ester hydrolysis with subsequent oxidative defluorination to butanoic acid metabolite (*m/z* 362, B4) detected in 16/20 urine samples may seemed to be a choice urinary marker as it appeared to have higher % peak area ratio when compared to ester hydrolysis dehydrogenation metabolite (B20). However, this metabolite was only detected in trace amounts in both the *C. elegans* and HLM models. Hence, structural elucidation could not

be confirmed unless a reference standard is made available. Despite the relatively high % peak area ratio and detection in 16/20 urine samples, ester hydrolysis followed by monohydroxylation at the *tert*-leucine moiety (*m/z* 366, B8) metabolite was not reported among the 17 urine samples from forensic psychiatric ward and prison in Haschimi *et al.*'s study. Hence, the use of this metabolite as urinary marker was not selected.

Finally, comparison of the results obtained from incubations of 4F-MDMB-BINACA with three different models showed that all of them were in agreement with the tentatively identified urinary metabolites. *C. elegans* and HLM models detected all of the *in vivo* metabolites (100 %), whilst HepG2 cells detected 7 out of the 8 *in vivo* metabolites (87.5 %). HepG2 model detected the major ester hydrolysis metabolite of 4F-MDMB-BINACA in abundance but the rest of the metabolites were found in small amount. This might be due to the low activity of numerous metabolizing enzymes resulting in lower drug biotransformation [42]. Comparison of *C. elegans* with *in vivo* metabolites showed that while *C. elegans* has limitations such as low abundance of ester hydrolysis metabolite, in general, the metabolic profiles were in good agreement. The findings also supported that *C. elegans* possessed enzymatic activity that mimics human metabolism of 4F-MDMB-BINACA. HLM possessed both the CYP and carboxylesterase enzymes accounted for biotransformation that matches with the *in vivo* findings. It should be noted that chemical structures of the tentative elucidated metabolites have not been unequivocally confirmed. With *C. elegans* model, scaling up of metabolites production for nuclear magnetic resonance (NMR) spectroscopy could provide unequivocal structural elucidation of the metabolites. *C. elegans* has also been reported to form and trap active metabolites using trapping agents such as glutathione [28]. Scaling up these potential active metabolites conjugates allows the identification of potential metabolite toxicities thus giving an enhanced understanding of the toxicity mechanism of 4F-MDMB-BINACA. Therefore, *C. elegans* is a useful complementary metabolic model for SCBs, especially when larger quantity of metabolites is required.

4.7 Conclusion

The present study showed that HLM proved to be a suitable predictive *in vitro – in vivo* extrapolation model for 4F-MDMB-BINACA. *C. elegans* demonstrated the ability to form all of the *in vivo* metabolites and has the potential to be used as a complementary model to predict and characterize human metabolites, as well as identifying possible drug toxicities for emerging SCBs. For the identification of 4F-MDMB-BINACA intake, ester hydrolysis (B22) and ester hydrolysis followed by dehydrogenation (B20) metabolites were identified as specific and relevant urinary markers. The difficulty in unequivocally identifying the structures of dehydrogenation metabolites including B20 by mass spectrometry demonstrate the need to utilise NMR spectroscopy. Future work will include isolation and confirmation of scaled-up reactions by *C. elegans* model to confirm the proposed chemical structure assignments to the metabolites identified here.

4.8 References

1. Cohen, K. & Weinstein, A. M. (2018) Synthetic and Non-synthetic Cannabinoid Drugs and Their Adverse Effects-A Review From Public Health Prospective, *Frontiers in public health.* **6**, 162.

2. Brandt, S., Poovendran, D. (2019) 4F-MDMB-BINACA. Critical Review Report, *World Health Organization Expert Committee on Drug Dependence (ECCD) Forty-second Meeting*, 1-24.

3. Banister, S. D., Longworth, M., Kevin, R., Sachdev, S., Santiago, M., Stuart, J., Mack, J. B. C., Glass, M., McGregor, I. S., Connor, M. & Kassiou, M. (2016) Pharmacology of Valinate and tert-Leucinate Synthetic Cannabinoids 5F-AMBICA, 5F-AMB, 5F-ADB, AMB-FUBINACA, MDMB-FUBINACA, MDMB-CHMICA, and Their Analogues, *ACS chemical neuroscience.* **7**, 1241-1254.

4. Schoeder, C. T., Hess, C., Madea, B., Meiler, J. & Muller, C. E. (2018) Pharmacological evaluation of new constituents of "Spice": synthetic cannabinoids based on indole, indazole, benzimidazole and carbazole scaffolds.(Report), *Forensic Toxicology.* **36**, 385.

5. Krotulski, A. J., Mohr, A. L. A., Kacinko, S. L., Fogarty, M. F., Shuda, S. A., Diamond, F. X., Kinney, W. A., Menendez, M. J. & Logan, B. K. (2019) 4F-MDMB-BINACA: A New Synthetic Cannabinoid Widely Implicated in Forensic Casework, *Journal of forensic sciences.* **64**, 1451-1461.

6. Krotulski, A. J., Mohr, A.L.A. & Logan, B.K. (2018) *Trend Report: Q4 2018 Synthetic Cannabinoids in the United States (Detailed)*, https://www.forensicscienceeducation.org/wp-content/uploads/2019/02/Synthetic-Cannabinoid-Trend-Report_Detailed_2018-Q4.pdf (Assessed Aug 1, 2020).

7. Krotulski, A. J., Mohr, A.L.A. & Logan, B.K. (2019) *Trend Report: Q1 2019 Synthetic Cannabinoids in the United States (Detailed)*, https://www.forensicscienceeducation.org/wp-content/uploads/2019/04/Synthetic-Cannabinoid-Trend-Report_Detailed_2019-Q1.pdf (Assessed Aug 1, 2020).

8. Krotulski, A. J., Mohr, A.L.A. & Logan, B.K. (2019) *Trend Report: Q2 2019 Synthetic Cannabinoids in the United States (Detailed)*, https://www.npsdiscovery.org/wp-

content/uploads/2019/07/Synthetic-Cannabinoid-Trend-Report_Detailed_2019-Q2.pdf (Assessed Aug 1, 2020).

9. Krotulski, A. J., Mohr, A.L.A. & Logan, B.K. (2019) *Trend Report: Q3 2019 Synthetic Cannabinoids in the United States (Detailed)*, https://www.npsdiscovery.org/wp-content/uploads/2019/11/Synthetic-Cannabinoid-Trend-Report_Detailed_2019-Q3.pdf (Accessed Aug 1, 2020).

10. Fantegrossi, W. E., Moran, J. H., Radominska-Pandya, A. & Prather, P. L. (2014) Distinct pharmacology and metabolism of K2 synthetic cannabinoids compared to Δ9-THC: Mechanism underlying greater toxicity?, *Life Sciences.* **97**, 45-54.

11. Tai, S. & Fantegrossi, W. E. (2017) Pharmacological and Toxicological Effects of Synthetic Cannabinoids and Their Metabolites in *Neuropharmacology of New Psychoactive Substances (NPS): The Science Behind the Headlines* (Baumann, M. H., Glennon, R. A. & Wiley, J. L., eds) pp. 249-262, Springer International Publishing, Cham.

12. Richter, L. H. J., Flockerzi, V., Maurer, H. H. & Meyer, M. R. (2017) Pooled human liver preparations, HepaRG, or HepG2 cell lines for metabolism studies of new psychoactive substances? A study using MDMA, MDBD, butylone, MDPPP, MDPV, MDPB, 5-MAPB, and 5-API as examples, *Journal of Pharmaceutical and Biomedical Analysis.* **143**, 32-42.

13. Li, J., Liu, C., Li, T. & Hua, Z. (2018) UPLC-HR-MS/MS-based determination study on the metabolism of four synthetic cannabinoids, ADB-FUBICA, AB-FUBICA, AB-BICA and ADB-BICA, by human liver microsomes, *Biomedical Chromatography.* **32**, 4113.

14. Staeheli, S. N., Poetzsch, M., Veloso, V. P., Bovens, M., Bissig, C., Steuer, A. E. & Kraemer, T. (2018) In vitro metabolism of the synthetic cannabinoids CUMYL-PINACA, 5F–CUMYL-PINACA, CUMYL-4CN-BINACA, 5F–CUMYL-P7AICA and CUMYL-4CN-B7AICA, *Drug Testing and Analysis.* **10**, 148-157.

15. Yeter, O. & Öztürk, Y. E. (2019) Metabolic profiling of synthetic cannabinoid 5F-ADB by human liver microsome incubations and urine samples using high-resolution mass spectrometry, *Drug Testing and Analysis.* **11**, 847-858.

16. Mogler, L., Franz, F., Rentsch, D., Angerer, V., Weinfurtner, G., Longworth, M., Banister, S. D., Kassiou, M., Moosmann, B. & Auwärter, V. (2018) Detection of the

recently emerged synthetic cannabinoid 5F–MDMB-PICA in 'legal high' products and human urine samples, *Drug Testing and Analysis.* **10**, 196-205.

17. Westerink, W. M. A. & Schoonen, W. G. E. J. (2007) Cytochrome P450 enzyme levels in HepG2 cells and cryopreserved primary human hepatocytes and their induction in HepG2 cells, *Toxicology in Vitro.* **21**, 1581-1591.

18. Guo, L., Dial, S., Shi, L., Branham, W., Liu, J., Fang, J.-L., Green, B., Deng, H., Kaput, J. & Ning, B. (2011) Similarities and differences in the expression of drug-metabolizing enzymes between human hepatic cell lines and primary human hepatocytes, *Drug Metabolism and Disposition.* **39**, 528-538.

19. O'Brien, P. J. & Edvardsson, A. (2017) Validation of a Multiparametric, High-Content-Screening Assay for Predictive/Investigative Cytotoxicity: Evidence from Technology Transfer Studies and Literature Review, *Chemical research in toxicology.* **30**, 804-829.

20. Asha, S. & Vidyavathi, M. (2009) Cunninghamella – A microbial model for drug metabolism studies – A review, *Biotechnology Advances.* **27**, 16-29.

21. Grafinger, K. E., Stahl, K., Wilke, A., König, S. & Weinmann, W. (2018) In vitro phase I metabolism of three phenethylamines 25D-NBOMe, 25E-NBOMe and 25N-NBOMe using microsomal and microbial models, *Drug Testing and Analysis.* **10**, 1607-1626.

22. Grafinger, K. E., Wilke, A., König, S. & Weinmann, W. (2019) Investigating the ability of the microbial model Cunninghamella elegans for the metabolism of synthetic tryptamines, *Drug Testing and Analysis.* **11**, 721-729.

23. Watanabe, S., Kuzhiumparambil, U., Winiarski, Z. & Fu, S. (2016) Biotransformation of synthetic cannabinoids JWH-018, JWH-073 and AM2201 by Cunninghamella elegans, *Forensic Science International.* **261**, 33-42.

24. Watanabe, S., Kuzhiumparambil, U., Nguyen, M., Cameron, J. & Fu, S. (2017) Metabolic Profile of Synthetic Cannabinoids 5F-PB-22, PB-22, XLR-11 and UR-144 by Cunninghamella elegans, *The AAPS Journal.* **19**, 1148-1162.

25. Watanabe, S., Kuzhiumparambil, U. & Fu, S. (2018) In vitro metabolism of synthetic cannabinoid AM1220 by human liver microsomes and Cunninghamella elegans using liquid chromatography coupled with high resolution mass spectrometry, *Forensic toxicology.* **36**, 435-446.

26. Gaunitz, F., Dahm, P., Mogler, L., Thomas, A., Thevis, M. & Mercer-Chalmers-Bender, K. (2019) In vitro metabolic profiling of synthetic cannabinoids by pooled human liver microsomes, cytochrome P450 isoenzymes, and Cunninghamella elegans and their detection in urine samples, *Analytical and Bioanalytical Chemistry.* **411**, 3561-3579.

27. Zhang, D., Yang, Y., Leakey, J. E. & Cerniglia, C. E. (1996) Phase I and phase II enzymes produced by Cunninghamella elegans for the metabolism of xenobiotics, *FEMS microbiology letters.* **138**, 221-226.

28. Rydevik, A., Hansson, A., Hellqvist, A., Bondesson, U. & Hedeland, M. (2015) A novel trapping system for the detection of reactive drug metabolites using the fungus Cunninghamella elegans and high resolution mass spectrometry, *Drug Testing and Analysis.* **7**, 626-633.

29. Wagmann, L., Frankenfeld, F., Park, Y. M., Herrmann, J., Fischmann, S., Westphal, F., Müller, R., Flockerzi, V. & Meyer, M. R. (2020) How to Study the Metabolism of New Psychoactive Substances for the Purpose of Toxicological Screenings—A Follow-Up Study Comparing Pooled Human Liver S9, HepaRG Cells, and Zebrafish Larvae, *Frontiers in Chemistry.* **8**, 539.

30. Haschimi, B., Mogler, L., Halter, S., Giorgetti, A., Schwarze, B., Westphal, F., Fischmann, S. & Auwärter, V. (2019) Detection of the recently emerged synthetic cannabinoid 4F-MDMB-BINACA in 'legal high' products and human urine specimens, *Drug Testing and Analysis.* **11**, 1377-1386.

31. Richter, L. H. J., Beck, A., Flockerzi, V., Maurer, H. H. & Meyer, M. R. (2019) Cytotoxicity of new psychoactive substances and other drugs of abuse studied in human HepG2 cells using an adopted high content screening assay, *Toxicology Letters.* **301**, 79-89.

32. Choudhary, M. I., Khan, N. T., Musharraf, S. G., Anjum, S. & Atta-Ur-Rahman, S. (2007) Biotransformation of adrenosterone by filamentous fungus, Cunninghamella elegans, *Steroids.* **72**, 923-929.

33. Rydevik, A., Bondesson, U., Thevis, M. & Hedeland, M. (2013) Mass spectrometric characterization of glucuronides formed by a new concept, combining Cunninghamella elegans with TEMPO, *Journal of pharmaceutical and biomedical analysis.* **84**, 278-284.

34. Diao, X. & Huestis, M. A. (2019) New Synthetic Cannabinoids Metabolism and Strategies to Best Identify Optimal Marker Metabolites, *Frontiers in Chemistry.* **7**, 109.

35. Wang, D., Zou, L., Jin, Q., Hou, J., Ge, G. & Yang, L. (2018) Human carboxylesterases: a comprehensive review, *Acta Pharmaceutica Sinica B.* **8**, 699.

36. Thomsen, R., Nielsen, L. M., Holm, N. B., Rasmussen, H. B. & Linnet, K. (2015) Synthetic cannabimimetic agents metabolized by carboxylesterases, *Drug Testing and Analysis.* **7**, 565-576.

37. Ross, M. K., Borazjani, A., Wang, R., Allen Crow, J. & Xie, S. (2012) Examination of the carboxylesterase phenotype in human liver, *Archives of Biochemistry and Biophysics.* **522**, 44-56.

38. Di, L. (2019) The Impact of Carboxylesterases in Drug Metabolism and Pharmacokinetics, *Current Drug Metabolism* **20**, 91-102.

39. Yeter, E. O. & Yeter, O. (2020) In Vitro Phase I Metabolism of the Recently Emerged Synthetic MDMB-4en-PINACA and its Detection in Human Urine Samples, *Journal of Analytical Toxicology*, 1-9.

40. Watanabe, S., Vikingsson, S., Åstrand, A., Gréen, H. & Kronstrand, R. (2019) Biotransformation of the New Synthetic Cannabinoid with an Alkene, MDMB-4en-PINACA, by Human Hepatocytes, Human Liver Microsomes, and Human Urine and Blood, *The AAPS journal.* **22**, 13.

41. Wohlfarth, A., Castaneto, M., Zhu, M., Pang, S., Scheidweiler, K., Kronstrand, R. & Huestis, M. (2015) Pentylindole/Pentylindazole Synthetic Cannabinoids and Their 5-Fluoro Analogs Produce Different Primary Metabolites: Metabolite Profiling for AB-PINACA and 5F-AB-PINACA, *The AAPS Journal.* **17**, 660-677.

42. Yokoyama, Y., Sasaki, Y., Terasaki, N., Kawataki, T., Takekawa, K., Iwase, Y., Shimizu, T., Sanoh, S. & Ohta, S. (2018) Comparison of Drug Metabolism and Its Related Hepatotoxic Effects in HepaRG, Cryopreserved Human Hepatocytes, and HepG2 Cell Cultures, *Biological & pharmaceutical bulletin.* **41**, 722-732.

Chapter 5
The Detox Factory: Toxicology Profile of New Psychoactive Substances

5.1 Foreword

The following manuscript was submitted for a peer-reviewed publication and details the investigation of the hepatotoxicity potential of butylone, pentylone, MDPV and 4F-MDMB-BINACA using HepG2 hepatoma cell line and the *in vitro* metabolic stability of using human liver microsomes. The manuscript was authored by Ms Huey Sze Leong (H.S.L.)[1,2], Dr Morgan Philp (M.P.)[1], Professor Paul Kenneth Witting (P.K.W.)[2] and Professor Shanlin Fu (S.F.)[1,*].

[1] Centre for Forensic Science, School of Mathematical and Physical Sciences, University of Technology Sydney, Thomas Street Broadway, Ultimo NSW 2007, Australia

[2] Discipline of Pathology, Faculty of Medicine and Health, The Charles Perkins Centre, The University of Sydney, Johns Hopkins Drive, Camperdown NSW 2006, Australia

* Corresponding author

Author Contributions: H.S.L.: Conceptualization, Methodology, Validation, Formal analysis, Investigation, Writing - original draft, Writing - review & editing, Visualization, Project administration. M.P.: Methodology, Resources, Writing - review & editing. P.K.W.: Resources, Writing - review & editing, Supervision. S.F.: Resources, Writing - review & editing, Supervision.

All authors have read and agreed to the version of the manuscript.

5.2 Abstract

New psychoactive substances (NPS), an emerging class of drugs continue to pose health risk and challenges for clinical and forensic laboratories as the majority have no available toxicokinetic or toxicity data. The aim of this study is to identify cytotoxic potency potential of butylone, pentylone, MDPV and 4F-MDMB-BINACA using human HepG2 cell line and to investigate the *in vitro* metabolic stability of these NPS in pooled human liver microsomes (HLM).

For the *in vitro* cytotoxicity study, NPS were incubated in HepG2 cells for 72 h before subsequent analysis. CyQUANT^{TM} XTT cell viability and tetramethylrhodamine ethyl ester mitochondrial membrane assays were employed to determine the NPS cytotoxicity potential in terms of EC_{50} and screening cut-off values, respectively. For the metabolic stability study, NPS were incubated in HLM for up to 30 min. Samples were collected at various time points for subsequent analysis by liquid chromatography-tandem mass spectrometry (LC-MS/MS).

All the NPS exhibited dose-dependent cytotoxicity after 72 h drug treatment. Both EC_{50} values and screening cut-off values approaches exhibited cytotoxicity potency in the following order: butylone (least cytotoxic) < pentylone < MDPV < 4F-MDMB-BINACA (most cytotoxic). The calculated *in vitro* half-lives ($t_{1/2}$) were 53.9 ± 16.0, 104 ± 32.6, 113 ± 33.8 and 7.57 ± 0.29 min for butylone, pentylone, MPDV and 4F-MDMB-BINACA, respectively. The estimated intrinsic clearance values together with calculated $t_{1/2}$ categorized butylone, pentylone and MPDV as low clearance drugs and 4F-MDMB-BINACA as a relatively high clearance drug in comparison. The toxicology profiles of the NPS in this study provide valuable information to toxicologists in the evaluation of the potential detrimental effects and toxicokinetic information of these drugs.

Keywords: New psychoactive substances, toxicokinetic, cytotoxicity, *in vitro*

5.3 Introduction

New psychoactive substances (NPS) continue to pose a challenge in the forensic toxicology field due to the growing number of NPS with unknown toxicities that have been associated with serious health effects. The number of NPS arriving on the illicit drug market in individual countries reported to United Nations Office on Drugs and Crime was at an overall rate of more than 500 NPS each year from 2015 - 2018. The majority of these NPS are stimulants (mainly synthetic cathinones, SCs) followed by the synthetic cannabinoids (SCBs) or synthetic cannabinoid receptor agonists (SCRAs) [1].

Among the SCs, 1-(1,3-benzodioxol-5-yl)-2-pyrrolidin-1-ylpentan-1-one (MDPV) is one of the most popular components of SCs products [2-4]. Second generation SCs, 1-(1,3-benzodioxol-5-yl)-2-(methylamino)pentan-1-one (bk-MBDP, pentylone) [5-7] and 1-(1,3-benzodioxol-5-yl)-2-(methylamino)butan-1-one (bk-MBDB, butylone) [2, 8] have been reported as alternatives to commonly abused traditional drugs such as N-methyl-1-(3,4-methylenedioxyphenyl)propan-2-amine (MDMA) [5, 9-12]. Indazole carboxamide-type of SCB, methyl (2S)-2-([1-(4-fluorobutyl)-1H-indazole-3-carbonyl]amino)-3,3-dimethylbutanoate (4F-MDMB-BINACA), was first reported in 2018 and has shown to exhibit severe adverse effects on gastrointestinal, neurological, and cardiovascular systems [13].

SCs are commonly insufflated (snorted) or orally ingested [14] with typical average doses between 2 – 1500 and 10 – 2500 mg for insufflation and oral ingestion, respectively [15]. Depending on the route of administration, median effect onset has been reported to be between 15 – 30 min with a duration of 120 - 210 min and a total experience over 6 - 8 h [14, 16-18]. 4F-MDMB-BINACA is primarily smoked (or vaped) with acute effects observed from 0 - 6 h after SCBs consumption [19], although reliable data on 4F-MDMB-BINACA's dosage are currently unavailable [13]. Inter- and intra-package inhomogeneities, and SCBs' preparation such as spraying of drug solution onto plant material resulted in a highly unpredictable SCBs active ingredients dosage [20, 21]. Blood concentrations from recreational users and post-mortem cases ranged from 6 - 20,000, 5 - 340 and 1 - 1,509 μg/L in butylone, pentylone and MDPV, respectively [14, 22-25]. Blood and serum concentrations ranging from 0.48 - 1.62 μg/L of 4F-MDMB-BINACA together with other SCBs was reported [19]. Often these blood concentrations do not accurately predict the fatalities' outcome nor reflect tissue concentrations. A fatal

overdose case found particularly higher drug concentration in the liver as compared to blood [26].

Hepatic injury following intake of SCs and SCBs have been reported [27-32], acknowledging that liver is one of the main target organs of toxicity. Although primary human hepatocytes serve as a "gold standard" for studies of toxicity and drug metabolism, their high batch-to-batch variation, high cost and limited availability have prevented their extensive use [33, 34]. In contrast, HepG2 hepatoma cells provide highly reproducible experiments, and are relatively easy to culture [35]. Despite low activities of certain drug-metabolizing enzymes in HepG2 cells, they have also been widely used for toxicity studies of NPS [36-38]. To overcome this limitation, HepG2 cells were treated with drugs for 3 days in order to develop its metabolic competence and expression of toxicity [39].

As liver is also the primary organ involved in drug metabolism, determination of the drug's susceptibility to biotransformation or metabolic stability study is useful as metabolism may produce chemically reactive metabolites that further triggers responses that may lead to drug-induced liver injury [40]. Human liver microsomes (HLM) are frequently used for metabolic stability studies instead of hepatocytes or liver tissues because its subcellular fractions contain higher concentrations of many drug metabolizing enzymes, hence small amounts could be used to minimize the proportion of protein bound to drugs [41, 42].

In vitro cytotoxicity and toxicokinetic studies provide critical information that could aid forensic and clinical toxicologists in interpreting findings and determining possible pharmacological and toxicological effects of NPS exposure in human. Currently, there are limited cytotoxicity and toxicokinetic details of newly emergent SCB, 4F-MDMB-BINACA. The aim of this study was to examine the toxicology profile of butylone, pentylone, MDPV and 4F-MDMB-BINACA, in particularly its cytotoxicity and metabolic stability using well-established HepG2 cell line and preparations of HLM, respectively.

5.4 Materials and Methods

5.4.1 Chemicals and reagents

4F-MDMB-BINACA was provided by Health Sciences Authority (Singapore). Hydrochloride salts of butylone, pentylone, and MDPV were synthesized in-house with a purity greater than 98 %. Details of the synthesis and characterization of these drugs has been published previously [43]. HepG2 cell line was purchased from CellBank (Sydney, NSW, Australia). Commercially sourced hundred fifty-donor HLM pool, NADPH system solution A and NADPH system solution B were from Corning (Corning, NY, USA). T75 tissue culture flasks, and 96-well cell culture plates were purchased from Corning (Corning, NY, USA). Minimum Essential Medium – Eagle with Earle's BSS (MEM Eagle EBSS) was purchased from Lonza (Basel, Switzerland). The Countess™ cell counting chamber slide, Trypan Blue (TB) Stain 0.4 % w/v and CyQUANT™ XTT Cell Viability Assay were purchased from Invitrogen (Eugene, OR, USA). TMRE (TetraMethylRhodamine Ethyl ester) Mitochondrial Membrane Potential Assay Kit and Hoechst 33342 (hydrochloride) were purchased from Cayman Chemical (Ann Arbor, MI, USA). Liquid chromatography–mass spectrometry (LC–MS) grade acetonitrile (ACN) was obtained from Honeywell (Muskegon, MI, USA). LC–MS grade formic acid was obtained from Sigma-Aldrich (St. Louis, MO, USA). The Axio Vert.A1 inverted fluorescence phase contrast microscope was purchased from Zeiss (Jena, Germany). The Infinite® M200 Pro plate reader was purchased from Tecan (Männedorf, Switzerland).

5.4.2 Cytotoxicity Studies

HepG2 cells were cultured (up to passage 8) in a T75 tissue culture flask using MEM Eagle EBSS media supplemented with 10 % heat-inactivated fetal bovine serum, L-glutamine (2 mM), penicillin: streptomycin (100 U/mL:100 µg/mL) and non-essential amino acid solution (NEAA, 1x). Cells were cultured at 37 °C in a humidified atmosphere incubator containing 95 % air and 5 % CO_2, and the media was changed every 2 - 3 days. General cell morphology was monitored at regular intervals using phase contrast inverted microscopy. Where required, cells were harvested by subculture with media containing trypsin/EDTA (0.12 % trypsin/ 0.02 % EDTA *w*/*v*) when cells reached about 80 %

confluence. Cells were counted under TB staining using an automated cell counter (Thermo Fisher Scientific, Waltham, MA, USA), and seeded at 15,000 cells/cm^2 onto 96-well plates in a volume of 100 µL of complete culture media to obtain confluent monolayers overnight. The following day, cells were incubated with butylone, pentylone, MDPV and 4F-MDMB-BINACA individually in complete culture media for 72 h.

Viability assessed with CyQuant assay

To ensure reliable and complete dose-response curves for each drug, a wide range of doses were employed (25 to 800 µM for SCs butylone, pentylone and MDPV; and 7.81 - 500 µM for 4F-MDMB-BINACA prepared in culture media). After 72 h of drug treatment, 70 µL of CyQuant working reagent (prepared according to the manufacturer's instruction) was added directly to each sample (containing individual drugs) and blank (containing culture media only) wells, and incubated for 4 h at 37 °C. After incubation, absorbance was measured at 450 and 660 nm with a Tecan plate reader. Data obtained from at least three independent experiments were subjected to the following specific absorbance calculation (Equation 1):

$$\text{Absorbance} = [\text{Abs}_{450\ \text{nm}}\ (\text{Sample}) - \text{Abs}_{450\ \text{nm}}\ (\text{Blank})] - \text{Abs}_{660\ \text{nm}}\ (\text{Sample}) \quad (1)$$

Viability assessed with TMRE and Hoechst 33342 Fluorescence Probes

After 72 h of drug treatment (100 and 300 µM for SCs, and 60 and 120 µM for 4F-MDMB-BINACA), culture media was aspirated from the black 96-well clear bottom plate. Sample, control (untreated) and blank wells were dispensed with 100 µL of two different fluorescence probes (200 nM TMRE to assess mitochondrial membrane potential and 1 µM Hoechst 33342 to stain nucleic acids) and incubated for 30 min at 37 °C, protected from light. Culture media was aspirated, cells were washed gently twice with the pre-warmed 1x assay buffer (150 µL first wash, 100 µL second wash) and 100 µL of 1x assay buffer (provided by manufacturer) was subsequently added. The plate was equilibrated at room temperature and fluorescence was read using a Tecan plate reader (TMRE: $\lambda_{ex/em}$ = 530/580 nm). Data obtained from four independent experiments were subjected to the following relative fluorescence unit (RFU) signal calculation (Equation 2):

$$RFU\ (\%) = [(RFU_{sample} - RFU_{blank})/ (RFU_{control} - RFU_{blank})] \times 100 \quad (2)$$

Average value from control was considered as 100 % TMRE uptake. The plate was also subjected to fluorescence imaging using the RFP and DAPI filter set for TMRE and Hoechst 33342, respectively. Images were collected using 20x objective with an inverted fluorescence phase contrast microscope (Zeiss, Jena, Germany).

5.4.3 Metabolic Stability Studies

Metabolic stability studies were conducted with HLM as previously described [44]. Briefly, individual NPS solutions (SCs: 40 µM; 4F-MDMB-BINACA: 44 µM) in acetonitrile/phosphate buffer (pH 7.4, 25 µL), phosphate buffer (0.1 M, pH 7.4, 855 µL), NADPH-A (50 µL) and NADPH-B (20 µL) were mixed in a 2 mL Eppendorf tube, to which HLM (50 µL = 1 mg total protein) was added. The final concentration of SCs and 4F-MDMB-BINACA in the mixture was 1.0 and 1.1 µM, respectively. The mixture was incubated in triplicate at 37 °C in a shaking water bath. At time 0, 5, 10, 16, 23 and 30 min, a 100 µL aliquot was removed and placed into ice-cold acetonitrile (100 µL) to quench the reaction. The cut-off was set to 30 min, due to decreasing enzyme activity after a period of time. The mixture was centrifuged at 13,000 r.p.m. for 10 min and supernatant was filtered using a 0.22 µm filter. 100 µL of the filtrate was diluted in 900 µL water/ acetonitrile (90:10, v/v) and 2 µL was injected into liquid chromatography–triple quadrupole mass spectrometer (LC-MS/MS) in triplicate. Chromatographic separation was performed on an Agilent 1290 LC system with Poroshell 120 EC-C18 analytical column (2.7 µm, 75 mm x 2.1 mm; Agilent Technologies, Santa Clara, CA, USA). The mobile phase consisted of 0.1 % formic acid in water (A) and 0.1 % formic acid in acetonitrile (B). The gradient elution was as follows: 10 % B until 2 min, increased to 40 % B until 10 min, ramped to 90 % B until 11 min, ramped down to 10 % B at 12 min and held until 14 min. The flow rate was 0.3 mL/min and the column temperature were kept at 30 °C. Mass spectrometry was run in multiple reaction monitoring mode on an Agilent 6490 Triple Quadrupole mass spectrometer with electrospray ionisation (ESI) source in positive ion mode. Two transitions with optimised collision energy [Butylone: *m/z* 222 → 204 (10 eV) and *m/z* 222 → 146 (34 eV); Pentylone: *m/z* 236 → 218 (10 eV) and *m/z* 236 → 188 (18 eV); MDPV: *m/z* 276 → 135 (26 eV) and *m/z* 276 → 126 (30

eV); and 4F-MDMB-BINACA: *m/z* 364 → 304 (14 eV) and *m/z* 364 → 219 (22 eV)] were monitored for each NPS.

In vitro microsomal half-life ($t_{1/2}$) of NPS was calculated from the plot of natural log of percentage of the drug remaining against time. Percentage of the drug remaining was calculated by dividing the peak area of the drug remaining at each time point by the peak area of the drug at time 0 min and multiplying by 100 %. The slope of linear regression (−k) was used to give $t_{1/2} = \ln 2/k$. *In vivo* estimated intrinsic clearance, CL_{int}, (mL/min/kg) was calculated based on the following formula (Equation 3) using the well-stirred model [45]:

$CL_{int} = (\ln 2/t_{1/2}) \times$ (mL of incubation/mg of microsomes) x (45 mg of microsomes/g of liver) x (20 g of liver/kg of body weight) (3)

Hepatic clearance (CL_H) and hepatic extraction ratio (E_H) were calculated from the well-stirred model from the following formulae (Equation 4 and 5, respectively) without considering blood protein and microsome binding. Human hepatic blood flow (Q_H) value of 21 mL/min/kg was used [45].

$$CL_H = (Q_H \times CL_{int})/ (Q_H + CL_{int}) \quad (4)$$

$$E_H = CL_H / Q_H \quad (5)$$

5.4.4 Data Analysis

Data was expressed as the mean ± standard deviation from at least three independent experiments. For comparisons, data were analysed using one-way analysis of variance (ANOVA) followed by Tukey's test using GraphPad Prism 7 (San Diego, CA, USA). Statistical significance was set at $p < 0.05$. EC_{50} values were obtained from the dose-response curve as determined using the GraphPad Prism software.

5.5 Results and Discussion

5.5.1 *In vitro* Cytotoxicity Potency of NPS

Dose-response curves determined via CyQuant assay showed a dose-dependent cytotoxicity for all the NPS studied (Figure 5.1 A-D). This is consistent with numerous *in vitro* studies relating NPS-induced dose-dependent cytotoxicity [36, 46-49] and the reported hypothesized dose-related hepatocellular necrosis involving an accumulation of oxidative damage [50]. The half maximal effective concentration (EC_{50}) of the NPS determined from the dose-response curves were as follows: butylone (200 ± μM), pentylone (150 ± 36 μM), MDPV (120 ± 26 μM) and 4F-MDMB-BINACA (79.2 ± 20.4 μM). EC_{50} values have an inversely proportional relationship with the order of potency. Hence, the order of cytotoxicity potency based upon EC_{50} values were determined as follows: butylone (least cytotoxic) < pentylone < MDPV < 4F-MDMB-BINACA (most cytotoxic).

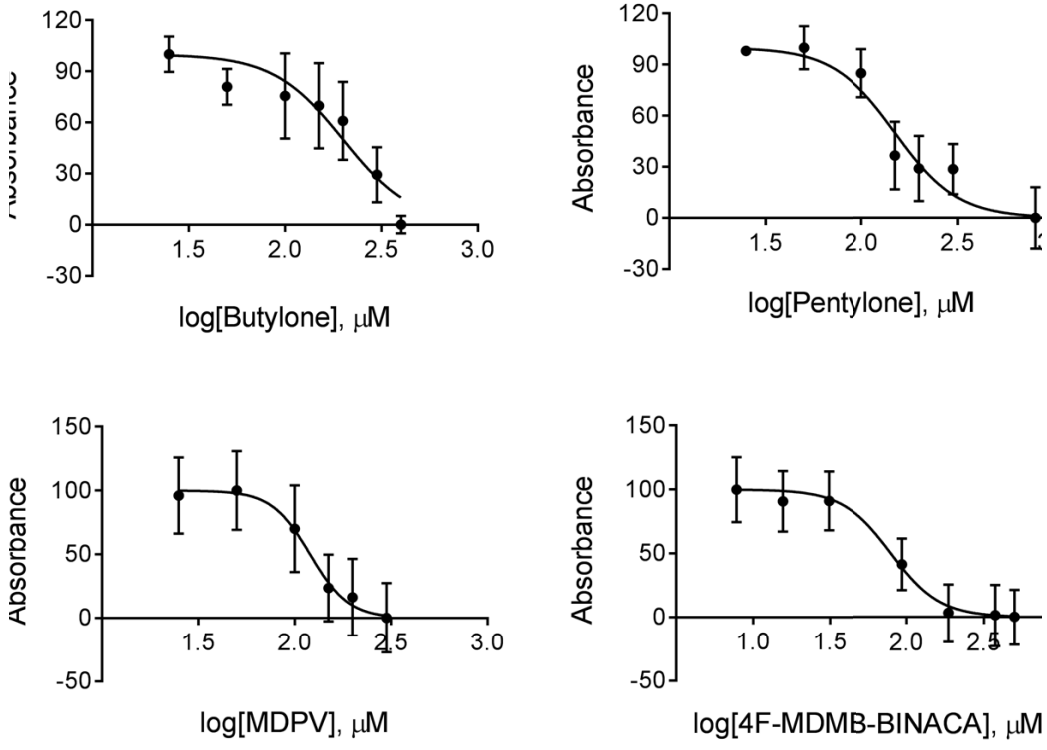

NPS	Butylone	Pentylone	MDPV	4F-MDMB-BINACA

Figure 5.1 Normalized dose-response curves after 72 h drug treatment with (A) butylone, (B) pentylone, (C) MDPV and (D) 4F-MDMB-BINACA in HepG2 cells. Data are mean ± SD obtained from at least three independent experiments for the CyQuant assay. Table: Mean EC_{50} values obtained from dose-response curves of CyQuant assay. ($^{\#}p < 0.1$ vs 4F-MDMB-BINACA)

Upon careful review of available data, it was determined that lipophilicity values (Consensus LogP) of NPS increases from butylone (1.86) to 4F-MDMB-BINACA (3.39), demonstrating a link between the cytotoxicity potency and the lipophilicity of the NPS. Linear regression analyses demonstrated that the lipophilicity parameter was strongly correlated with the EC_{50} values ($R^2 > 0.90$) with p value < 0.05, suggesting that lipophilicity is one of the factors contributing to enhancing overall cytotoxicity observed (Figure 5.2).

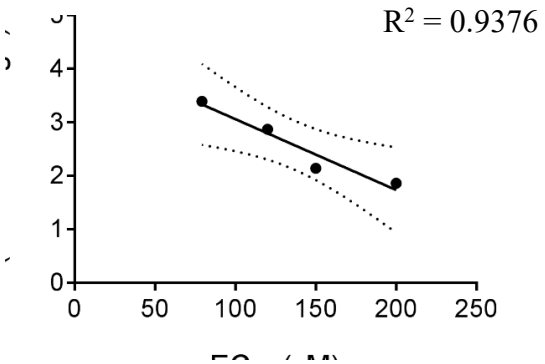

Figure 5.2 Linear regression plot of lipophilicity and EC_{50} values of butylone, pentylone, MDPV and 4F-MDMB-BINACA

The length of aliphatic side-chain influencing the lipophilicity properties have been reported to affect the cytotoxicity potency of drugs [51]. Butylone and pentylone differ in the length of the aliphatic side-chain, butylone contains an ethyl group and pentylone a propyl group. MDPV is similar in chemical structure to pentylone with methyl group on the amine being replaced by a pyrrolidine ring, whilst 4F-MDMB-BINACA possess a butyl group side-chain (Figure 5.3). The findings in this study supported that increasing aliphatic side-chain from ethyl to butyl group, increased the lipophilicity of NPS, and hence the cytotoxicity potency. Studies have supported that increasing lipophilicity and

dosage together with the extent of metabolism increases the risk factors of drug-induced liver injury [52].

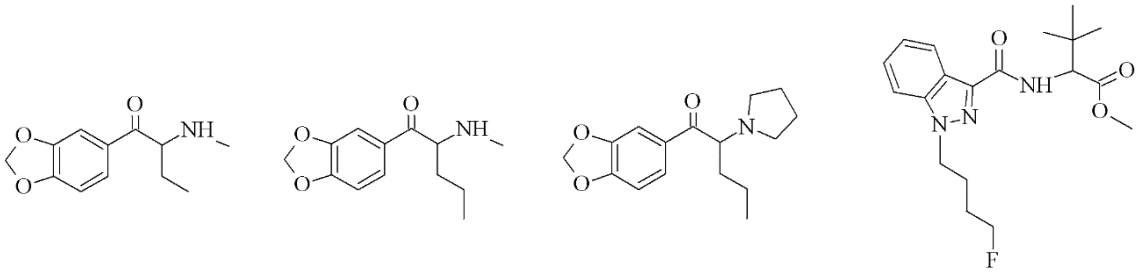

Figure 5.3 Chemical structures and lipophilicity values (expressed in terms of Consensus LogP [53]) of butylone, pentylone, MDPV and 4F-MDMB-BINACA

Mitochondrial membrane potential has been identified as one of the more sensitive parameters in high-content analysis using multi-parameter cell-based assays [37]. TMRE, a fluorescent lipophilic cationic dye was employed in this study to assess whether added NPS-induced mitochondrial dysfunction consistent with previous reports [36, 37]. In addition, Hoechst 33342, a cell permeant nuclear counterstain, was added to define the nuclear envelop relative to the mitochondrial fluorescence. Thus, simultaneous detection of nuclear morphology and mitochondrial membrane potential enabled investigations of NPS cytotoxicity and its underlying preliminary mechanism at the cellular level. Two doses were chosen based upon the obtained EC_{50} values (above and below EC_{50} values) defined here as 100 and 300 μM for the SCs and 60 and 120 μM for 4F-MDMB-BINACA to elucidate possible mitochondrial impairment as determined by TMRE staining. Dispersed orange-red with decreased TMRE fluorescence intensity in mitochondria (demonstrating depolarization of mitochondrial membrane potential) and decreased nuclei DNA Hoechst 33342 blue stain was observed in drug-treated HepG2 cells (Figure 5.4 A-D) compared the corresponding control cells (Figure 4 E). HepG2 cells were significantly affected at higher doses of NPS (Figure 4 F-G): 300 μM of pentylone (** $p < 0.01$), MDPV (**** $p < 0.0001$) and 120 μM of 4F-MDMB-BINACA (* $p < 0.1$). The effect is dose-dependent for both pentylone and MDPV (**** $p < 0.0001$). Mitochondrial membrane potential was not significantly affected by butylone at these doses. Using an approach where TMRE fluorescence was screened as a baseline (first minimal dose

reported with statistical significance different from control), the order of cytotoxicity potency was as follows: butylone (least cytotoxic) < pentylone < MDPV < 4F-MDMB-BINACA (most cytotoxic). Overall, both approaches showed a similar level of cytotoxicity potency in ranking of the NPS tested here.

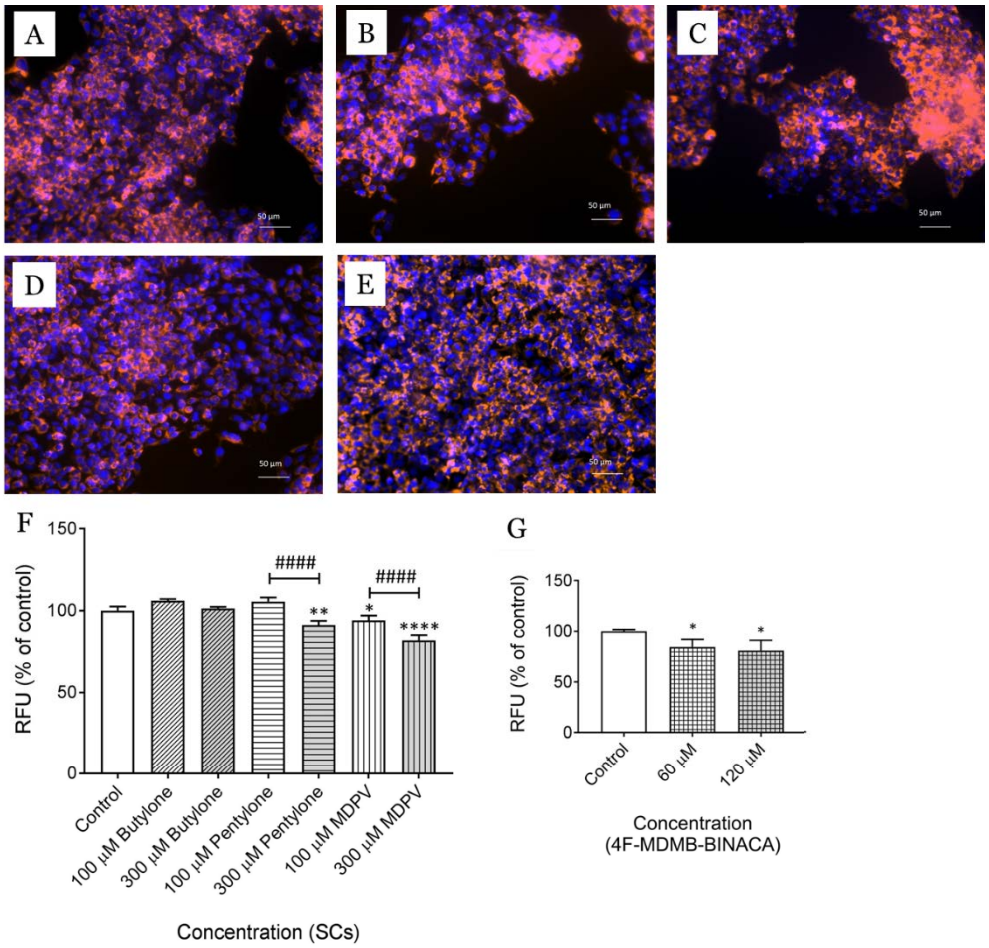

Figure 5.4 Representative merged images of orange-red TMRE and blue Hoechst 33342 staining in 300 µM of (A) butylone, (B) pentylone, (C) MDPV; 120 µM of (D) 4F-MDMB-BINACA; and (E) the control using fluorescence phase-contrast microscope with a 20x objective (scale bar: 50 µm) after 72 h of drug treatments in HepG2 cells. Quantification of TMRE fluorescence after 72 h of treatment in (F) 100 and 300 µM of SCs: butylone, pentylone and MDPV, and (G) 60 and 120 µM of 4F-MDMB-BINACA. Data shown in panel F and G are mean ± SD obtained from four independent experiments. #### $p < 0.0001$ vs 300 µM pentylone and 300 µM MDPV. Different to the control; * $p <$ 0.1, ** $p < 0.01$ and **** $p < 0.0001$. RFU: Relative Fluorescence Unit

It should be noted that the number of NPS used in this study was relatively small. Future studies should include greater number of screening cut-off levels to be tested together with different groups of NPS. A possible key application of the TMRE screening cut-off approach described here is expected to be in the early toxicological assessment of the safety profile of emergent NPS using known toxicity of NPS as positive controls. Irregularities with this approach may be likely if drugs are concentrated in specific tissues other than liver, or undergo extensive metabolism. Drug metabolism must also be taken into consideration when determining emerging drugs' *in vivo* toxicity and this is presently outside the scope of this study.

5.5.2 Metabolic Stability

Metabolic stability refers to the drug susceptibility to biotransformation and can be expressed by the *in vitro* $t_{1/2}$ and intrinsic clearance values that is scaled to the *in vivo* values. Toxicokinetic data of SCs butylone, pentylone and MDPV have been reported in various *in vivo* rat studies [16, 54-56], however these data are currently unavailable for 4F-MDMB-BINACA. Selected literature from *in vivo* toxicokinetic data of the SCs were compared to the *in vitro* findings in this study (Table 5.1). Careful inspection of this data indicates that MDPV has the longest microsomal $t_{1/2}$ and lowest clearance rate, whereas 4F-MDMB-BINACA has the shortest $t_{1/2}$ with the highest clearance rate, with the assumption made that non-specific blood protein binding had a minimal effect on the overall metabolic stability result. *In vitro* microsomal $t_{1/2}$ (min) was observed in the following order: 4F-MDMB-BINACA (7.57 ± 0.29) < butylone (53.9 ± 16) < pentylone (104 ± 32.6) < MDPV (113 ± 33.8). Calinski *et al.* demonstrated that SCs scaffold modifications could alter the toxicokinetic profile of SCs and ultimately produces SCs with longer $t_{1/2}$ [57].

Toxicokinetic Parameters	Butylone	Pentylone	MDPV	4F-MDMB-BINACA
Human liver microsomes				
$t_{1/2}$ (min)	53.9 ± 16	104 ± 32.6	113 ± 33.8	7.57 ± 0.29
CL_{int} (mL/min/kg)	11.6 ± 2.27	6.28 ± 1.96	5.78 ± 1.73	82.4 ± 3.21

CL_H (mL/min/kg)	7.46 ± 1.07	4.79 ± 1.17	4.50 ± 1.07	16.7 ± 0.132
E_H	0.355 ± 0.051	0.228 ± 0.056	0.214 ± 0.051	0.797 ± 0.006
Rat plasma				
$t_{1/2}$ (min)	81.9 [c]	253 [c]	77.8 - 97.8 [a] 79 - 99[b]	N.A.
CL/F (mL/min/kg)	20 [c]	9.80 [c]	N.A.	N.A.
C_{max} (µg/L)	1840 [c]	5740 [c]	74.2 – 271 [a] 20 – 135 [b]	N.A.
T_{max} (min)	30 [c]	30 [c]	12.9 - 18.6 [a] 10 [b]	N.A.

[a] Anizan et al. [55]:
Subcutaneous administration; 0.5, 1.0 and 2.0 mg/kg (Each dose: n = 7)
[b] Baumann et al. [58]:
Intraperitoneal administration; 0.5, 1.0 and 2.0 mg/kg (Each dose: n = 6 - 7)
[c] Grecco et al. [54]:
Subcutaneous administration; 20 mg/kg (n = 4)

Classification of drugs according to $t_{1/2}$ and CL_{int}:

$t_{1/2}$ [59]	**CL_{int}**	
$t_{1/2} > 60$ min	$CL_{int} < 15$ mL/min/kg	Low clearance compound
$20 < t_{1/2} < 60$ min	15 < CLint < 45 mL/min/kg	Intermediate clearance compound
$t_{1/2} < 20$ min	$CL_{int} > 45$ mL/min/kg	High clearance compound

Table 5.1 Toxicokinetic parameters of butylone, pentylone, MDPV and 4F-MDMB-BINACA incubated via *in vitro* human liver microsomes (n = 3) and *in vivo* rat plasma from selected literatures. $t_{1/2}$: Half-life, CL/F: observed apparent clearance; CL_H: estimated hepatic clearance; CL_{int}: estimated intrinsic clearance; C_{max}: maximum observed concentration; E_H: hepatic clearance ratio; T_{max}: time of C_{max}; N.A.: Not applicable

In this present study, increasing length of aliphatic side-chain from ethyl to propyl in butylone to pentylone, respectively and ultimately addition of pyrrolidine ring in MDPV yielded longer $t_{1/2}$. The low estimated intrinsic clearance, CL_{int} (< 15 mL/min/kg) and *in vitro* $t_{1/2}$ > 60 min indicated that SCs butylone, pentylone and MDPV showed relative low clearance drugs. Metabolic studies have demonstrated that metabolic pathways of MDPV is relatively simple and occurs mainly at the methylenedioxy functional group [60], with demethylenation via human CYP1A2, CYP2D6, and CYP2C19 followed by O-methylation identified as metabolites. Both butylone and pentylone have similar metabolic pathways as MDPV [10, 61, 62]. Most SCBs are highly lipophilic and distributed quickly into fat tissue where they can accumulate, causing rapid decline of parent drug in blood after administration [63]. From the findings, 4F-MDMB-BINACA was the most lipophilic drug in the tested group with very short $t_{1/2}$ (< 20 min) and high CL_{int} values (> 45 mL/min/kg), indicated that 4F-MDMB-BINACA is a high clearance drug. This is supported by recently published metabolism data where 4F-MDMB-BINACA underwent several phase I metabolic transformations, which primarily were that of 4F-MDMB-BINACA ester hydrolysis metabolite, followed by other metabolites which were oxidative in nature via CYP1A2, CYP2C8, CYP2C19, CYP3A4 and CYP3A5 [64-66]. Further studies would be required to ascertain whether the 4F-MDMB-BINACA metabolites formed are chemically reactive resulting in the higher cytotoxicity observed. While it is difficult to make direct comparison to available *in vivo* literature values due to the wide-ranging factors such scale-up physiological parameters and *in vivo* clearance data variation [67], the *in vitro* toxicokinetic data of butylone, pentylone and MDPV in this study compared favourably with the *in vivo* literatures to the overall classification of the low clearance drugs' category. Metabolic stability *in vivo-in vitro* extrapolation in this study was conducted using the drug depletion approach. The advantage of this approach is that the depletion of the rate of the unchanged drug could be simply determined without knowing the main metabolic pathway. Conversely, metabolically stable drugs may suffer from prediction bias [67]. Future work should also include studies on protein binding and volume of distribution calculation to supplement existing $t_{1/2}$ and estimated *in vivo* CL_{int}.

5.6 Conclusion

Preliminary *in vitro* cytotoxicity and metabolic stability studies are useful in the prediction of *in vivo* human toxicity and toxicokinetics of NPS. The order of cytotoxicity potency according to EC_{50} values and screening cut-off approach using human HepG2 hepatoma cell line was found to be similar. The *in vitro* kinetic calculations provide important data on the NPS half-life which ultimately would be needed to properly design *in vitro* incubation for drug metabolic pathway studies. 4F-MDMB-BINACA being highly lipophilic has short half-life and high intrinsic clearance, implied extensive hepatic metabolism that might be implicated with the cytotoxicity observed.

5.7 References

1. UNODC (2020) World Drug Report: Cross-cutting Issues: Evolving Trends and New Challenges, *United Nations publication, Sales No E20XI6.* **Booklet 4**, 1-119.

2. Leffler, A. M., Smith, P. B., de Armas, A. & Dorman, F. L. (2014) The analytical investigation of synthetic street drugs containing cathinone analogs, *Forensic Science International.* **234**, 50-56.

3. Schneir, A., Ly, B. T., Casagrande, K., Darracq, M., Offerman, S. R., Thornton, S., Smollin, C., Vohra, R., Rangun, C., Tomaszewski, C. & Gerona, R. R. (2014) Comprehensive analysis of "bath salts" purchased from California stores and the internet, *Clinical Toxicology.* **52**, 651-658.

4. Uralets, V., Rana, S., Morgan, S. & Ross, W. (2014) Testing for designer stimulants: metabolic profiles of 16 synthetic cathinones excreted free in human urine, *Journal Of Analytical Toxicology.* **38**, 233-241.

5. Brandt, S. D., Freeman, S., Sumnall, H. R., Measham, F. & Cole, J. (2011) Analysis of NRG 'legal highs' in the UK: identification and formation of novel cathinones, *Drug Testing and Analysis.* **3**, 569-575.

6. Sadeg, N., Darie, A., Vilamot, B., Passamar, M., Frances, B. & Belhadj-Tahar, H. (2014) Case Report of Cathinone-Like Designer Drug Intoxication Psychosis and Addiction With Serum Identification, *Addictive Disorders & Their Treatment.* **13**, 38-43.

7. Liakoni, E., Dolder, P. C., Rentsch, K. & Liechti, M. E. (2015) Acute health problems due to recreational drug use in patients presenting to an urban emergency department in Switzerland, *Swiss medical weekly.* **145**, w14166-w14166.

8. Zuba, D. & Byrska, B. (2013) Prevalence and co-existence of active components of 'legal highs': Analysis of 'legal highs' composition, *Drug Testing and Analysis.* **5**, 420-429.

9. Brandt, S. D., Sumnall, H. R., Measham, F. & Cole, J. (2010) Analyses of second-generation 'legal highs' in the UK: initial findings, *Drug testing and analysis.* **2**, 377-382.

10. Zaitsu, K., Katagi, M., Kamata, H. T., Kamata, T., Shima, N., Miki, A., Tsuchihashi, H. & Mori, Y. (2009) Determination of the metabolites of the new designer drugs bk-MBDB and bk-MDEA in human urine, *Forensic Science International.* **188**, 131-139.

11. Palamar, J., Salomone, A., Gerace, E., Di Corcia, D., Vincenti, M. & Cleland, C. (2017) Hair testing to assess both known and unknown use of drugs amongst ecstasy users in the electronic dance music scene, *The International Journal on Drug Policy.* **48**, 91.

12. Salomone, A., Palamar, J. J., Gerace, E., Di Corcia, D. & Vincenti, M. (2017) Hair Testing for Drugs of Abuse and New Psychoactive Substances in a High-Risk Population, *Journal of Analytical Toxicology.* **41**, 376-381.

13. Brandt, S., Poovendran, D. (2019) 4F-MDMB-BINACA. Critical Review Report, *World Health Organization Expert Committee on Drug Dependence (ECCD) Forty-second Meeting*, 1-24.

14. Horsley, R. R., Lhotkova, E., Hajkova, K., Feriancikova, B., Himl, M., Kuchar, M. & Pa lenA-Aek, T. (2018) Behavioural, Pharmacokinetic, Metabolic, and Hyperthermic Profile of 3,4-Methylenedioxypyrovalerone (MDPV) in the Wistar Rat, *Frontiers in Psychiatry.* **9**, 144.

15. Assi, S., Gulyamova, N., Kneller, P. & Osselton, D. (2017) The effects and toxicity of cathinones from the users' perspectives: A qualitative study, *Human Psychopharmacology: Clinical and Experimental.* **32**, e2610.

16. Ross, E. A., Reisfield, G. M., Watson, M. C., Chronister, C. W. & Goldberger, B. A. (2012) Psychoactive "bath salts" intoxication with methylenedioxypyrovalerone, *The American journal of medicine.* **125**, 854.

17. Johnson, P. S. & Johnson, M. W. (2014) Investigation of "Bath Salts" Use Patterns Within an Online Sample of Users in the United States, *Journal of Psychoactive Drugs.* **46**, 369.

18. Bertol, E., Mari, F., Boscolo Berto, R., Mannaioni, G., Vaiano, F. & Favretto, D. (2014) A mixed MDPV and benzodiazepine intoxication in a chronic drug abuser: Determination of MDPV metabolites by LC–HRMS and discussion of the case, *Forensic Science International.* **243**, 149-155.

19. Kleis, J., Germerott, T., Halter, S., Héroux, V., Roehrich, J., Schwarz, C. S. & Hess, C. (2020) The synthetic cannabinoid 5F-MDMB-PICA: A case series, *Forensic Science International.* **314**, 110410.

20. Moosmann, B., Angerer, V. & Auwärter, V. (2015) Inhomogeneities in herbal mixtures: a serious risk for consumers, *Forensic Toxicology.* **33**, 54-60.

21. Frinculescu, A., Lyall, C. L., Ramsey, J. & Miserez, B. (2017) Variation in commercial smoking mixtures containing third-generation synthetic cannabinoids, *Drug Testing and Analysis.* **9**, 327-333.

22. Paillet-Loilier, M., Cesbron, A., Le Boisselier, R., Bourgine, J. & Debruyne, D. (2014) Emerging drugs of abuse: current perspectives on substituted cathinones, *Substance abuse and rehabilitation - Journal Article.* **5**, 37.

23. Elliott, S. & Evans, J. (2014) A 3-year review of new psychoactive substances in casework, *Forensic science international.* **243**, 55-60.

24. Glicksberg, L., Winecker, R., Miller, C. & Kerrigan, S. (2018) Postmortem distribution and redistribution of synthetic cathinones, *Forensic Toxicology.* **36**, 291-303.

25. Beck, O., Franzen, L., Bäckberg, M., Signell, P. & Helander, A. (2015) Intoxications involving MDPV in Sweden during 2010-2014: Results from the STRIDA project, *Clinical Toxicology.* **53**, 865-873.

26. García-Repetto, R., Moreno, E., Soriano, T., Jurado, C., Giménez, M. P. & Menéndez, M. (2003) Tissue concentrations of MDMA and its metabolite MDA in three fatal cases of overdose, *Forensic Science International.* **135**, 110-114.

27. Borek, H. A. & Holstege, C. P. (2012) Hyperthermia and multiorgan failure after abuse of "bath salts" containing 3,4-methylenedioxypyrovalerone, *Annals of Emergency Medicine.* **60**, 103-105.

28. Murray, B. L., Murphy, C. M. & Beuhler, M. C. (2012) Death Following Recreational Use of Designer Drug “Bath Salts” Containing 3,4-Methylenedioxypyrovalerone (MDPV), *Journal of Medical Toxicology.* **8**, 69-75.

29. Fröhlich, S., Lambe, E. & O'Dea, J. (2011) Acute liver failure following recreational use of psychotropic "head shop" compounds, *Irish journal of medical science.* **180**, 263.

30. Kesha, K., Boggs, C. L., Ripple, M. G., Allan, C. H., Levine, B., Jufer-Phipps, R., Doyon, S., Chi, P. & Fowler, D. R. (2013) Methylenedioxypyrovalerone (“Bath Salts”),Related Death: Case Report and Review of the Literature, *Journal of Forensic Sciences.* **58**, 1654-1659.

31. Behonick, G., Shanks, K. G., Firchau, D. J., Mathur, G., Lynch, C. F., Nashelsky, M., Jaskierny, D. J. & Meroueh, C. (2014) Four Postmortem Case Reports with Quantitative Detection of the Synthetic Cannabinoid, 5F-PB-22, *Journal of Analytical Toxicology.* **38**, 559-562.

32. Solimini, R., Busardò, F. P., Rotolo, M. C., Ricci, S., Mastrobattista, L., Mortali, C., Graziano, S., Pellegrini, M., Di Luca, N. M. & Palmi, I. (2017) Hepatotoxicity associated to synthetic cannabinoids use, *European review for medical and pharmacological sciences.* **21**, 1-6.

33. Fraczek, J., Bolleyn, J., Vanhaecke, T., Rogiers, V. & Vinken, M. (2013) Primary hepatocyte cultures for pharmaco-toxicological studies: at the busy crossroad of various anti-dedifferentiation strategies, *Archives of Toxicology.* **87**, 577-610.

34. Gómez-Lechón, M. J., Tolosa, L., Conde, I. & Donato, M. T. (2014) Competency of different cell models to predict human hepatotoxic drugs, *Expert Opin Drug Metab Toxicol.* **10**, 1553-68.

35. Guo, L., Dial, S., Shi, L., Branham, W., Liu, J., Fang, J.-L., Green, B., Deng, H., Kaput, J. & Ning, B. (2011) Similarities and differences in the expression of drug-metabolizing enzymes between human hepatic cell lines and primary human hepatocytes, *Drug metabolism and disposition: the biological fate of chemicals.* **39**, 528-538.

36. Luethi, D., Liechti, M. E. & Krahenbuhl, S. (2017) Mechanisms of hepatocellular toxicity associated with new psychoactive synthetic cathinones, *Toxicology.* **387**, 57-66.

37. Richter, L. H. J., Beck, A., Flockerzi, V., Maurer, H. H. & Meyer, M. R. (2019) Cytotoxicity of new psychoactive substances and other drugs of abuse studied in human HepG2 cells using an adopted high content screening assay, *Toxicology Letters.* **301**, 79-89.

38. Dias-da-Silva, D., Arbo, M. D., Valente, M. J., Bastos, M. L. & Carmo, H. (2015) Hepatotoxicity of piperazine designer drugs: Comparison of different in vitro models, *Toxicology in Vitro.* **29**, 987-996.

39. O'Brien, P. J. & Edvardsson, A. (2017) Validation of a Multiparametric, High-Content-Screening Assay for Predictive/Investigative Cytotoxicity: Evidence from Technology Transfer Studies and Literature Review, *Chemical research in toxicology.* **30**, 804-829.

40. Zhang, Z. & Tang, W. (2018) Drug metabolism in drug discovery and development, *Acta Pharmaceutica Sinica B.* **8**, 721.

41. Castell, J. V., Jover, R., Martnez-Jimnez, C. P. & Gmez-Lechn, M. J. (2006) Hepatocyte cell lines: their use, scope and limitations in drug metabolism studies, *Expert Opinion on Drug Metabolism & Toxicology.* **2**, 183-212.

42. Asha, S. & Vidyavathi, M. (2010) Role of Human Liver Microsomes in In Vitro Metabolism of Drugs—A Review, *Applied Biochemistry and Biotechnology.* **160**, 1699-1722.

43. Huey Sze, L., Morgan, P., Martin, S., Paul Kenneth, W. & Shanlin, F. (2020) Synthetic Cathinones Induce Cell Death in Dopaminergic SH-SY5Y Cells via Stimulating Mitochondrial Dysfunction, *International journal of molecular sciences.* **21**, 1370.

44. Watanabe, S., Kuzhiumparambil, U. & Fu, S. (2018) In vitro metabolism of synthetic cannabinoid AM1220 by human liver microsomes and Cunninghamella elegans using liquid chromatography coupled with high resolution mass spectrometry, *Forensic toxicology.* **36**, 435-446.

45. Obach, R. S., Baxter, J. G., Liston, T. E., Silber, B. M., Jones, B. C., Macintyre, F., Rance, D. J. & Wastall, P. (1997) The prediction of human pharmacokinetic parameters from preclinical and in vitro metabolism data, *The Journal of pharmacology and experimental therapeutics.* **283**, 46-58.

46. Valente, M. J., Araújo, A. M., Silva, R., Bastos, M. d. L., Carvalho, F., Guedes de Pinho, P. & Carvalho, M. (2016) 3,4-Methylenedioxypyrovalerone (MDPV): in vitro mechanisms of hepatotoxicity under normothermic and hyperthermic conditions, *Archives of Toxicology.* **90**, 1959-1973.

47. Araújo, A. M., Valente, M. J., Carvalho, M., Dias da Silva, D., Gaspar, H., Carvalho, F., de Lourdes Bastos, M. & Guedes de Pinho, P. (2015) Raising awareness of new psychoactive substances: chemical analysis and in vitro toxicity screening of 'legal high' packages containing synthetic cathinones, *Archives of Toxicology.* **89**, 757-771.

48. Valente, M. J., Araújo, A. M., Bastos, M. d. L., Fernandes, E., Carvalho, F., Guedes de Pinho, P. & Carvalho, M. (2016) Characterization of hepatotoxicity mechanisms triggered by designer cathinone drugs (β-keto amphetamines), *Toxicological Sciences.* **153**, 89-102.

49. Gaspar, H., Bronze, S., Oliveira, C., Victor, B. L., Machuqueiro, M., Pacheco, R., Caldeira, M. J. & Santos, S. (2018) Proactive response to tackle the threat of emerging drugs: Synthesis and toxicity evaluation of new cathinones, *Forensic Science International.* **290**, 146-156.

50. Sheikh, I. A., Lukšič, M., Ferstenberg, R. & Culpepper-Morgan, J. A. (2014) Spice/K2 synthetic marijuana-induced toxic hepatitis treated with N-acetylcysteine, *The American journal of case reports.* **15**, 584-588.

51. Wojcieszak, J., Andrzejczak, D., Kedzierska, M., Milowska, K. & Zawilska, J. B. (2018) Cytotoxicity of α-Pyrrolidinophenones: an Impact of α-Aliphatic Side-chain Length and Changes in the Plasma Membrane Fluidity, *Neurotoxicity Research.* **34**, 613-626.

52. McEuen, K., Borlak, J., Tong, W. & Chen, M. (2017) Associations of Drug Lipophilicity and Extent of Metabolism with Drug-Induced Liver Injury, *International Journal of Molecular Sciences.* **18**, 1335.

53. Antoine, D., Olivier, M. & Vincent, Z. (2017) SwissADME: a free web tool to evaluate pharmacokinetics, drug-likeness and medicinal chemistry friendliness of small molecules, *Scientific Reports.* **7**, 42717.

54. Grecco, G. G., Kisor, D. F., Magura, J. S. & Sprague, J. E. (2017) Impact of common clandestine structural modifications on synthetic cathinone "bath salt" pharmacokinetics, *Toxicology and Applied Pharmacology.* **328**, 18-24.

55. Anizan, S., Concheiro, M., Lehner, K. R., Bukhari, M. O., Suzuki, M., Rice, K. C., Baumann, M. H. & Huestis, M. A. (2016) Linear pharmacokinetics of 3,4-methylenedioxypyrovalerone (MDPV) and its metabolites in the rat: relationship to pharmacodynamic effects, *Addiction Biology.* **21**, 339-347.

56. Baumann, M. H., Bukhari, M. O., Lehner, K. R., Anizan, S., Rice, K. C., Concheiro, M. & Huestis, M. A. (2017) Neuropharmacology of 3,4-Methylenedioxypyrovalerone (MDPV), Its Metabolites, and Related Analogs, *Current Topics in Behavioral Neurosciences.* **32**, 93-117.

57. Calinski, D. M., Kisor, D. F. & Sprague, J. E. (2019) A review of the influence of functional group modifications to the core scaffold of synthetic cathinones on drug pharmacokinetics, *Psychopharmacology (Berl).* **236**, 881-890.

58. Baumann, M. H., Bukhari, M. O., Lehner, K. R., Anizan, S., Rice, K. C., Concheiro, M. & Huestis, M. A. (2017) Neuropharmacology of 3,4-methylenedioxypyrovalerone (MDPV), its metabolites, and related analogs in *Current Topics in Behavioral Neurosciences* pp. 93-117

59. McNaney, C., Drexler, D., Hnatyshyn, S., Zvyaga, T., Knipe, J., Belcastro, J. & Sanders, M. (2008) An Automated Liquid Chromatography-Mass Spectrometry Process

to Determine Metabolic Stability Half-Life and Intrinsic Clearance of Drug Candidates by Substrate Depletion, *Assay and Drug Development Technologies.* **6**, 121-129.

60. Strano-Rossi, S., Cadwallader, A. B., de la Torre, X. & Botrè, F. (2010) Toxicological determination and in vitro metabolism of the designer drug methylenedioxypyrovalerone (MPDV) by gas chromatography/mass spectrometry and liquid chromatography/quadrupole time-of-flight mass spectrometry, *Rapid Communications in Mass Spectrometry.* **24**, 2706-2714.

61. Meyer, M. R., Wilhelm, J., Peters, F. T. & Maurer, H. H. (2010) Beta-keto amphetamines: studies on the metabolism of the designer drug mephedrone and toxicological detection of mephedrone, butylone, and methylone in urine using gas chromatography–mass spectrometry, *Analytical and Bioanalytical Chemistry.* **397**, 1225-1233.

62. Mueller, D. & Rentsch, K. (2012) Generation of metabolites by an automated online metabolism method using human liver microsomes with subsequent identification by LC-MS(n), and metabolism of 11 cathinones, *Analytical and Bioanalytical Chemistry.* **402**, 2141-2151.

63. Castaneto, M. S., Wohlfarth, A., Desrosiers, N. A., Hartman, R. L., Gorelick, D. A. & Huestis, M. A. (2015) Synthetic cannabinoids pharmacokinetics and detection methods in biological matrices, *Drug Metabolism Reviews.* **47**, 124-74.

64. Haschimi, B., Mogler, L., Halter, S., Giorgetti, A., Schwarze, B., Westphal, F., Fischmann, S. & Auwärter, V. (2019) Detection of the recently emerged synthetic cannabinoid 4F-MDMB-BINACA in 'legal high' products and human urine specimens, *Drug Testing and Analysis.* **11**, 1377-1386.

65. Krotulski, A. J., Mohr, A. L. A., Kacinko, S. L., Fogarty, M. F., Shuda, S. A., Diamond, F. X., Kinney, W. A., Menendez, M. J. & Logan, B. K. (2019) 4F-MDMB-BINACA: A New Synthetic Cannabinoid Widely Implicated in Forensic Casework, *Journal of forensic sciences.* **64**, 1451-1461.

66. Wagmann, L., Frankenfeld, F., Park, Y. M., Herrmann, J., Fischmann, S., Westphal, F., Müller, R., Flockerzi, V. & Meyer, M. R. (2020) How to Study the Metabolism of New Psychoactive Substances for the Purpose of Toxicological Screenings—A Follow-Up Study Comparing Pooled Human Liver S9, HepaRG Cells, and Zebrafish Larvae, *Frontiers in Chemistry.* **8**, 539.

67. Morita, K., Kato, M., Kudo, T. & Ito, K. (2020) In vitro-in vivo extrapolation of metabolic clearance using human liver microsomes: factors showing variability and their normalization, *Xenobiotica; the fate of foreign compounds in biological systems.* **50**, 1064-1075.

Chapter 6

Conclusions, limitations, recommendations and future work

Synthetic cathinones (SCs) are psychostimulants designed to mimic the effects of traditional psychostimulants such as cocaine, methamphetamine and 3,4-methylenedioxymethamphetamine (MDMA). Neurotoxic effects involving oxidative stress, metabolic compromise, induction of apoptosis and so on have been reported from the traditional psychostimulant counterparts. The first section of the study hypothesizes similar mechanisms and processes occurring following chronic SCs intake. The findings from this study demonstrated that SCs exert significant neurotoxic effects on cultured dopaminergic neuronal SH-SY5Y cells in a dose-dependent neurotoxicity pattern, showing the detrimental impact of these SCs when administered in high dosage. Mitochondrial-mediated toxicity mechanisms were found to be the key player as implicated by the apoptotic cell death pathway, changes in intracellular calcium homeostasis, oxidative stress and compromised bioenergetics balance. These findings provide an important first insight into the mechanisms of SCs' neurotoxicity like to the traditional psychostimulant, paving the way for further studies in cultures of primary neuronal cell cultures and *in vivo* models. It would be interesting to employ the use of antioxidants to assess whether its use could mitigate the SCs-induced neurotoxicity, hence defining the critical role of oxidative stress in these neurotoxic effects if applicable. The study sheds light on the neurotoxicity potency and the underlying mechanisms of psychostimulant SCs butylone, pentylone and 3,4-methylenedioxypyrovalerone (MDPV). Understanding the relationship between the molecular mechanisms underlying the neurotoxicity of these psychostimulants and related clinical manifestations is imperative to provide more effective treatments for SCs users. Substantial work remains before translating the *in vitro* data to human practice in the prevention of the devastating neurotoxic effects associated with the abuse of these drugs.

Different cell system might response differently to toxic injury. In the second section of this study, previously mentioned SCs butylone, pentylone and MDPV, together with synthetic cannabinoid, methyl (2S)-2-([1-(4-fluorobutyl)-1H-indazole-3-carbonyl]amino)-3,3-dimethylbutanoate (4F-MDMB-BINACA) were investigated for its hepatoxicity potency potential using HepG2 hepatoma cell line. To evaluate whether an assessment of the order of cytotoxic potential was possible without EC_{50} determination, another screening cut-off method using mitochondrial membrane potential assay was employed. The two different assay approaches (Viability and mitochondrial membrane

potential assay) showed similar order of cytotoxicity findings in HepG2 cells: butylone (least toxic) < pentylone < MDPV < 4F-MBDB-BINACA (most toxic). More work is needed to establish an appropriate baseline screening cut off using the mitochondrial membrane potential assay and the plausible insertion of positive control of known toxicity in determining the relative cytotoxicity potency of different NPS. As increasing use of unknown NPS toxicities poses severe risk for public health, predicting which NPS is likely to result in severe effects, prior to the actual occurrence of severe effects, could improve public health.

The order of cytotoxicity potency of SCs butylone, pentylone and MDPV observed in the HepG2 liver cells was the same as that in the human dopaminergic neuronal SH-SY5Y cells, suggesting that the cellular damage mechanism might be similar in both cell system. It was observed that lipophilicity of the NPS, augmented with increasing length of alkyl chains is one of the factors contributing to the overall cytotoxicity. Future work could include the *in silico* investigation on how lipophilicity and other physicochemical properties could be linked with the induced cytotoxicity of NPS.

The later part of the second section of this study was to assess the correlation between *in vitro* and *in vivo* estimated intrinsic clearance (CL_{int}) and half-life ($t_{1/2}$) of the NPS. *In vitro – in vivo* extrapolation (IVIVE) using human liver microsomes (HLM) has been widely used to predict metabolic clearance. The calculated *in vitro* $t_{1/2}$ were 53.9 ± 16.0, 104 ± 32.6, 113 ± 33.8 and 7.57 ± 0.29 min for butylone, pentylone, MPDV and 4F-MDMB-BINACA, respectively. The CL_{int} values together with calculated $t_{1/2}$ categorized butylone, pentylone and MPDV as low clearance drugs ($t_{1/2}$ > 60 min, CL_{int} < 15 mL/min/kg) and 4F-MDMB-BINACA ($t_{1/2}$ < 20 min, CL_{int} > 45 mL/min/kg) as a relatively high clearance drug. The *in vitro* kinetic $t_{1/2}$ values obtained from the metabolic stability study via HLM is essential to properly design *in vitro* incubation for drug metabolism studies. The kinetic calculation in this study is based upon the assumption that non-specific blood protein and microsome binding was negligible. Future work should include studies on protein binding and volume of distribution calculation to supplement the existing available kinetics data.

Highly lipophilic 4F-MDMB-BINACA with short half-life and high intrinsic

clearance, implied the extensive hepatic metabolism of 4F-MDMB-BINACA. To prove the reliability of the *in vitro* toxicokinetic data obtained, the last section of this study includes the metabolism study of 4F-MDMB-BINACA. To understand and monitor the metabolism of 4F-MDMB-BINACA, three *in vitro* models (HepG2, HLM and *Cunninghamella elegans* (*C. elegans*)) were employed, and the resultant findings were compared with the *in vivo* authentic human urine samples. A total of 25 different *in vitro* metabolites and eight *in vivo* metabolites were tentatively identified, demonstrating the extensive metabolism of 4F-MDMB-BINACA. HepG2 identified the major *in vivo* metabolite of 4F-MDMB-BINACA in abundance but the rest of the metabolites were found in low abundances. HLM was found to be a suitable IVIVE model for the metabolism study of 4F-MDMB-BINACA. *C. elegans* demonstrated the potential to be used as a complementary model to predict and characterize human metabolites, as well as identifying possible drug toxicities for emerging synthetic cannabinoids (SCBs), especially when large quantities of metabolites are required. Suitable urinary markers of 4F-MDMB-BINACA identified (ester hydrolysis and ester hydrolysis dehydrogenation 4F-MDMB-BINACA metabolites) in this study aid the forensic and clinical toxicologists in the detection of metabolites of 4F-MDMB-BINACA in biological fluids. Future work should include unequivocally identifying the structures of postulated dehydrogenation metabolites and potentially toxic hydroxyl metabolites of 4F-MDMB-BINACA found in this study via the nuclear magnetic resonance spectroscopy, which includes the isolation of metabolites using scaled-up metabolism experiments by *C. elegans*.

Overall, the present study demonstrated the cytotoxic potency potential and metabolic profile of NPS butylone, pentylone, MDPV and 4F-MDMB-BINACA. *In vitro* toxicokinetic data of 4F-MDMB-BINACA revealed the high clearance nature of this NPS, and the findings were supported with the metabolism study whereby 4F-MDMB-BINACA was found to be extensively metabolized. The extensive metabolism of 4F-MDMB-BINACA might result in the cytotoxicity observed in this study. Hydroxylated urinary metabolites that are even more toxic than the parent SCBs have been reported. Future work should also include the cytotoxic investigation of the active hydroxyl metabolites formed by 4F-MDMB-BINACA. Preliminary *in vitro* cytotoxicity and metabolic stability studies data are useful in the prediction of *in vivo* human toxicity and

understanding the toxicokinetics of NPS. Understanding the toxicology profile of these NPS could potentially provide the key to effective policy decisions and interventions.

Appendices

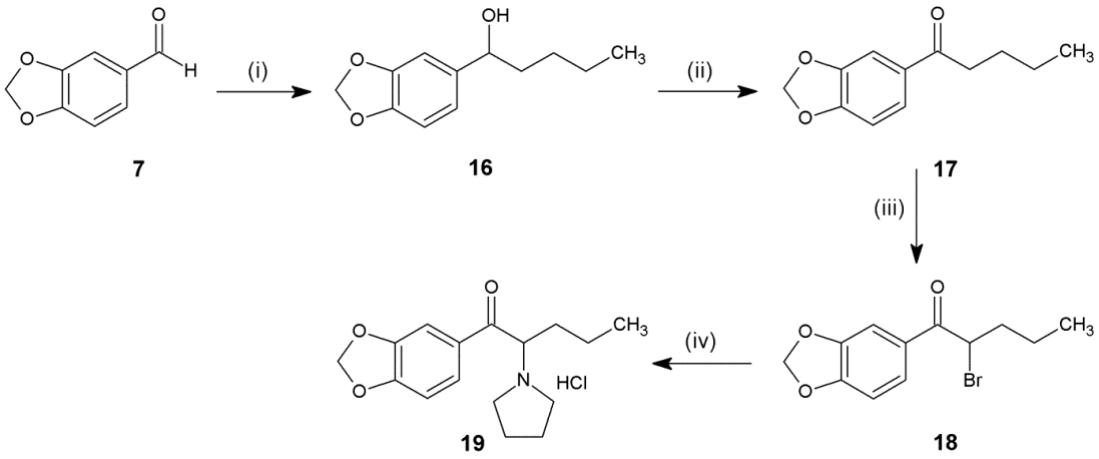

Figure A.1 Synthesis of MDPV HCl (**19**) via a four step reaction sequence: (i) Grignard reaction of piperonal (**7**), (ii) oxidation of **16**, (iii) α-bromination of **17** and (iv) nucleophilic substitution of **18** with pyrrolidine.
Reagents and conditions: (i) BuMgCl, Et_2O, N_2 atm., RT, 2 h; *(ii)* PCC/celite, DCM, 18 h; *(iii)* bromine, glacial acetic acid, RT, 17.5 h; *(iv)* pyrrolidine, Et_2O, RT, 19 h.

Detailed synthesis of MDPV HCl (**19**):
In a round-bottom flask (RBF), the α-bromoketone **18** (2.016 g, 7.07 mmol) was dissolved in diethyl ether (15 mL) and cooled on an ice bath. Pyrrolidine (1.5 mL, 18 mmol) was added all at once and the reaction left to stir for 19 h. Diethyl ether (10 mL) and water (10 mL) were added to the RBF before extracting the mixture with diethyl ether (3 x 15 mL) and washing the ethereal extracts with water (3 x 15 mL). The mixture was back-extracted with 1 M HCl (3 x 15 mL) and the aqueous extracts were washed with diethyl ether (3 x 10 mL). The water was removed via rotary evaporation and the residue dried under vacuum overnight to afford a crude brown coloured residue with a toffee-like texture. The crude material was washed with small portions of acetone to afford an off-white, bone coloured powder **19** (0.776 g, 2.49 mmol).

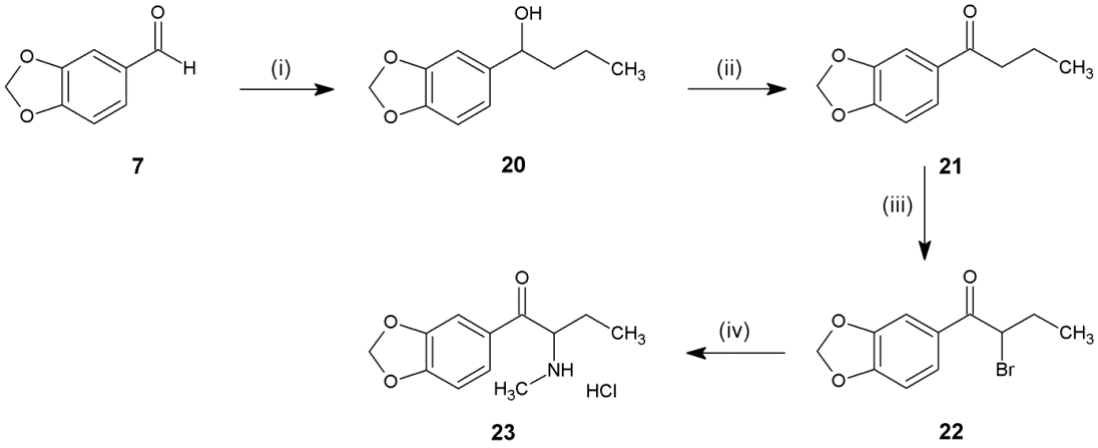

Figure A.2 Synthesis of butylone HCl (**23**) via a four step reaction sequence: (i) Grignard reaction of piperonal (**7**), (ii) oxidation of **20**, (iii) α-bromination of **21** and (iv) nucleophilic substitution of **22** with methylamine.
Reagents and conditions: (i) PropMgCl, Et_2O, N_2 atm., RT, 4 h; *(ii)* PCC/celite, DCM, 21 h; *(iii)* bromine, glacial acetic acid, RT, 18 h; *(iv)* pyrrolidine, Et_2O, RT, 20 h.

Detailed synthesis of butylone HCl (**23**):
In a RBF, the α-bromoketone **22** (2.09 g, 7.71 mmol) was dissolved in toluene (5 mL) and stirred at room temperature briefly. Separately in two beakers, sodium hydroxide pellets (1.28 g, 32.0 mmol) were dissolved in cold water (2.5 mL) and added to a solution of methylamine hydrochloride (2.16 g, 32.0 mmol) in cold water (2 mL). This combined solution was quickly added dropwise to the RBF using a Pasteur pipette and the reaction mixture left to stir for 20 h. The reaction was quenched by pouring the mixture into ice-cold water (30 mL). The toluene layer was separated, and the aqueous layer further extracted with toluene (3 x 10 mL). Combined toluene extracts were washed with water (3 x 10 mL) and acidified with 1 M HCl (5 x 10 mL). Acidic extracts were washed with toluene (3 x 10 mL) and evaporated to dryness to afford an off-white coloured crystalline material **23** (1.48 g, 5.74 mmol).

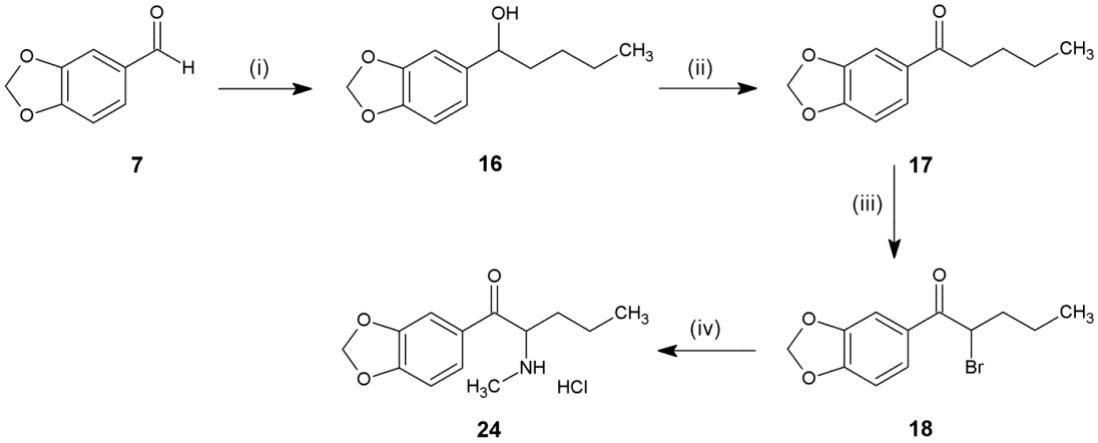

Figure A.3 Synthesis of pentylone HCl (**24**) via a four step reaction sequence: (i) Grignard reaction of piperonal (**7**), (ii) oxidation of **16**, (iii) α-bromination of **17** and (iv) nucleophilic substitution of **18** with methylamine.
Reagents and conditions: (i) ButMgCl, Et_2O, N_2 atm., RT, 4 h; *(ii)* PCC/celite, DCM, RT, 21 h; *(iii)* bromine, glacial acetic acid, RT, 18 h; *(iv)* pyrrolidine, Et_2O, RT, 19 h.

Detailed synthesis of pentylone HCl (**24**):
In a RBF, the α-bromoketone **18** (2.30 g, 8.01 mmol) was dissolved in toluene (5 mL) and stirred at room temperature briefly. Separately in two beakers, sodium hydroxide pellets (1.28 g, 32.0 mmol) were dissolved in cold water (2.5 mL) and added to a solution of methylamine hydrochloride (2.16 g, 32.0 mmol) dissolved in cold water (2 mL). The combined solution was quickly added (dropwise) to the RBF using a Pasteur pipette and the reaction mixture left to stir for 19 h. The reaction was quenched by pouring the mixture into ice-cold water (30 mL). The toluene layer was separated, and the aqueous layer further extracted with toluene (3 x 15 mL). Combined toluene extracts were washed with water (3 x 10 mL) and acidified with 1 M HCl (3 x 10 mL). Acidic extracts were washed with toluene (3 x 10 mL) and evaporated to dryness to afford an off-white coloured crystalline material **24** (1.61 g, 5.94 mmol).

Detailed synthesis of intermediates **16**, **17** and **18**:

To a RBF maintained under nitrogen atmosphere was added piperonal **7** (1.2013 g, 8.00 mmol). Diethyl ether (10 mL) was added via syringe and the solution stirred to dissolve the solid. The flask was kept on an ice bath while butylmagnesium chloride solution (6.0 mL, 12 mmol) was added dropwise via syringe over 3 min. The ice bath was removed after 10 min and the reaction stirred for 2 h. To the RBF was added 1 M HCl (6 mL, 6 mmol) and the mixture stirred briefly. The ether layer was separated and washed with water (3 x 5 mL). The ether extract was dried over anhydrous sodium sulphate before removing the solvent via rotary evaporation to afford a light yellow oil **16** (1.55 g, 7.42 mmol). The oil was dissolved in dichloromethane (12 mL) in a RBF before adding pyridinium chlorochromate (1.0 g, 4.6 mmol) and celite (1.0 g) sequentially and leaving the mixture to stir for 17 h. Diethyl ether (30 mL) was added to the flask and the reaction stirred for a further 1 h. The reaction mixture was filtered through a pad of silica in a sintered glass funnel and the filtrate rotary evaporated to afford a yellow oil with dark droplets on the surface **17** (1.53 g, 7.42 mmol). In a RBF, the ketone **17** (1.530 g, 7.42 mmol) was dissolved in glacial acetic acid (60 mL) and a pressure equalising dropping funnel containing bromine (0.41 mL, 8.0 mmol) was attached. One drop of bromine was initially added, and the mixture stirred for 30 min. The remaining bromine was added dropwise over 10 min and the mixture left to stir for 17.5 h. The reaction was quenched by pouring the mixture into ice-cold water (100 mL). The aqueous mixture was extracted with dichloromethane (3 x 50 mL) and the combined extracts were washed with saturated sodium carbonate solution (3 x 50 mL) before drying over magnesium sulphate. The solvent was removed via rotary evaporation to afford an orange oil **18** (2.02 g, 7.07 mmol).

Detailed synthesis of intermediates **20**, **21** and **22**:

To a RBF maintained under nitrogen atmosphere was added piperonal **7** (1.50 g, 10.0 mmol). Diethyl ether (10 mL) was added via syringe and the solution stirred to dissolve the solid. The flask was kept on ice while propylmagnesium chloride solution (6.0 mL, 12 mmol) was added via syringe over 3 min. The ice bath was removed after 10 min and the reaction stirred for 4 h before carefully adding 1 M HCl (10 mL, 10 mmol). The ether layer was separated, washed with water (3 x 5 mL) and dried over magnesium sulphate before removing the solvent via rotary evaporation to afford a cloudy oil **20** (1.76 g, 9.06

mmol). The oily residue **20** was dissolved in dichloromethane (20 mL) in a RBF before adding PCC (2.5 g, 11.5 mmol) and celite (2.5 g) and leaving the reaction to stir for 20.5 h. Diethyl ether (30 mL) was added to the mixture and the reaction stirred for a further 30 min. The reaction mixture was filtered through a pad of silica in a sintered glass funnel and the filtrate was rotary evaporated to afford a yellow-brown oil **21** (1.58 g, 8.22 mmol). The ketone **21** (1.58 g, 8.22 mmol) was dissolved in glacial acetic acid (50 mL) in a RBF and a pressure equalising dropping funnel containing bromine (0.50 mL, 9.0 mmol) was attached. A few drops of bromine were added initially, and the reaction stirred for 30 min, after which, the remaining bromine was added dropwise. After 18 h of stirring, the reaction was quenched by pouring the mixture into ice-cold water (100 mL). The mixture was extracted with dichloromethane (3 x 40 mL) and carefully washed with sodium carbonate solution (3 x 30 mL). The organic fraction was dried over magnesium sulphate before decanting and removing the solvent via rotary evaporation to afford an orange-brown oil **22** (2.09 g, 7.71 mmol).

Abbreviations:
BuMgCl: butylmagnesium chloride
Et_2O: diethyl ether
N_2: nitrogen
PCC: pyridinium chlorochromate
DCM: dichloromethane
HCl: hydrochloric acid
RT: room temperature
PropMgCl: propylmagnesium chloride

Table **A1**. Percentage yields obtained for synthetic cathinone analogues and their respective intermediates

Synthetic Cathinone Analogue	Percent yield (%)[a]				Melting point (°C)
	Ketone	α-Bromoketone	Crude amine HCl	Pure amine HCl	Pure amine HCl
MDPV (**19**)	93	95[c]	- [d]	35	235-238
Butylone (**23**)	82	94[c]	- [b]	74	222-227
Pentylone (**24**)	93[c]	95[c]	- [b]	74	216-222

[a] Calculated per one step reaction. Intermediates not applicable to synthesis are blank

[b] Amine salt did not require further purification

[c] Repeated procedure from synthesis of different analogue

[d] Yield not calculated

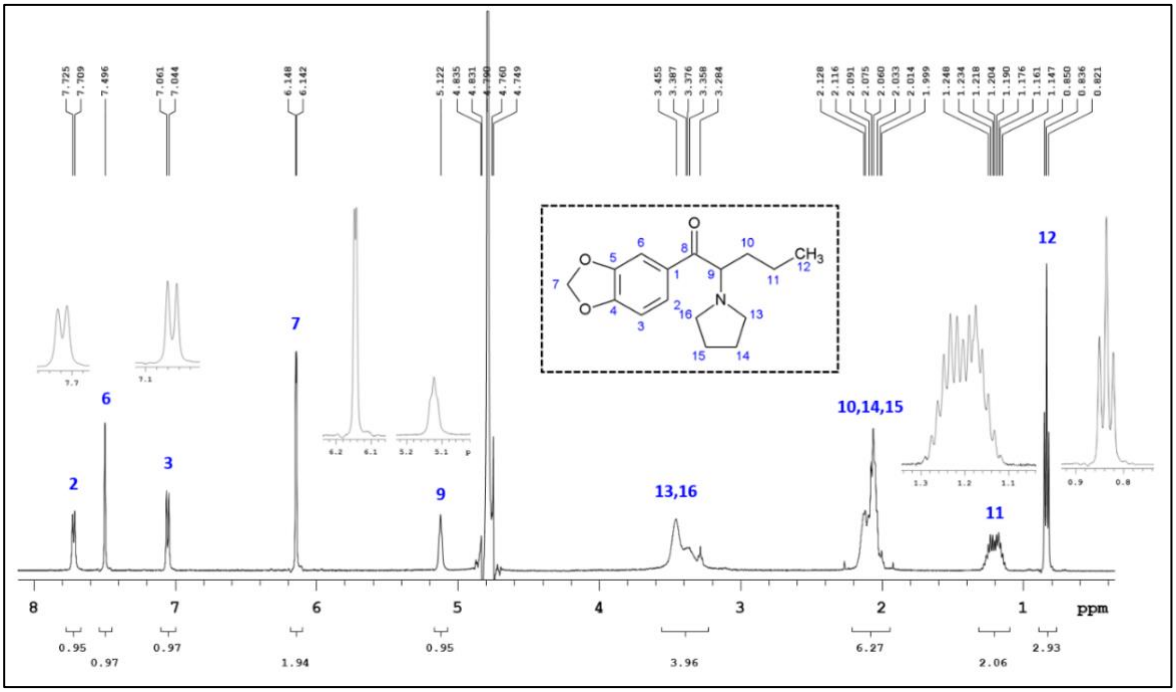

Figure B.1 Annotated ^{1}H-NMR spectrum of MDPV HCl (**19**) measured in deuterated water (δ 4.79 ppm). Inset: zoomed regions containing splitting patterns

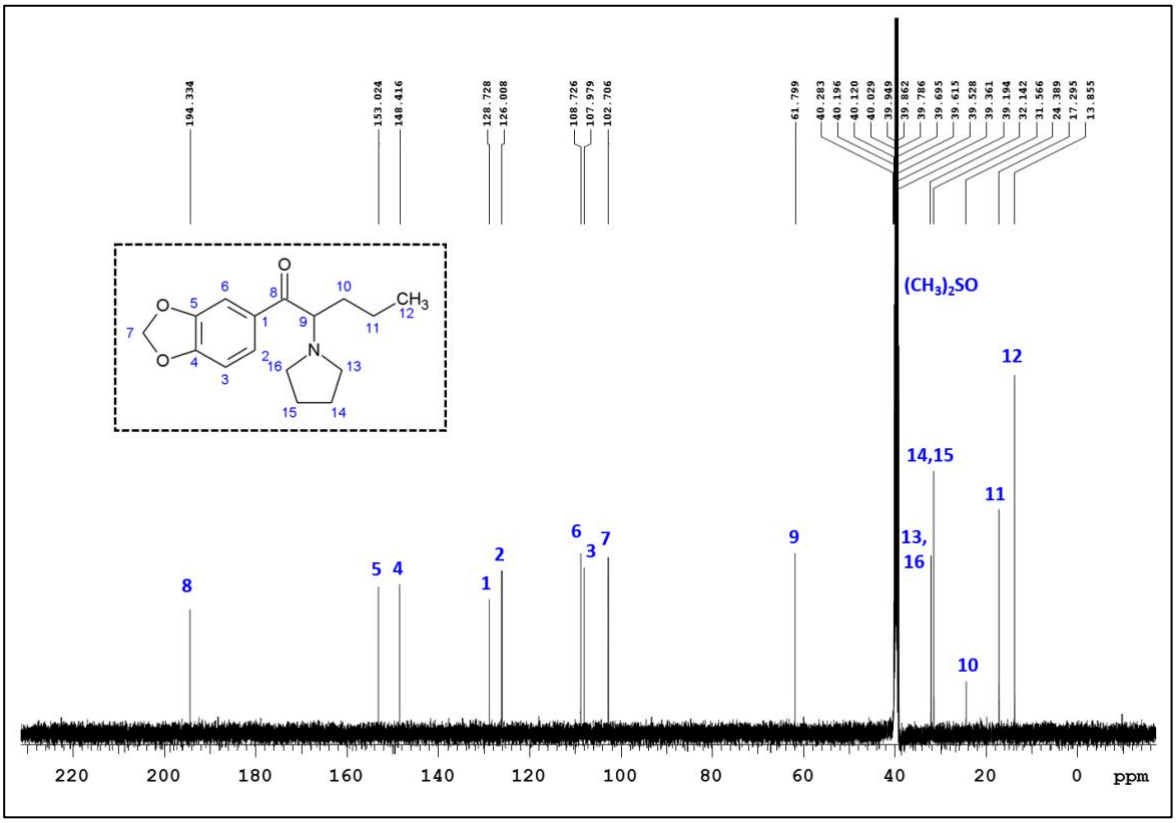

Figure B.2 Annotated ^{13}C-NMR spectrum of MDPV HCl (**19**) measured in deuterated dimethyl sulfoxide (δ 39.52 ppm)

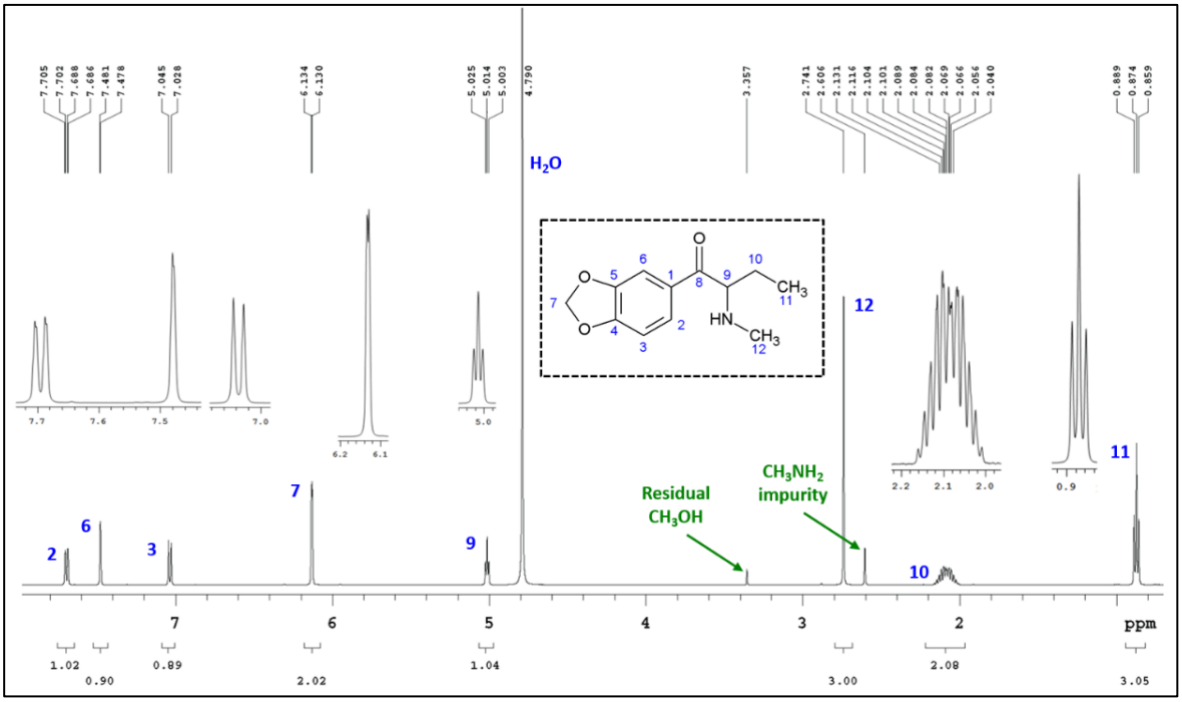

Figure B.3 Annotated ^{1}H-NMR spectrum of butylone HCl (**23**) measured in deuterated water (δ 4.79 ppm). Inset: zoomed regions containing splitting patterns

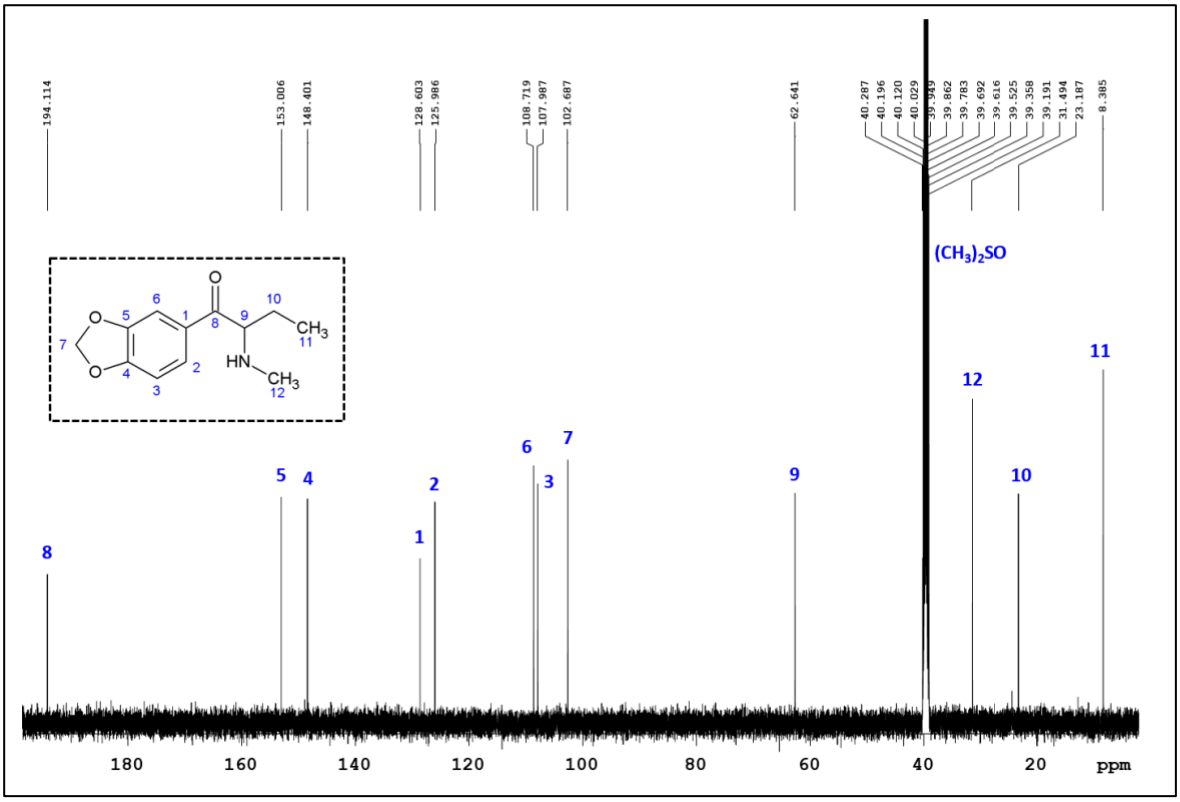

Figure B.4 Annotated ^{13}C-NMR spectrum of butylone HCl (**23**) measured in deuterated dimethyl sulfoxide (δ 39.52 ppm)

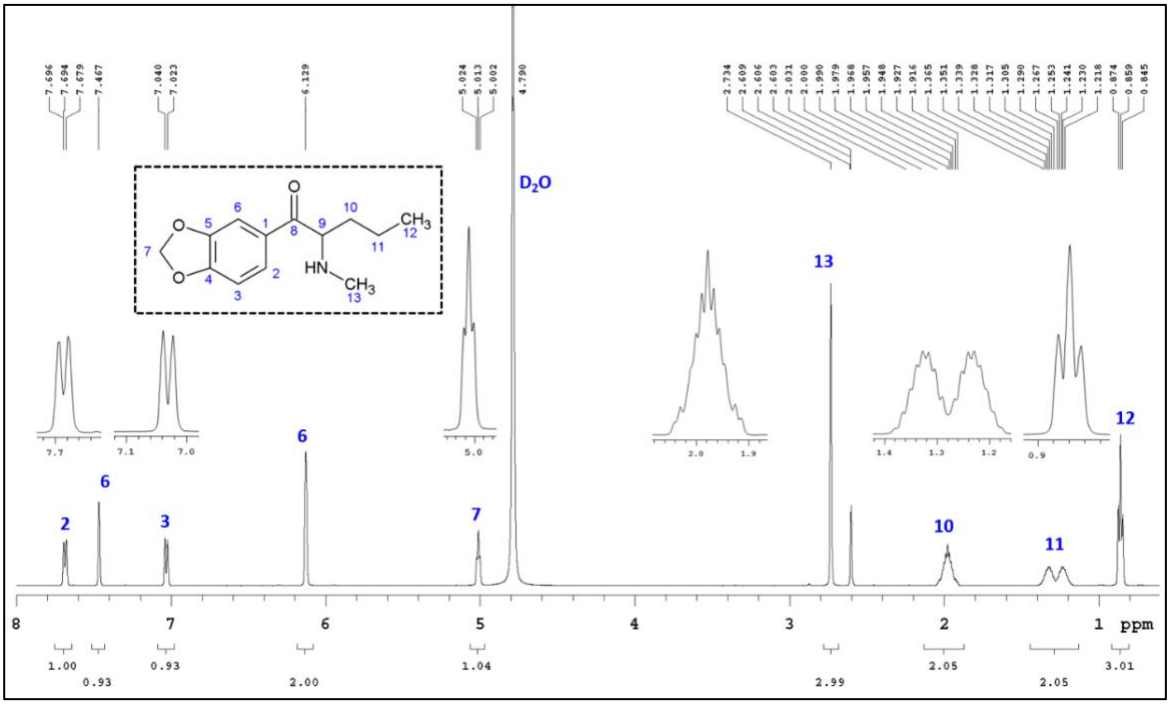

Figure B.5 Annotated ^{1}H-NMR spectrum of pentylone HCl (**24**) measured in deuterated water (δ 4.79 ppm). Inset: zoomed regions containing splitting patterns

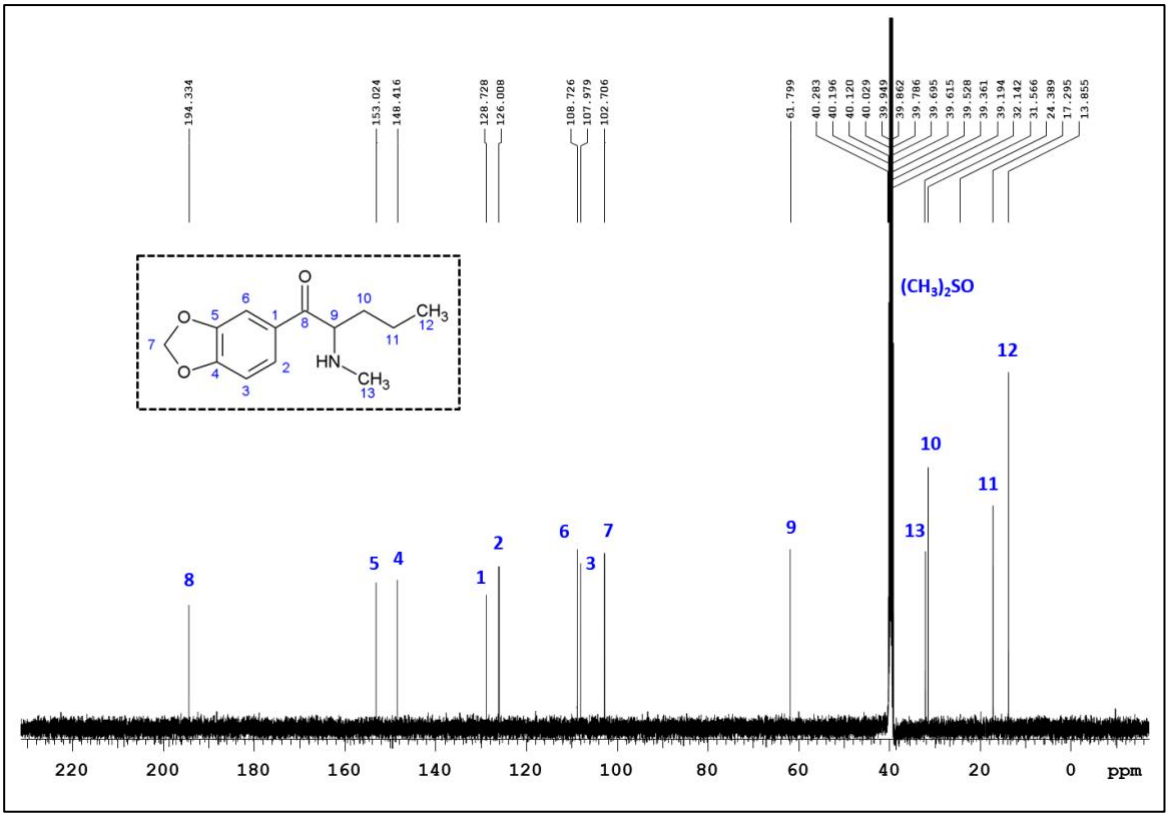

Figure B.6 Annotated ^{13}C-NMR spectrum of pentylone HCl (**24**) measured in deuterated dimethyl sulfoxide (δ 39.52 ppm)